Spring 5-13-2016

Barrier spit evolution and primary consolidation of backbarrier facies: West Belle Pass Barrier, LA

John N. Kramer III
University of New Orleans, New Orleans, jnkramer@uno.edu

Barrier spit evolution and primary consolidation of backbarrier facies: West Belle Pass Barrier, LA

A Thesis

Submitted to the Graduate Faculty of the
University of New Orleans
in partial fulfillment of the
requirements for the degree of

Master of Science
in
Earth and Environmental Sciences
Coastal Geology

by

John Norbert Kramer III

B.S. University of West Florida, 2013

May, 2016

Acknowledgements

I would first like to thank the University of New Orleans for accepting me in to the Earth and Environmental Science department and giving me the opportunity to work with such passionate and knowledgeable faculty. I am extremely appreciative for the chances I was given to represent the University of New Orleans EES department at APPG's Imperial Barrel Award and professional conferences. The life-lessons and hands-on experience I gained from my time here will stay with me for years to come, and I hope that many more students will have the same opportunities.

I am very grateful for the guidance and motivation from my committee. My advisor, Dr. Mark Kulp, provided the inspiration and much-needed guidance for this study. Our discussions on coastal-related issues led to a friendship that I will surely treasure. Dr. Ioannis Georgiou participated in field sampling and discussions that helped focus the aim of this study early on in its development. I would also like to thank Dr. Klaus Meyer-Arendt, whose methods and desire of teaching instilled in me an interest for the Louisiana coast during my time at the University of West Florida. Dr. Malay Ghose Hajra provided outside geotechnical support, and he is certainly deserving of thanks as well.

Finally, I would like to thank my fiancée, Alexa Bonadona, for her love and encouragement during the last three years. Without her, this thesis would not be. Thank you to my parents, John and Anne Kramer, who provided me every opportunity imaginable no matter the expense.

Table of Contents

List of Figures

List of Tables

Abstract

West Belle Pass Barrier is a barrier spit that formed during the last delta lobe progradation associated with the Lafourche delta complex. Located on the western flank of the Caminada-Moreau Headland, West Belle Pass Barrier and Raccoon Pass are located downdrift of the Belle Pass jetties. Morphological changes stemming from storms, jetty infrastructure, and an expanding tidal inlet are evaluated using historical shoreline data and imagery. Littoral transport around the jetties combined with inlet growth created a framework wherein sediment is transported through Raccoon Pass and sequestered as a flood-tidal delta. These events aided in the landward migration of West Belle Pass Barrier, which ultimately loaded and consolidated previously unconsolidated facies. A conceptual model illustrating the primary consolidation of backbarrier facies resulting from washover deposits during one storm is presented. The primary consolidation settlement associated with loading near-surface, water-saturated backbarrier facies is substantially larger than current subsidence rates.

Keywords: Caminada-Moreau Headland, Bayou Lafourche, Raccoon Pass, barrier spit, consolidation

Chapter 1. Introduction and Significance

1.1 Introduction

Sustaining barrier islands within the Mississippi River delta plain (MRDP) is of social, ecological, industrial, and environmental importance. Barrier islands are the seaward-most subaerial boundary of the MRDP that protect valuable wetlands from saltwater intrusion and erosion by wind and waves generated during cold fronts, subtropical storms, as well as daily marine processes. Barrier islands form and evolve in response to relative sea-level changes and alongshore and cross-shore sediment transport processes, all of which contribute to the migration, extension, and ultimately, inundation of Louisiana coastal barriers. Multiple theories on barrier formation exist; however, three distinctive hypotheses stand out: 1) accretion of submerged bars (De Beaumont, 1845), 2) spit progradation and inlet segmentation (Gilbert, 1885), and 3) submergence of beach ridges (McGee, 1890; Hoyt, 1967). Although there are numerous theories regarding the origin of barriers, it is widely accepted that Louisiana's barrier islands are in danger of drowning because of high rates of relative sea-level rise. One component that contributes to relative sea-level rise (i.e., compaction of strata) stems from the location and deposition of facies within a barrier system. There are three main environments of barrier systems (barrier beach, lagoon, and tidal channel-delta complex), and each environment is comprised of numerous sub-environments categorized by distinct lithofacies (Reinson, 1976). Specifically, lagoonal deposits consist predominantly of mud with interbedded sand layers that load and compress saturated mud strata. Loading compressible strata along deltaic coastlines results in elevation changes, ultimately making barrier shorelines more susceptible to overwash, wave attack, and ultimately drowning (Rosati et al., 2010).

Within the last two decades, State and Federal agencies have embarked on a suite of ambitious plans that are focused on renourishing deteriorating coastal barriers and shorelines of Louisiana. For instance, Fourchon Beach, located between Grand Isle and the study area, was the site of the Caminada-Moreau Subsidence Study (State Project Number LA-12.6). This paramount study examined the geological profile along Fourchon Beach in order to evaluate pre-project subsidence and post-fill settlement using numerous borings, soil samples, and surface monuments. The success of these efforts and others to come, however, will be strongly contingent upon a solid understanding of the geologic framework and morphologic evolution of these threatened systems. Only through a robust understanding of how these systems have changed and respond to forcing mechanisms can economically and environmentally sensitive coastal restoration efforts be truly feasible.

This study focuses specifically on documenting the natural and anthropogenically-modified geomorphologic history of a south-central Louisiana barrier system through an analysis of historic maps, imagery, and stratigraphic framework (Fig. 1). Additionally, this study quantifies the primary consolidation settlement of backbarrier facies upon conceptual loading from washover deposits during a singular overwash event.

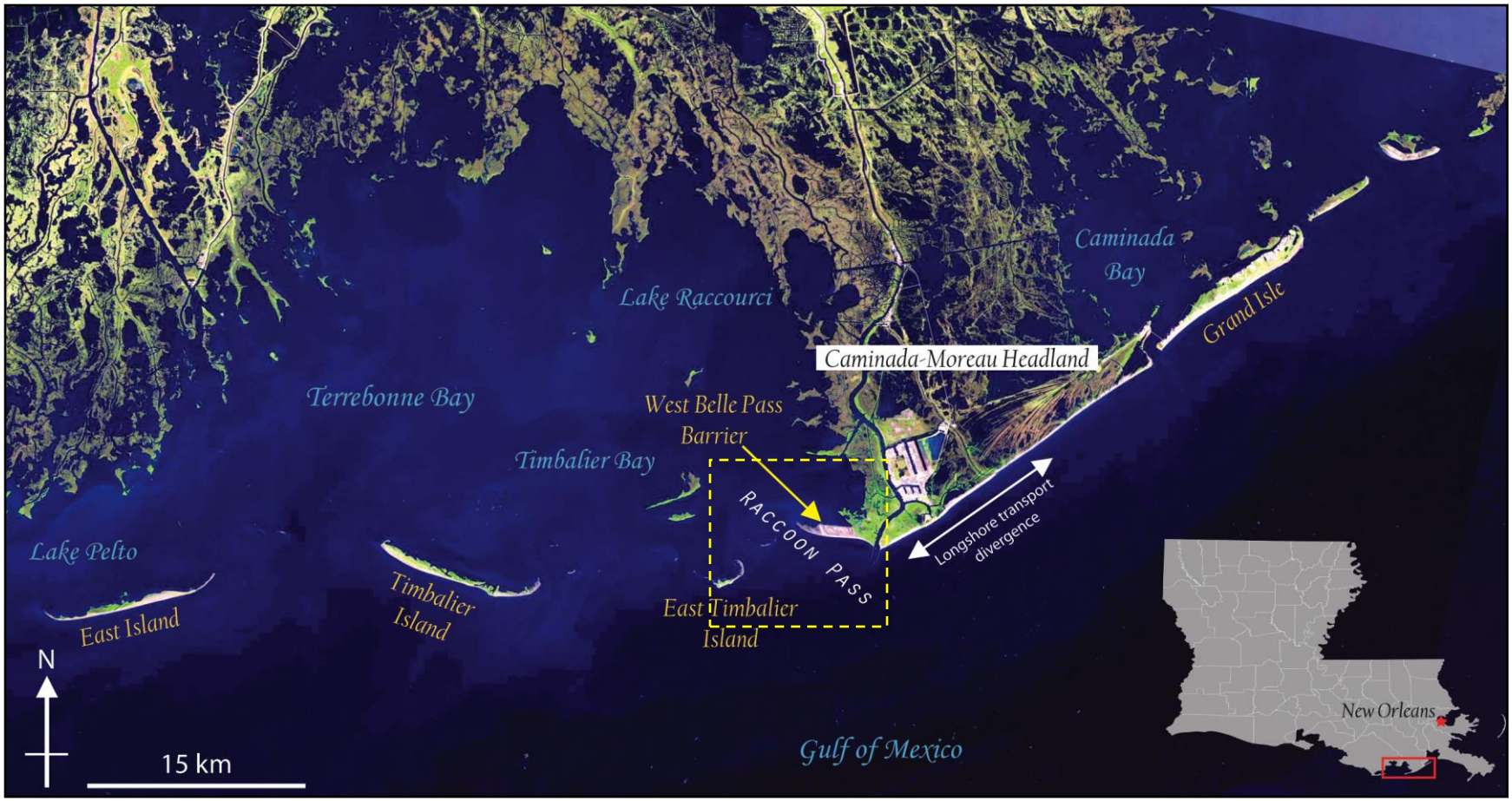

Figure 1. Study Site Location. Satellite image showing the location of the study site located within the yellow dashed box. Raccoon Pass is located between East Timbalier Island to the west and West Belle Pass Barrier Headland to the east, both of which are located downdrift of Belle Pass, west of where there is a divergence of the longshore transport pattern along the Caminada-Moreau headland (2015 image from USGS Landsat Look Viewer.)

1.2 Objectives and Hypotheses

1.2.1 Objectives

This study is focused on two specific objectives: 1) to reconstruct the natural and anthropogenic-induced evolution of West Belle Pass Barrier and adjacent Raccoon Pass using imagery, historic shorelines, and shallow stratigraphic relationships, and 2) to quantify the primary consolidation settlement accredited to the near-surface (0-2 m), unconsolidated, water-saturated backbarrier facies after loading. The goal of this study is to evaluate the mechanisms that are driving the evolution of a south-central Louisiana barrier system including the effects of marine reworking, anthropogenic shoreline modifications, and loading backbarrier facies with storm washover deposits. Collectively, these processes have been shown to affect barrier evolution and longevity in a regime of rapid relative sea-level rise.

1.2.2 Hypotheses

Two hypotheses were formulated for this study: 1) anthropogenic shoreline modifications caused the deterioration of West Belle Pass Barrier, and 2) washover from one storm event has the potential to consolidate shallow backbarrier stratigraphy two to three times more than the long-term rate of subsidence of 7.59 ±0.23 mm/yr for Grand Isle, Louisiana (Kolker et al., 2011). Although the time associated with the degree of primary consolidation will not be calculated specifically for this thesis, the author assumes that more than 95% of the primary consolidation of backbarrier facies will be completed within one year.

1.3 Importance

Prior to the construction of artificial levees along the Mississippi River and its distributaries these fluvial systems debouched sediment throughout the mid to late Holocene to create several, aerially expansive deltaic complexes across the north-central Gulf of Mexico

through the process of delta switching (e.g. Fisk, 1944; McIntire, 1954; Kolb and van Lopik, 1958; Frazier, 1967; Roberts, 1997 and many others). Progradation of distributaries leads to the creation of deltaic headlands, the seaward most landforms associated with distributary growth (Penland et al., 1988a). Deltaic headlands and the fluvial transport of distributaries that lead to their creation are ephemeral, and these prograded landmasses are inevitably subjected to net erosion in contrast to distributary activity that results in net deposition. Erosion by marine processes is accentuated by the regionally high rates of relative sea-level rise and, consequently, previously subaerial landmasses are eventually converted to open-water areas. The changing courses of distributary systems means these open-water regions can become reoccupied by distributaries and be the sites of renewed fluvial sedimentation; collectively, the sequence of distributary growth, abandonment, land loss, and reinvigorated distributary progradation is cyclical and has become widely known as the "delta cycle" (Roberts, 1997). Much of Louisiana's wetlands and barrier islands no longer receive sediment and nutrients in sufficient quantities for their maintenance above an increasing sea-level because of artificial leveeing that impedes the natural progress of distributary switching, leaving wetlands adjacent to open-water areas that were recently converted from subaerial landforms exposed to intensified and prolonged wave attack. Eustatic sea-level rise of approximately 2.0 mm year coupled with subsidence and marine reworking has resulted in a net land loss of approximately 4,877 km^2 between 1932 and 2010 (Couvillion et al., 2011).

It is becoming progressively more important to understand all of the processes affecting barrier island longevity, particularly, since major barrier renourishments have been formulated (e.g., 2012 LA Master Plan), completed (e.g., TE-52, TE-23, BA-45, etc.), or commenced (e.g., 2017 LA Master Plan) within the immediate vicinity of the West Belle Pass Barrier Headland

(Fig. 2). From an economical standpoint, hundreds of millions of dollars have been invested in renourishment projects within the immediate vicinity of West Belle Pass Barrier, and $42.2 million was spent on West Belle Pass Barrier alone (TE-52). Understanding the historical evolution of West Belle Pass Barrier and quantifying the primary consolidation settlement of backbarrier deposits is one step to enhance the effectiveness of high-cost barrier-related projects along Louisiana's coastline.

Figure 2. Project Infrastructure. At least eight projects are located within 8 km of West Belle Pass Barrier. The TE-52 project (pink) created 291 acres of land along West Belle Pass Barrier and cost approximately $42.2 million (satellite image from USGS Earth Explorer, 2013 NAIP JPG 2000).

1.4 Description of Study Site

The majority of wetland loss within Lafourche Parish, Louisiana has been attributed to two subsurface processes: 1) consolidation of recently deposited sediment, and 2) active faulting (Kuecher, 1994). Consolidation data of seven facies within the Lafourche and Terrebonne Parishes from Kuecher (1994) show that the three most consolidation-prone facies of the MRDP are peat, prodelta clay, and bay mud facies, respectively. Kuecher (1994) did not sample the lagoonal/bay mud facies located directly behind Louisiana's barriers that are part of the focus of this study.

The study area for this project is the southwest edge of the Caminada-Moreau Headland in Lafourche Parish, which helps protect an interior located, offshore hub known as Port Fourchon. Located near the mouth of Bayou Lafourche, Port Fourchon sustains a multi-billion dollar petroleum industry by acting as a prolific seaport that provides services to approximately 90% of deepwater rigs in the Gulf of Mexico and operates as the host for the Louisiana Offshore Oil Port (LOOP) (Scott, 2008). As a younger deltaic headland in a prime location along the Louisiana coast, the Caminada-Moreau Headland was an ideal site for the development of a major Gulf of Mexico port. Human modification of the Gulf-fronting shore aiding in the stabilization of coastal lands proximal to Port Fourchon and other oil and gas infrastructure appears to have played a significant role in the evolution of the study area, West Belle Pass Barrier (Fig. 1). Necessary shoreline modifications including jetty construction and channel dredging projects have been undertaken to ensure the port's efficacy as a leading port along the Gulf Coast through the 21st century. These projects along with natural processes resulted in the deterioration of the downdrift shore that aided in the protection of valuable petroleum infrastructure and wetlands from storm surge and wave attack.

West Belle Pass Barrier, located approximately 97 km SE of New Orleans and 24 km WSW of Grand Isle (Fig. 1), has a historical (1884-2005) shoreline average rate of change of -25.5 m/yr (Martinez et al., 2009). This barrier system is part of the Lafourche delta complex, which began forming sometime between 2,000 (Frazier, 1967) and 1,490 years BP (Törnqvist et al., 1996). A continued lack of sediment input, relative sea-level rise, and storms cause barrier systems along Louisiana's coastline to progressively lose land area, and well-documented land loss has taken place within historic time frames (Couvillion et al., 2011). Little is known, however, about the sediment budget of barrier coastlines such as West Belle Pass Barrier, and the fate of sediment lost during transgression is not well constrained.

Chapter 2. History and Geologic Framework

2.1 Holocene Evolution of the Mississippi River Delta Plain

The modern-day MRDP is located along the northern boundary of the Gulf of Mexico and is comprised of distinct sedimentary packages that formed due to changes in sea-level, climate, sediment supply, and accommodation space since the Marine Isotope Stage 2 last glacial maximum and deglaciation (11-25 ka) (Blum and Roberts, 2012; and many others). Currently, this delta plain has a subaerial area more than 30,000 km^2 and contains approximately 41% of the U.S. coastal wetlands (Coleman et al., 1998). The modern delta plain was created by the distribution of sediment from distributaries of the Mississippi River to form overlapping delta complexes. Delta complexes are 2nd order deltaic deposits that are comprised of temporally and spatially linked delta lobes (3rd order), subdeltas (4th order), and crevasse splays or overbank splays (5th order) (Roberts, 1997). Delta complexes are active for 1,000 to 2,000 years (Roberts, 1997), and their development within the Mississippi River delta plain is well understood (e.g. Fisk & McFarlan, 1955; Frazier, 1967; Penland et al., 1988b; Roberts, 1997; Kulp et al., 2005a). The names and dates of deltaic complexes used herein were spatially and temporally identified by Frazier (1967) using multiple borings and radiocarbon dating and updated by Törnqvist et al. (1996) and Kulp et al. (2005a). The Mississippi River and its distributaries have contributed to the formation of six delta complexes and sixteen delta lobes between 7-8 ka (Frazier, 1967).

Two factors controlling the location of delta complexes on the Pleistocene continental shelf has been the growth and decay of continental-scale ice sheets along with the location of the Mississippi River. During the late Wisconsinan glacial maximum, sea-level was approximately 120 m lower than it is today, which allowed for the development of shelf-edge deltas (Fairbanks, 1989). From the end of the glacial maximum to the onset of the Holocene, eustatic sea-level rise

flooded shelf-edge deltas and forced the Mississippi River to backstep landward, forming a series of undifferentiated outer-shelf complexes between 7-10 ka. As eustatic sea-level rise began to "stabilize," six, well-documented shelf-phase deltas prograded onto the continental shelf within 7-8 ka (Frazier, 1967) (Fig. 3).

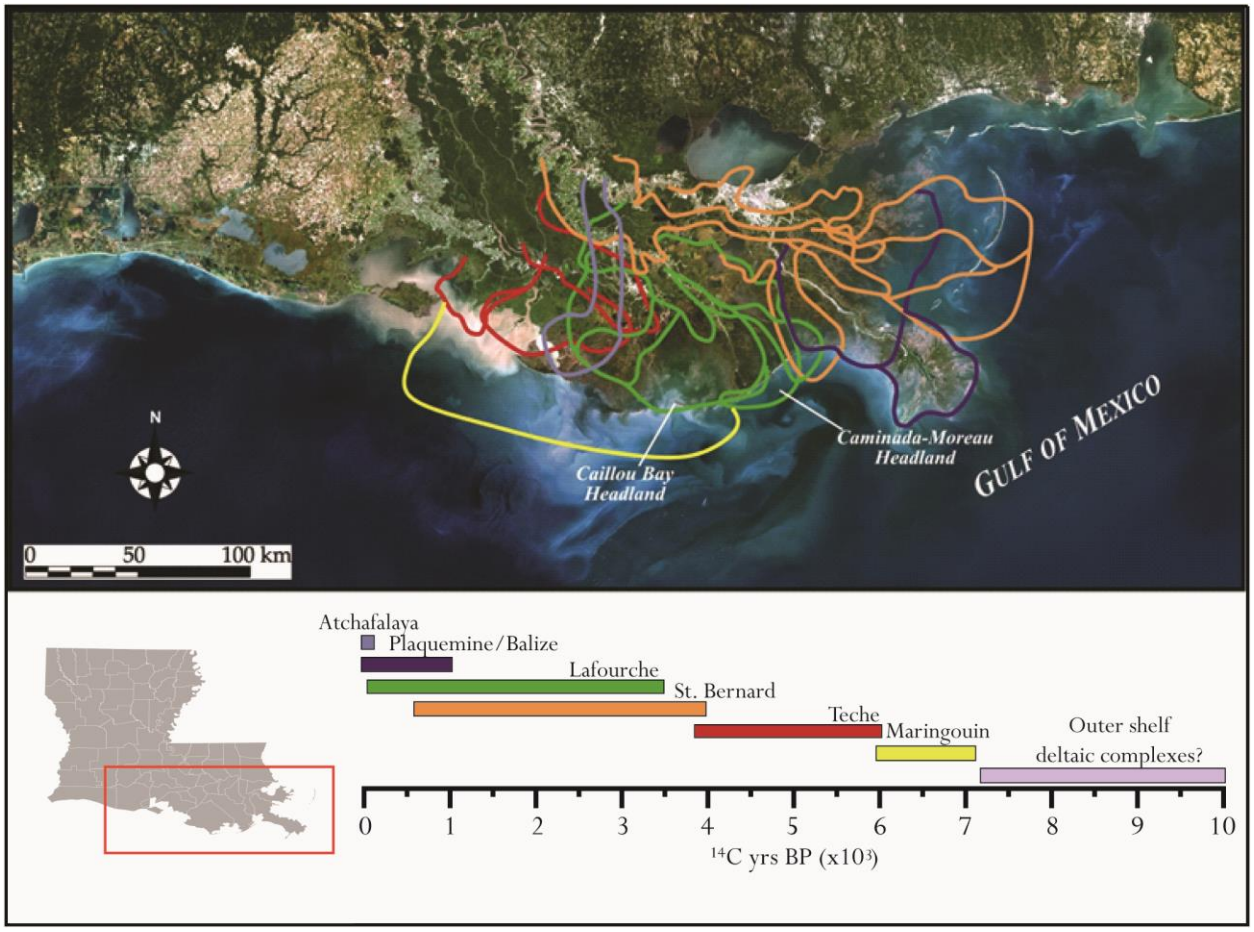

Figure 3. Holocene Mississippi River Delta Complexes. The Mississippi River and its distributaries created six delta complexes within the last 7-8 ka (modified from Kulp et al., 2005a based on data from Frazier, 1967).

The six delta complexes of the MRDP are (oldest to youngest) the Maringouin, Teche, St. Bernard, Lafourche, Plaquemines/Balize, and Atchafalaya. All of the delta complexes, except for the Plaquemines/Balize and Atchafalaya, have been abandoned and are in various stages of degradation. The study area is located within the Lafourche delta complex; therefore, it is

necessary to understand the timing and construction of this complex in order to better understand the formation and processes affecting West Belle Pass Barrier.

2.2 Lafourche Delta Complex

The Lafourche delta complex is located along the south-central portion of the Louisiana coast within Lafourche Parish. Törnqvist et al.'s (1996) chronology of the Lafourche delta complex suggests first sedimentation at approximately 1,491 ± 13 ka. Frazier (1967), however, argued that deposition began 2,000 years earlier at approximately 3,500 ka. Five distinct delta lobes filled an open-water area between the Teche and St. Bernard complexes, the result of which formed the Lafourche delta complex. The bayous that created these delta lobes are Bayou Terrebonne, Bayou Blue, Bayou Black, and Bayou Lafourche (Frazier, 1967). Bayou Lafourche produced the fifth and final delta lobe of the Lafourche delta complex and remained active until approximately 300 years before present (Frazier, 1967). Erosion of the complex resulted in the formation of the modern Caminada-Moreau headland, which is of particular importance to the study area since West Belle Pass Barrier is located on the western flank of the headland.

2.2.1 The Caminada-Moreau Headland

The Caminada-Moreau Headland is unique in that it is the location of a longshore sediment divergence due mainly to a dominant wave approach from the southeast and a convex shoreline (Penland et al., 1986). This longshore sediment separation resulted in the formation of barrier islands such as Grand Isle to the east and the Timbalier Islands to the west as described in the Penland et al. (1988a) model for barrier development (see fig. 1). The headland contains a series of sandy beach ridges that formed during headland progradation (Kulp et al., 2005b), and presumably supply sediment to the region by longshore transportation during transgression.

2.2.2 West Belle Pass Barrier

According to the Penland et al. (1988a) model of headland evolution, West Belle Pass Barrier is a Stage 1 barrier spit that flanks the west side of the Caminada-Moreau Headland (Fig. 4). This barrier environment provides a unique opportunity to observe and document a barrier spit's response to changes in sediment supply in an early stage of development.

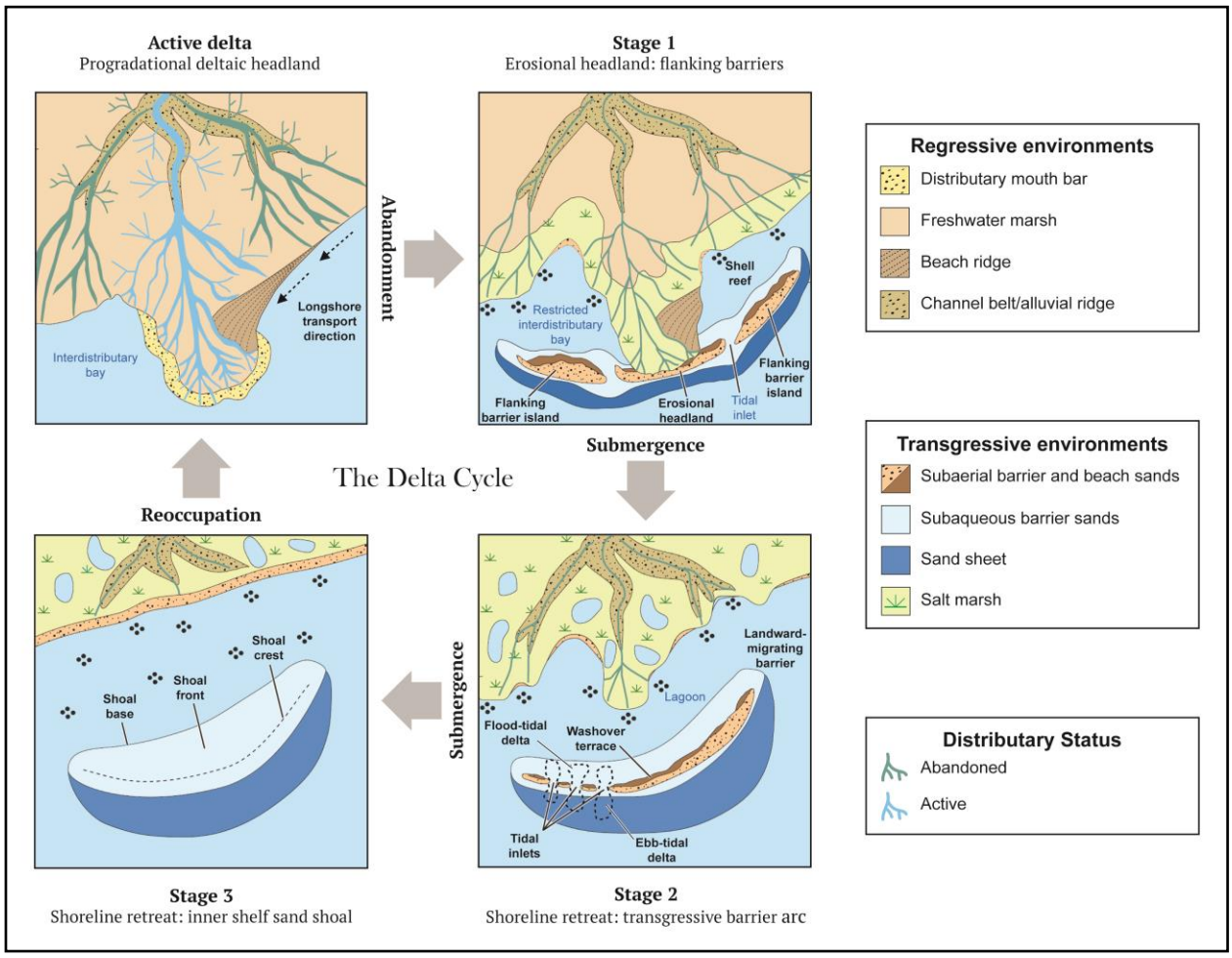

Figure 4. The Delta Cycle Model. Penland et al.'s (1988a) model of deltaic headland evolution illustrates the morphological changes and sediment distribution patterns of headlands as they are abandoned, subjected to marine processes and subsidence, and reoccupied (created by Penland et al., 1988a and modified from Blum and Roberts, 2012).

Reduced flow from the Mississippi River began around 1 ka when abandonment of Bayou Lafourche began and flow was diverted to the Plaquemines/Balize system. Bayou Lafourche was completely separated from the Mississippi River in 1904, when a dam

constructed at Donaldsonville, Louisiana, deprived Bayou Lafourche of freshwater input and lead to the introduction of saline waters 61 km upstream to the Intracoastal Canal (Winehurst, 1974; Mossa et al., 1985). It was not until the 1950's that water from the Mississippi River would find its way back into Bayou Lafourche through a pumping system (Dantin et al., 1978). Fundamentally, Bayou Lafourche is an abandoned Mississippi River distributary starved of fresh water and sediment input and is influenced more by tides than fluvial processes (Dantin et al., 1978).

The introduction of a jetty updrift of West Belle Pass Barrier in 1935 and subsequent modifications throughout the 1960's possibly disrupted and altered sediment transport patterns from the sediment divergence point to the east. Furthermore, rock revetments were installed in 1964 on East Timbalier Island in order to protect valuable petroleum infrastructure. The goal of these revetments was to keep sediment in place and contained on the bay side of the rocks in hopes of protecting oil and gas infrastructure in Timbalier Bay. Lastly, coastal engineers approved the design and construction of the TE-52 West Belle Pass Barrier Headland Restoration project in 2006, and it was completed in 2012. Approximately 2.1 million m^3 of dredged sand was used to create 3,000 m of beach and dune habitat. Since the completion of the TE-52 renourishment project, the barrier is 2.9 km long and 0.6 km wide as of 2013.

Chapter 3. Geomorphic Evolution

3.1 Methodology

3.1.1 Database Development

This study examined the shallow stratigraphic framework and historical evolution of West Belle Pass Barrier by combining a database spanning 130 years of data along with newly acquired vibracores, push-cores, and grab samples. In addition to the sedimentary database, bathymetric surveys, historical shorelines, and satellite and aerial imagery were used to interpret sediment distribution patterns through time and across space from East Timbalier Island to West Belle Pass Barrier. Using ESRI's *ArcMap 10.1*, a database combining 72 vibracores, 7 push-cores, and 61 grab samples was constructed for the study area.

3.1.2 Sampling Techniques

A. Vibracores

In addition to vibracores previously collected by the Louisiana Geological Survey, Coastal Protection and Restoration Authority, and the University of New Orleans, six additional vibracores were collected in the summer of 2014. These cores were taken within the adjacent backbarrier environment West Belle Pass Barrier between the island and Devil's Point to the north (Fig. 5). Vibracore locations were selected in backbarrier areas that lacked historic core data. This study did not focus specifically on seismic acquisition or interpretation, but vibracores were examined in the context of previously interpreted high-resolution seismic data collected in 2002 (Kulp et al., 2002).

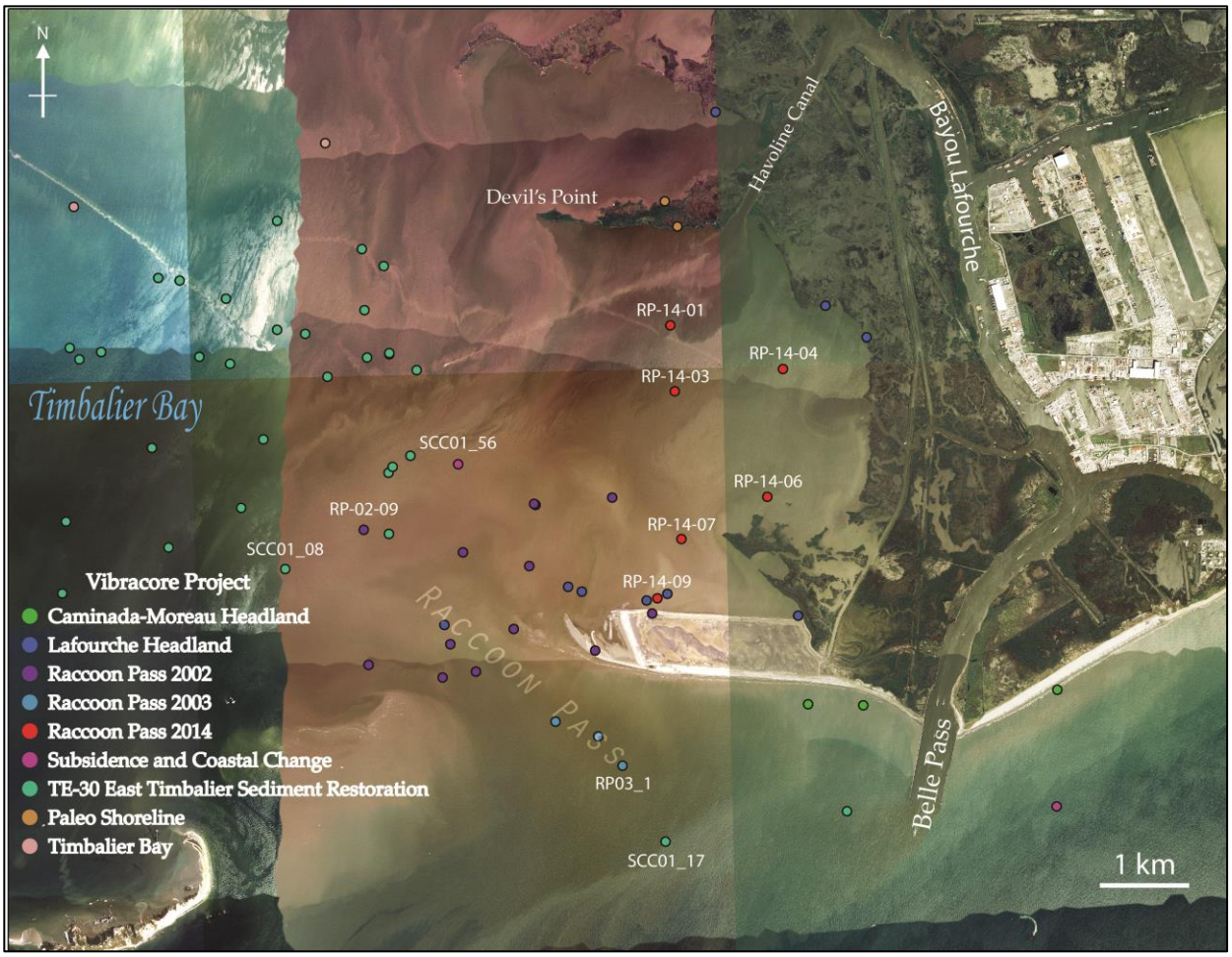

Figure 5. Vibracore Locations. Location of vibracores within the immediate vicinity of Raccoon Pass categorized by project name. The cores in red were collected in the summer of 2014 specifically for this study. Core names are displayed for the ones used in creating stratigraphic lines of section (satellite image from USGS Earth Explorer, 2013 NAIP JPG 2000).

Vibracores were obtained on the *R/V Greenhead* vessel using a STOW Model G550H vibrator and a 5.5 hp gasoline-powered motor (Fig. 6). The vibracore setup is coupled with a 6.1 m-long, 76.2 mm diameter aluminum pipe with a 1.27 mm wall thickness. The aluminum tubing is hoisted in to the air using a portable tripod. Vibracore pipes are lowered through the water column and penetrate the subsurface due to the weight and vibrating motion of the vibracoring equipment. Vibracoring continues until refusal or the sampling limit of the equipment is reached. Water depth and depth-to-sediment measurements were recorded. These measurements combined with the maximum depth of penetration provide a measure of compaction undergone

by the section within the tube. The aluminum tubing is capped, plugged, and sealed before being hoisted out of the water. Vibracores were transported to a sediment analysis laboratory. Each vibracore was cut into halves and visually analyzed to document the sedimentary structure, lithofacies, and textural characteristics. Cores were photographed and archived in U.N.O.'s database. Multiple, high-resolution images covering 0.9-1.2 m sections of each core were mosaicked to create a single, composite photograph of the core.

Figure 6. Vibracore Setup. A tripod-mounted vibracoring rig was used to collect cores within the backbarrier environment of West Belle Pass Barrier.

B. Grab Samples

Grab sample data was obtained in 2008 as a collaborative research effort by the University of New Orleans as part of the Louisiana Barrier Island Comprehensive Monitoring (BICM) study. The majority of these samples are located on the gulfside of West Belle Pass Barrier; therefore, new samples within the backbarrier were acquired during the summer of 2014.

A total of 17 grab samples were collected using a Petit Ponnar along a transect starting in the northeast corner of Timbalier Bay approximately 2 km from the Havoline Canal that trends south-southwest for approximately 3.8 km into Raccoon Pass (Fig. 7). Slowly lowering the Petit Ponnar into the water column allows for the open clam-shaped device to impact surficial bay-floor sediments. A quick pull on the line releases a safety pin, closing the device and retaining sediment. Grab samples were hoisted back to the surface, packaged, and labeled for transport. After arriving at UNO's CRL, samples were dried and sieved through ASTM No. 45, 60, 80, 120, 170, and 230 sieves according to ASTM D422 standard procedures to determine grain size distribution. Hydrometer analyses were subsequently performed on samples containing greater than 50 g of silt/clay. Grain size analyses of all core tops (upper 5 cm) and all grab samples were compiled and classified using USGS's SedPlot program (Poppe et al., 2008) based on Shepard's (1954) classification method. Results were used to classify water-bottom surficial sediments in to their respective categories.

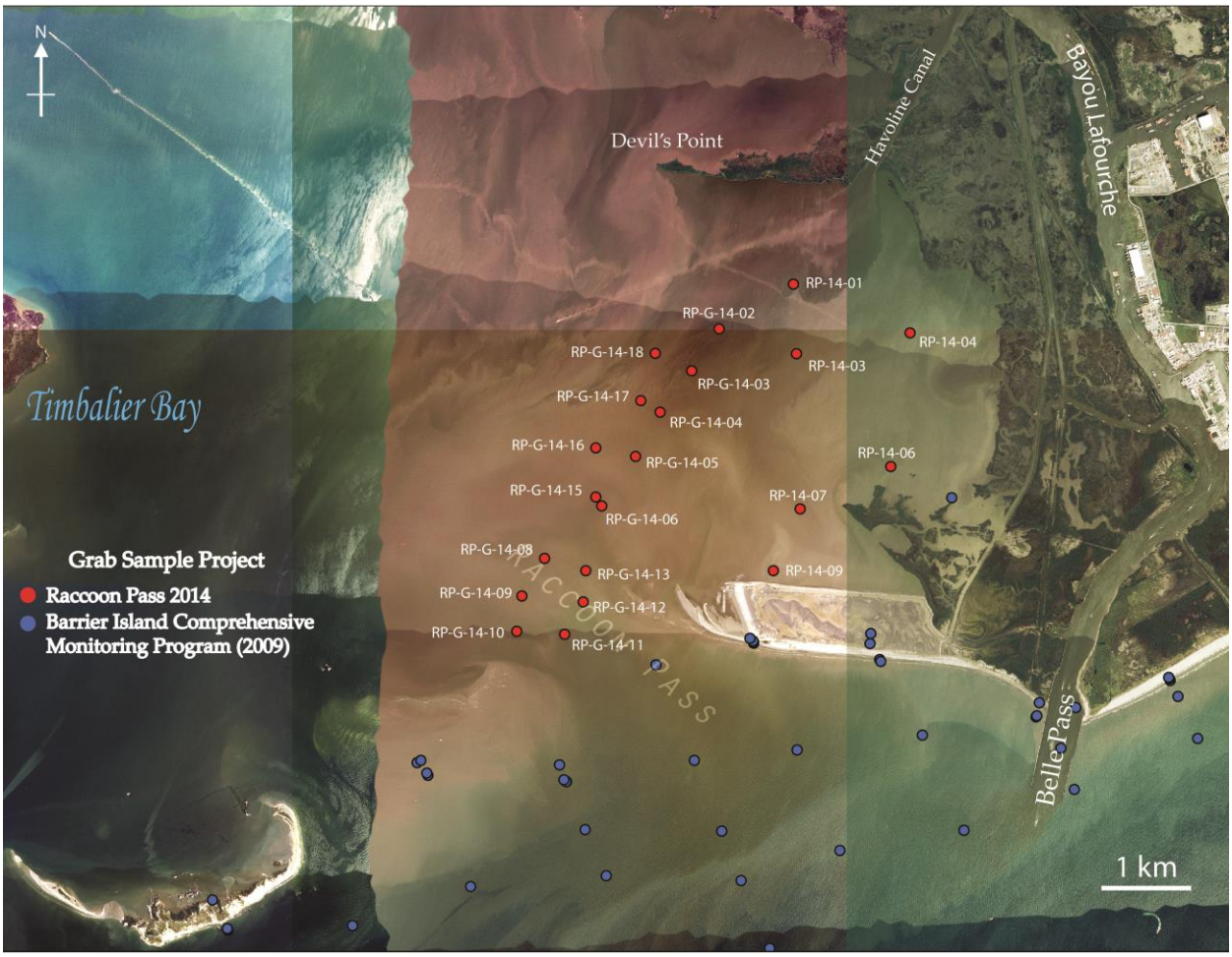

Figure 7. Grab Sample Locations. Location of grab samples within the vicinity of Raccoon Pass categorized by project name. Grab samples in red were taken during the summer of 2014. The blue samples were acquired in 2008 as part of Louisiana's Barrier Island Comprehensive Monitoring Program in 2009 (satellite image from USGS Earth Explorer, 2013 NAIP JPG 2000).

3.1.3 Shoreline Digitization

Shoreline data of the Lafourche region is available through the Barrier Island Comprehensive Monitoring Program: Shoreline Changes and Barrier Island Loss 1800s-2005 (Martinez et al., 2009). Digitized shorelines from 1884, 1933, 1996, 2004, and 2005 are readily available and were added to the database. In order to record shoreline migration patterns at adequate intervals between 1933 and 1996, maps of the study area for the years of 1956, 1978, and 1988 were scanned from the USGS Atlas of Shoreline Changes in Louisiana from 1853 to 1989 (McBride et al., 1992) and added to the database. Maps were georeferenced and plotted in

ArcMap 10.1. Once referenced, shorelines were digitized with polylines to represent the parameter of subaerial portions surrounding East Timbalier, West Belle Pass Barrier, and the Caminada-Moreau Headland. These shorelines are useful for developing a historical model of shoreline evolution when combined with shoreline modifications and storms impacts.

3.1.4 Imagery

A. Satellite Imagery

Satellite imagery used in this study is from Landsat 8. Specifically, the imagery was captured by the Operational Land Imager (OLI) sensor, which has a band resolution ranging from 15 to 30 m. All satellite imagery was acquired from USGS using the LandsatLook Viewer database.

B. Aerial Imagery

Aerial imagery used in this study is a combination of the National Agriculture Imagery Program (NAIP) JPEG2000, High Resolution Orthoimagery (HRO), and Digital Orthophoto Quadrangles (DOQs) acquired from the USGS's Earth Explorer database. These images aided in interpreting the recent evolution of West Belle Pass Barrier from 1989 – 2013.

3.2 Results

3.2.1 Historical Shorelines

Eight shorelines between 1884 and 2005 were digitized and plotted in *ArcMap 10.1*. Shorelines from the Barrier Island Comprehensive Monitoring Program (Martinez et al., 2009) and USGS Atlas of Shoreline Changes in Louisiana from 1853 to 1989 (McBride et al., 1992) between Timbalier Island and Fourchon Beach were acquired for the years 1884, 1933, 1956, 1978, 1988, 1996, 2004, and 2005 (Figures 8-15). Shorelines were determined using the high-water line on the basis of the wet and dry-beach contact and/or debris line. The Barrier Island Comprehensive Monitoring Program calculated the rate of change for four time periods: historical (1884-2005), long term (1904-2005), short term (1996-2005), and near term (2004-2005). Table 1 shows the results of the time-averaged rate of shoreline change for the respective time periods for West Belle Pass Barrier (Martinez et al., 2009). These rates are useful for evaluating morphological changes and their possible causes. Every map contains a list of significant events that may have led to the morphology of the corresponding year. The locations of the events are drawn on the appropriate figure when possible (labeled by number). The list of events is not complete, specifically with regard to storms. Criteria for choosing storms focused on the year of landfall, landfall location, and storm intensity. The 1884 shoreline is the earliest shoreline dataset available and serves as the baseline for shoreline comparison and does not contain a list of significant events.

Table 1. West Belle Pass Shoreline Change Rates. Time-averaged rates of shoreline change for West Belle Pass Barrier. These rates provided a quantitative analysis of shoreline change for different time periods (from Martinez et al., 2009).

Dates	Average Rate of Change (m/yr)
Historical (1884-2005)	-25.5
Long Term (1933-2005)	-10.9
Short Term (1996-2005)	-17.8
Near Term (2004-2005)	-41.5

Shoreline datasets are separated into two distinct groups on the basis of magnitude of morphological change and shoreline modification proximal to the West Belle Pass Barrier. Epoch 1 (1884 – 1956) depicts a barrier system that, even with natural and anthropogenic influences, maintains a much larger subaerial portion of land when compared to the area of the island anytime between 1978 and pre-restoration morphology. During Epoch 1 a few shoreline modifications and one upstream control on Bayou Lafourche are undertaken. Epoch 2 (1976 – 2005), however, is dominated by shoreline transgression and contains several shoreline projects that influenced the morphological response of the barrier. It is worth noting that morphological changes and interpretations were composed on the basis of comparing the map in question against the previous shoreline dataset.

Epoch 1

A. 1884

The 1884 shoreline is the oldest shoreline dataset available for the study area and is used as the starting point for evaluation (Figure 8). In 1884 a tidal inlet that is approximately 2 km wide separated West Belle Pass Barrier and East Timbalier Island. On the basis of the location of this inlet and modern day morphology, the inlet on the 1884 map is most likely Raccoon Pass. Although not completely visible in figure 8, the 1884 map shows three outlets to the Gulf of

Mexico stemming from Bayou Lafourche: Belle Pass, Pass Fourchon, and Bayou Moreau. The latter two passes are located just east of the area shown in Figure 8.

B. 1933

The 1933 shoreline represents the first shoreline which morphological comparisons can be made (Figure 9). Significant events leading up to the 1933 morphology include both natural and anthropogenic influences. In 1904 Bayou Lafourche was separated from the Mississippi River at Donaldsonville, Louisiana, minimizing freshwater input, along with any sediment sourced outside of the Bayou Lafourche channel network (i.e., negligible Mississippi River sediment input). In 1915 an unnamed category 3 hurricane made direct landfall on East Timbalier Island. East Timbalier Island and West Belle Pass Barrier had a net loss of subaerial land from 1884 to 1933, along with widening of Raccoon Pass. Furthermore, all but one of Bayou Lafourche's passes is closed to the Gulf by 1933. The damming in 1904 reduced the flow of water reaching the passes, which lead to the partial closure of Belle Pass and full closure of Pass Fourchon and Bayou Moreau (Dantin et al., 1978). Dantin et al. (1978) showed that the shoreline just east of Belle Pass receded 1,128 m from 1885 to 1932 at an average rate of 24 m/yr. However, Dantin et al. (1978) argue that if the damming of Bayou Lafourche in 1904 represents the time of sediment deprivation then the rate of shoreline change becomes even more drastic at 41 m/yr (1904-1932).

C. 1956

The 1956 dataset depicts a rather dramatic change in the morphology of East Timbalier Island and West Belle Pass Barrier compared to the 1933 shoreline (Figure 10). In 1935 Belle Pass jetty construction began at the mouth of Bayou Lafourche. Two tropical storms impacted the study site approximately 3.7 km to the east of Belle Pass in 1936 and 1939. By 1940 the

installation of the jetties at Belle Pass was complete, leaving stone jetties 152 m long and 61 m apart at the entrance of Belle Pass (Dantin et al., 2978). Five years later, the jetties were extended 90 m shoreward along with a groin east of the jetty system in 1950 (Mossa et al., 1985). The new jetty extensions were 122 m apart and attached to the older jetty sections through transitional sections (Dantin et al., 1978). Nonetheless, the entire flanking barrier system is nearly continuous at this time with less than 0.4 km of water between East Timbalier Island and West Belle Pass Barrier. Even with the installation and modification of the jetties, both barrier systems had a net increase of subaerial acreage from 1933 to 1956. After the 1956 dataset, the distance between East Timbalier Island and West Belle Pass Barrier only increases.

Epoch 2

D. 1978

From 1978 through 2005 the shoreline orientation changed within the area of West Belle Pass Barrier and East Timbalier Island. Between 1956 and 1978 the West Belle Pass region underwent a tremendous amount of shoreline modification, marking this dataset as the beginning of Epoch 2 (Figure 11). A total of six significant events occurred between 1958 and 1969. In 1958 Belle Pass at the mouth of Bayou Lafourche was dredged and widened to a bottom width of 30 m and a depth of 3.7 m (Dantin et al., 1978). In 1963 only the west jetty was relocated to make the distance between jetties 98 m. In the same year Bayou Lafourche was widened again, making the channel 38 m wide and 3.7 m deep (Dantin et al., 1978). During this widening the channel was moved west of the already in-place west jetty. The previous channel contained by the jetties was plugged, and there was essentially no west jetty as the old west jetty acted as the "new" east jetty.

Two major hurricanes impacted the region before 1978. Hurricane Betsy made landfall in 1965 as a category 4 storm less than 9.2 km east of Belle Pass. The second storm, Hurricane Carmen, made landfall in 1974 as a category 4 storm just west of the Isles Dernieres 101 km west of Belle Pass. Sometime prior to 1978, Raccoon Pass established itself as the main tidal inlet separating East Timbalier from the Caminada-Moreau Headland. The shoreline no longer continued to translate landward in a continuous, linear fashion. Rather, signs of slight clockwise rotation begin to emerge on west side of West Belle Pass Barrier.

E. 1988

The events prior to the 1988 shoreline configuration are generally quiet in terms of modification and storm impact (Figure 12). The only notable modification occurs on East Timbalier Island, where T-groins were installed on the island to limit the movement of sediment (Mossa et al., 1985), and limit the magnitude of island thinning indicated by the 1978 dataset. Despite these mitigation efforts East Timbalier continued to thin at its center during this time. At West Belle Pass Barrier, continued shoreline rotation took place along with net widening of Raccoon Pass leading up to 1988.

F. 1996

From 1996 to 2005 only the gulf-side shoreline data is available and estimates of subaerial barrier acreage cannot be accurately determined on shoreline data alone. Although changes in land area are inferred by the location and direction of movement of available shoreline data, satellite imagery was used to aid in the interpretation. Before the shoreline dataset was captured, Hurricane Andrew made landfall less than 74 km west of Belle Pass as a category 4 hurricane.

By 1996 the clockwise rotation seen in previous datasets is masked by a well-pronounced spit, suggesting that sediment supply was adequate enough for the spit to prograde westward into Raccoon Pass (Figure 13). Furthermore, a section of East Timbalier Island detached from the main island and was situated between East Timbalier and Raccoon Pass. For simplicity, this island will be referred to as remnant East Timbalier. Interestingly, the orientation of East Timbalier proper and the separated section compared to West Belle Pass Barrier were not the same. Both sections of East Timbalier Island had a shoreline strike of northeast to southwest, whereas West Belle Pass Barrier had a shoreline strike of east to west.

G. 2004

The 2004 shoreline dataset has the imprint of three important events that had the potential to alter the barrier morphology (Figure 14). Captured in the 2004 image is an indication that the West Belle Pass Barrier was transgressing landward and concomitantly eastward through the clockwise translation. By 2004 the length of the West Belle Pass Barrier shoreline is approximately half of the 1996 length, and Raccoon Pass appears to have widened additionally since 1996.

Two coastal mitigation projects were completed within the study are between 1998 and 2000. TE-23 and TE-25 projects resulted in an array of coastal modifications including marsh creation, shoreline protection structures, and channel dredging. The outlines of these projects are shown on figure 14, as well as the direct path of Tropical Storm Isidore's in 2002 through the study site, which directly impacted the longevity and shoreline protection efforts of 1998 and 2000.

H. 2005

Imagery reveals that by 2005 East Timbalier proper and West Belle Pass Barrier were separated by approximately 6.4 km. The 2005 shoreline shows signs of significant erosion and the addition of sediment to maintain a subaerial status, particularly for the remnant island of East Timbalier and West Belle Pass Barrier (Figure 15). Two major storm impacts to the area occurred prior to the 2005 morphology. Hurricanes Cindy (category 1) and Hurricane Katrina (category 3) made landfall less than 18.5 and 74 km east of Belle Pass, respectively. The result of these impacts and preceding shoreline morphology prompted legislators to approve the TE-52 project in 2006.

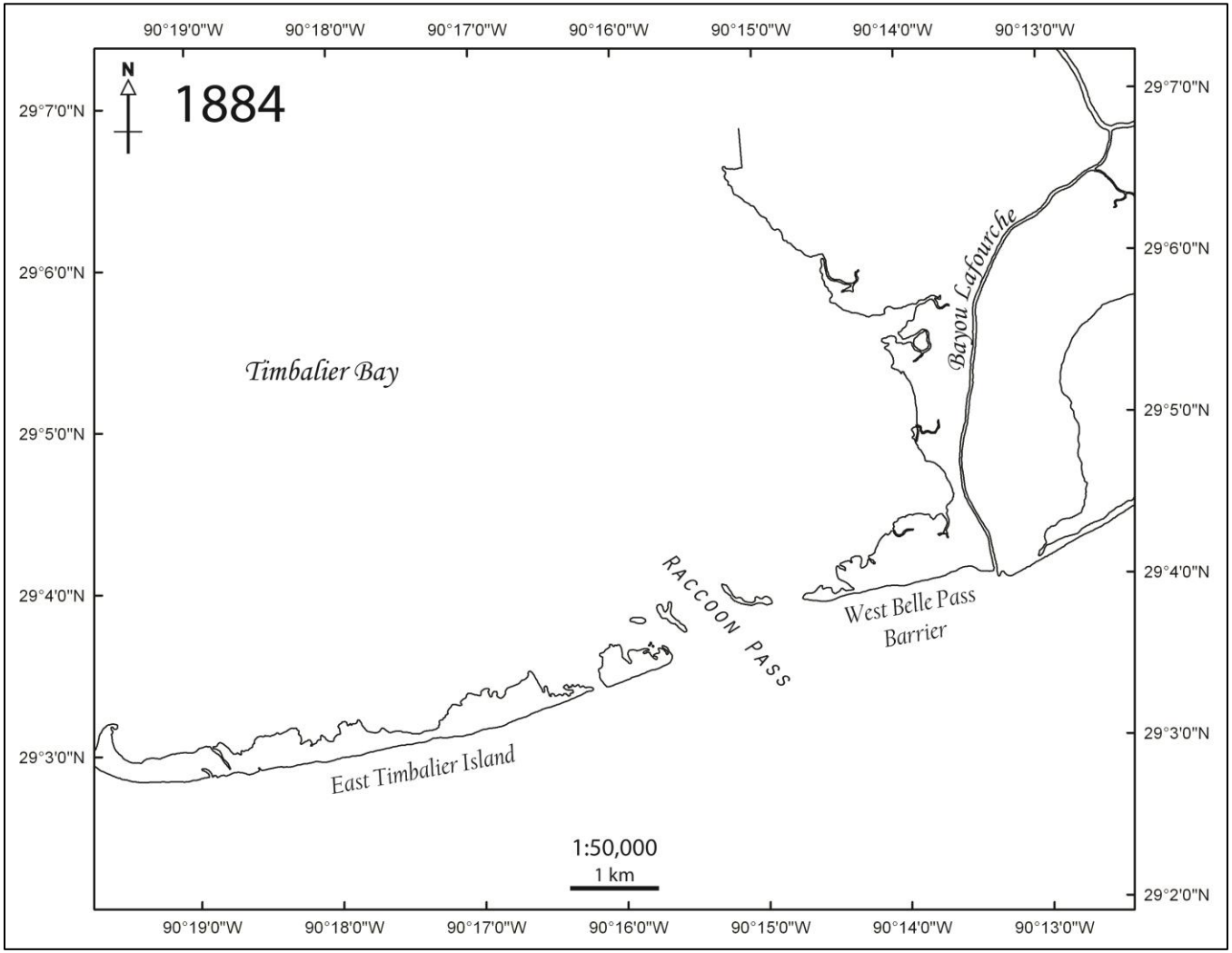

Figure 8. 1884 Shoreline. 1884 map of the study area showing the barrier system immediately west of the Caminada-Moreau Headland (shoreline from Martinez et al., 2009). East Timablier Island and West Belle Pass are separated by Raccoon Pass, and both islands had a very similar shoreline strike orientation. This is the earlierst map of the study area and represents the basis for morphological comparison.

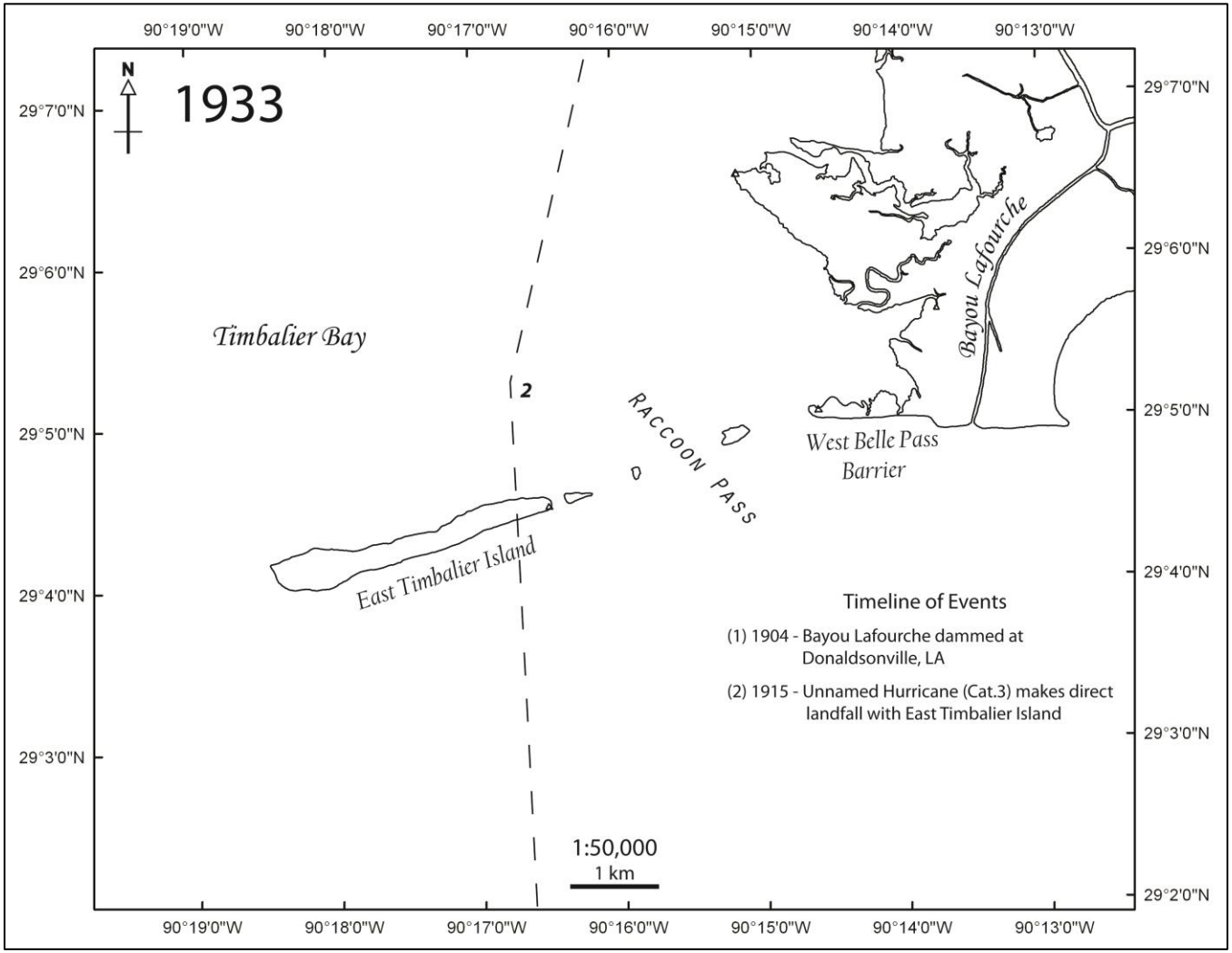

Figure 9. 1933 Shoreline. 1933 map of the barrier system immediately west of the Caminada-Moreau Headland (shoreline from Martinez et al., 2009). Note that in comparison to the 1884 map (Fig. 8) there has been a northward translation of the entire barrier system, a reduction in the footprint of East Timbalier Island, an increased width of Raccoon Pass and reduction in the area of West Belle Pass Barrier. There also appears to be clockwise rotation of the West Belle Pass Barrier relative to the 1884 map.

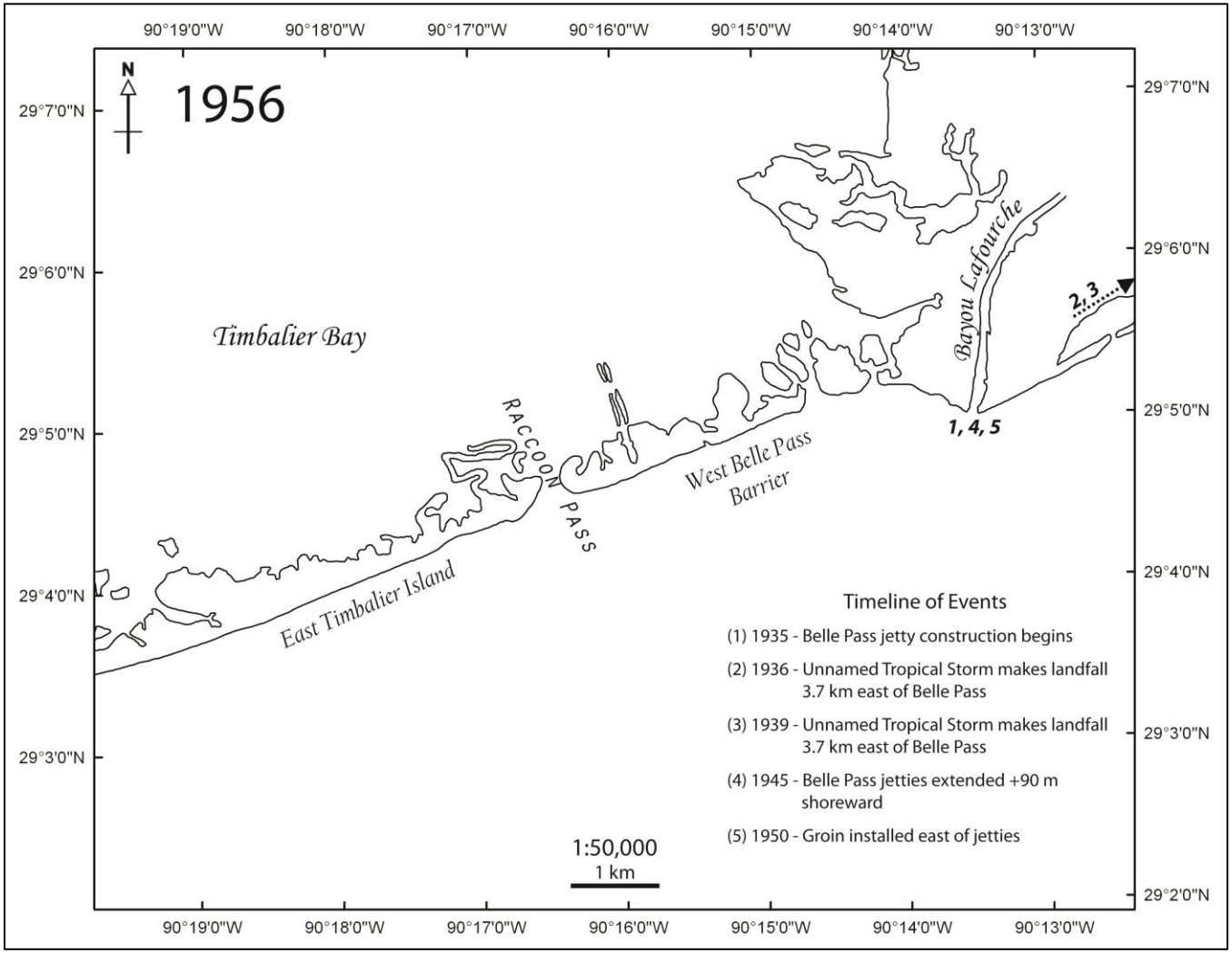

Figure 10. 1956 Shoreline. 1956 USGS-georeferenced map of the barrier system immediately west of the Caminada-Moreau Headland (shoreline from McBride et al., 1992). Note that in comparison to the 1933 map both East Timbalier Island and West Belle Pass Barrier have an increased aerial extent, the width of Raccoon Pass has been reduced, and the shoreline immediately east of Belle Pass continued to rotate clockwise.

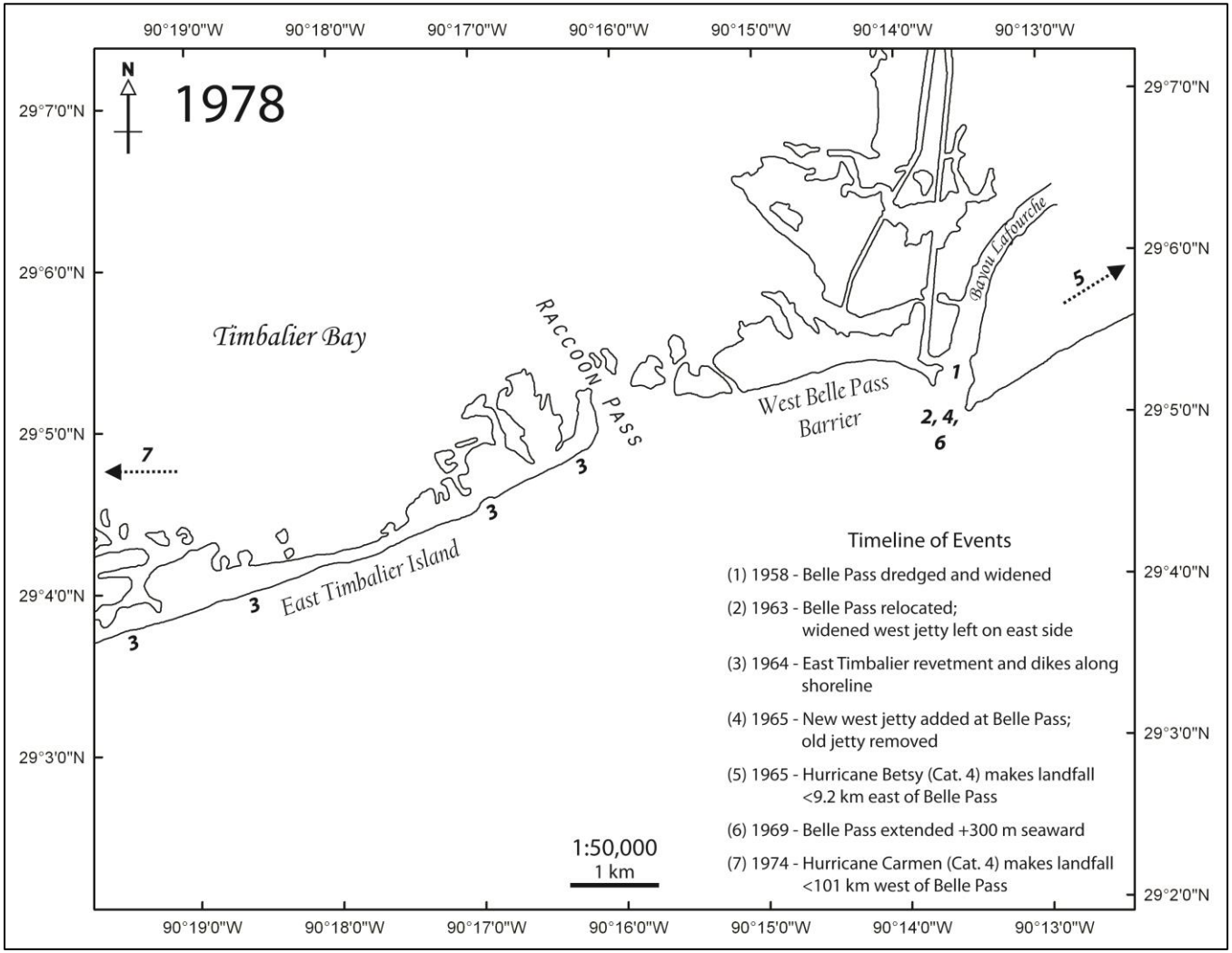

Figure 11. 1978 Shoreline. The USGS georeferenced 1978 shoreline map of the barrier system immediately west of the Caminada-Moreau Headland (shoreline from McBride et al., 1992). East Timbalier appeared to undergo thinning at its center, and West Belle Pass Barrier continued to translate east evidenced by the widening of Raccoon Pass.

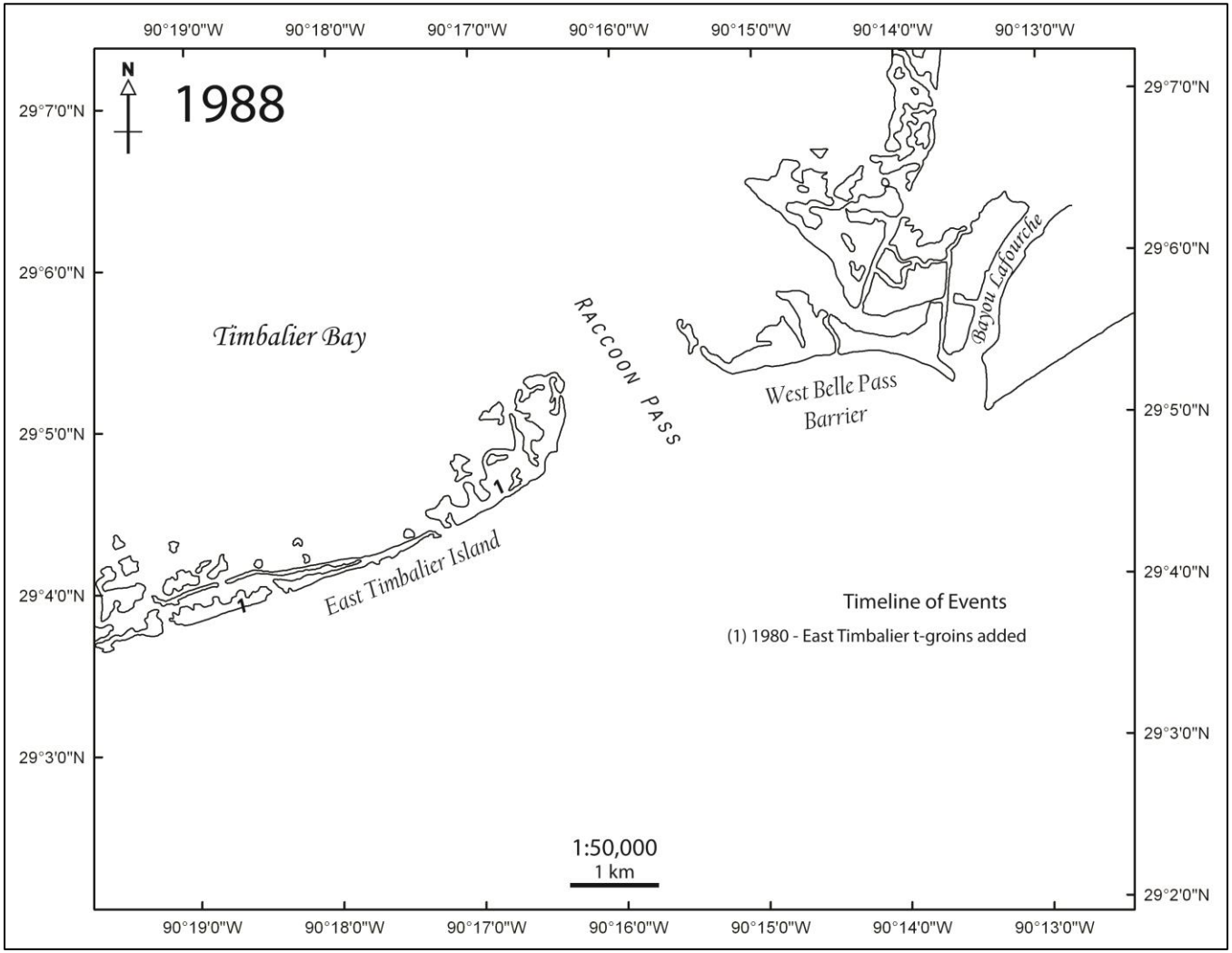

Figure 12. 1988 Shoreline. The USGS georeferenced 1988 shoreline map of the barrier system immediately west of the Caminada-Moreau Headland (shoreline from McBride et al., 1992). This map shows the East Timbalier Island at its thinnest point before it separated in to two distinct islands. Raccoon Pass continued to widen and forced West Belle Pass to translate northward and eastward.

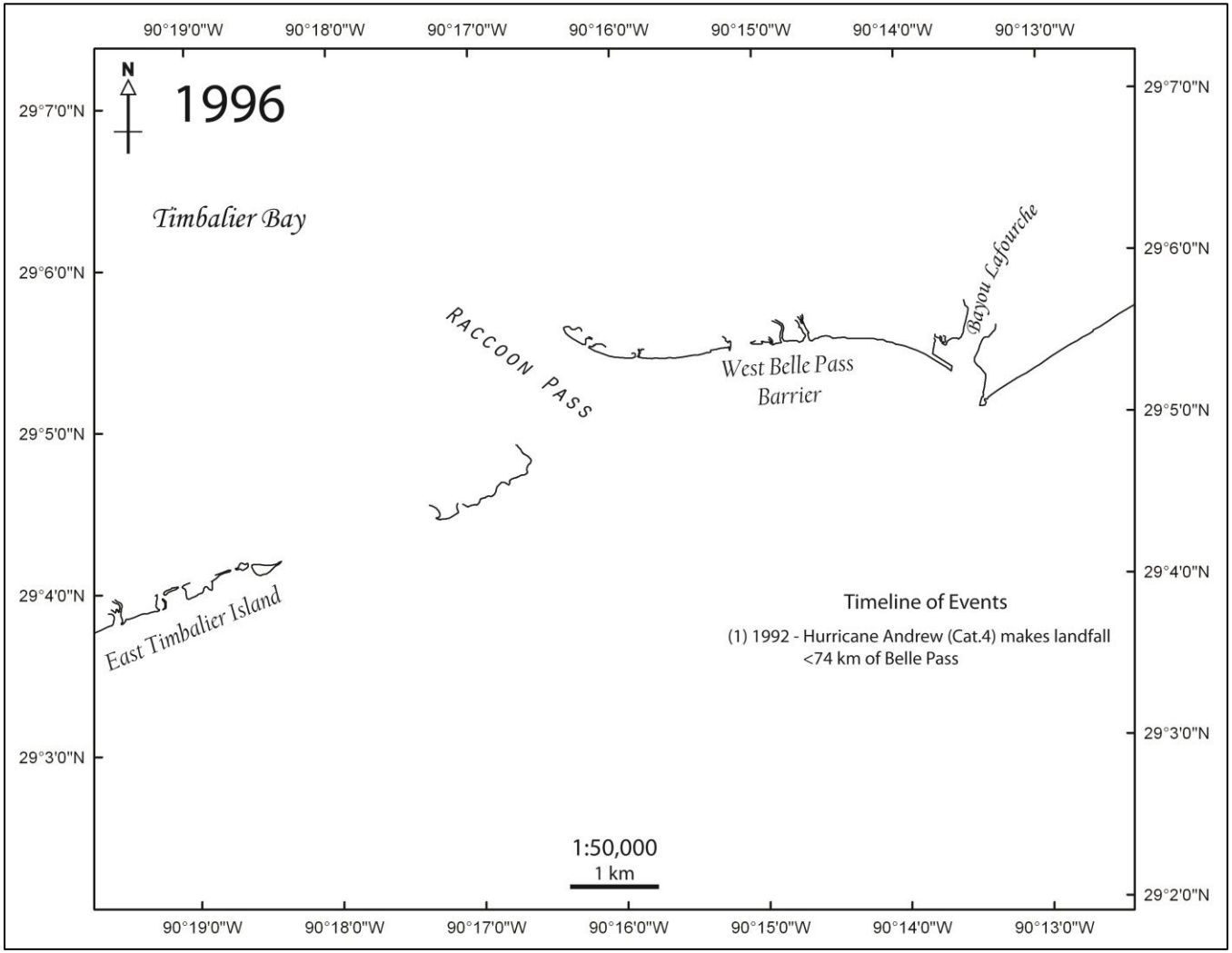

Figure 13. 1996 Shoreline. The BICM program 1884 shoreline map of the barrier system immediately west of the Caminada-Moreau Headland (shoreline data from Martinez et al., 2009). By 1996 East Timbalier Island was completed separated in two islands. Raccoon Pass appeared to shift 5-10° to the west. This shift potentially allowed for the extentioning of the spit seen on the west side of West Belle Pass Barrier.

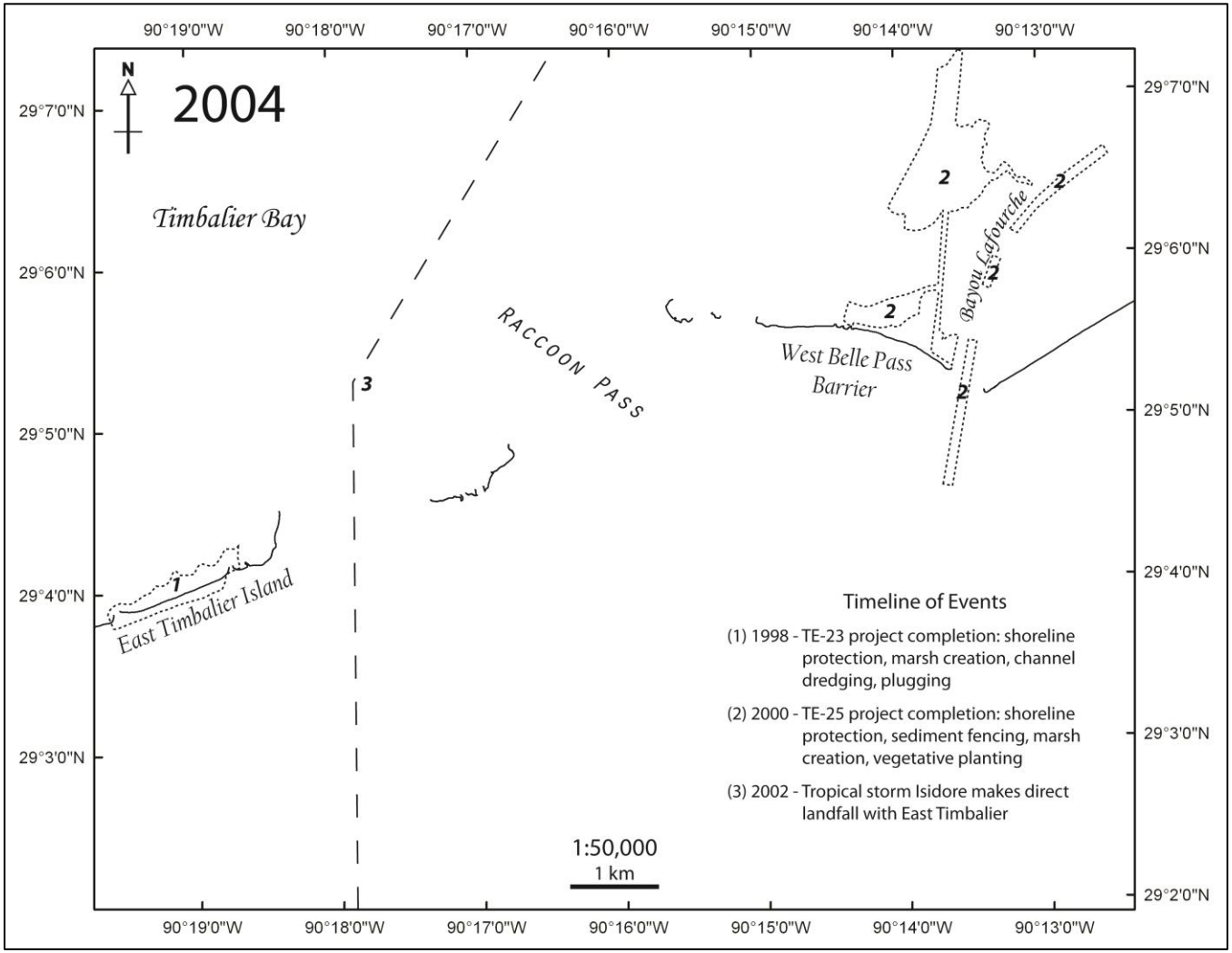

Figure 14. 2004 Shoreline. The USGS georeferenced 2004 shoreline map of the barrier system immediately west of the Caminada-Moreau Headland (shoreline data from Williams et al., 1992). In 2004 West Belle Pass Barrier is approximately half as long as the 1996 shoreline. Multiple renourishment projects were completed in the area to help protect valuable wetlands and infrastructure.

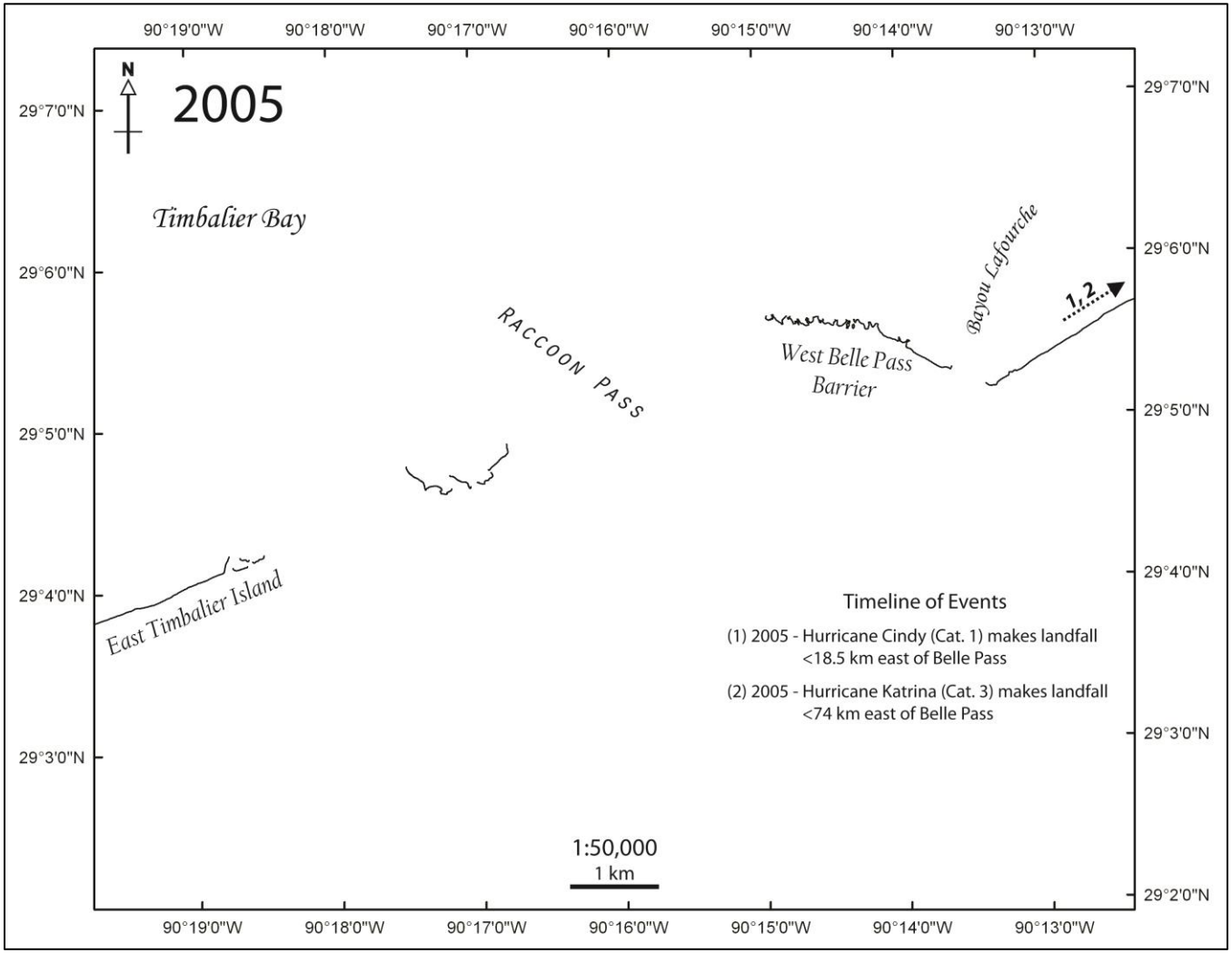

Figure 15. 2005 Shoreline. The BICM program 2005 shoreline map of the barrier system immediately west of the Caminada-Moreau Headland (shoreline data from Martinez et al., 2009). By 2005 both East Timbalier Island and West Belle Pass Barrier continued to lose shoreline. Raccoon Pass nearly tripled its width since 1884.

3.2.2 Recent Imagery

Numerous satellite images and aerial photographs between the 1980's and 2013 are available from the USGS. Eight images corresponding to eight timeframes were acquired from USGS Earth Explorer in order to document morphologic change on the west side of the Caminada-Moreau Headland, primarily focusing on West Belle Pass Barrier and the eastern portion of East Timbalier Island within the last 30 years (Figures 16-17). Although there is some temporal overlap between the shoreline maps and imagery, the same events and morphologies are discussed in further detail.

A. November 1989 DOQ

The 1989 DOQ image shows West Belle Pass Barrier separated from East Timbalier Island by a well-developed tidal inlet (Raccoon Pass) and its associated flood-tidal delta. West Belle Pass Barrier was approximately 3.1 km long from the end of the recurved spits (where it was cut by an overwash channel) to the west jetty rocks at Belle Pass. There appeared to be one main tidal channel with two smaller channels branching away. Three or four recurved spits were present on the west end of West Belle Pass Barrier. All of these spits were cut by overwash channels. Spits on both sides of Raccoon Pass indicated the dominant sediment transportation pathways, as well as the formation of the flood tidal delta located within Timbalier Bay. This is the earliest image in which hard structures such as rock revetments were visible on the gulf side of East Timbalier Island. Furthermore, it is the only image that clearly showed the extent of the tidal channels associated with Raccoon Pass.

B. February 1998 DOQ

In 1998 a 1.3 km-long section of East Timbalier separated from the main island (Figure 16), which remains in the same location until it is completely submerged in 2013. This is the

first image in which separation is visible between the gulf-side rocks and remnant East Timbalier. West Belle Pass Barrier thinned and elongated towards the west, forming a well-developed spit. At this time it was approximately 4.5 km from the end of the spit to the west jetty rocks at Belle Pass. Approximately 1.6 km east of the spit, West Belle Pass Barrier was breached, allowing for the temporary transportation of sediment from the shoreface to the backbarrier. Raccoon Pass trended approximately northwest to southeast with a slight bend towards the north in the most northern reaches of the inlet. The various tidal channels were not as visible as in the 1989 image; however, the main channel was noticeable enough to infer the direction of transportation through the inlet. Erosion of West Belle Pass Barrier prompted state organizations to pass the TE-23 restoration project in 1992, and it was completed later in 1998.

C. January 2004 DOQ

A 2004 DOQ shows drastic changes to the morphology of West Belle Pass Barrier, as well as the location and orientation of Raccoon Pass. In 2004 the subaerial portion of West Belle Pass Barrier decreased in size relative to the 1998 image. In 2004 West Belle Pass Barrier was only 2.4 km long from the west end of the mainland to the west jetty rocks at Belle Pass. However, extensive washover platforms along with numerous breaches were present. By 2004 the thalweg of Raccoon Pass striked approximately west with a meander toward the northeast on the bayside of the inlet.

These changes were most likely due to the development of three tropical cyclones between 2002 and 2003, one of which, Isidore, was a direct hit to East Timbalier Island. Hurricane Isidore reached maximum strength off the Yucatan Peninsula as a category 3 hurricane. As it continued to move north, it was downgraded to a tropical storm that made landfall within 1.6 km of Raccoon Pass. Isidore made landfall as a tropical storm on September

26, 2002 with sustained winds of 56 knots (Roth, 2010). Tropical storms Bertha and Bill made landfall within 83 km of Raccoon Pass in August 2002 and June 2003, respectively, and would have contributed to the 2004 morphology.

D. October 2005 DOQ

The subaerial extent of the barrier system in 2005 is comparable to 2004, especially toward the most eastern portion of West Belle Pass Barrier. West Belle Pass Barrier proper was 2.3 km long and contained numerous breaches. The west side of the image captured subaqueous sand dunes that were not visible in any earlier images. The dunes were essentially oriented along a northwest trend and approximately 152 m long and 183 m wide. In 2005 Raccoon Pass maintained an east to west orientation, suggesting that processes at work in the 2004 image continued to act on the tidal inlet in 2005. Sections of the rocks at remnant East Timbalier Island were either submerged or relocated from their original position. In the summer 2005 Hurricane Cindy with sustained winds of 65 knots (Stewart, 2006) made landfall as a category 1 hurricane less than 19 km east of Raccoon Pass and Hurricane Katrina made landfall less than 74 km east of Raccoon Pass with north winds of 110 knots (Roth, 2010).

E. August 2009 NAIP 2000

By 2007 West Belle Pass Barrier partially annealed the erosional effects of Hurricanes Cindy and Katrina with infilling of all the earlier formed breaches and a continuous 2.7 km of West Belle Pass Barrier shoreline. In 2008 Hurricane Gustav made landfall as a category 2 hurricane less than 28 km west of Raccoon Pass with gusts up to 75 knots in the vicinity of Raccoon Pass (Beven II and Kimberlain, 2009). Close examination of the 2009 image revealed two sand deposits with an array of recurved spits that were not present in the 2007 image, mostly along the western terminus of West Belle Pass Barrier. By 2009 West Belle Pass Barrier had an

extended spit, relative to earlier time periods, and a shoreline length of 3.2 km measured from spit end to the west jetty rocks at Belle Pass. Remnant East Timbalier and West Belle Pass Barrier proper were separated by 3.4 km of water. The rocks at remnant East Timbalier are completely submerged or destroyed by this time, as they are not visible on the image. Additionally, oil and gas infrastructure originally located on the backside of East Timbalier had now been removed from the shoreface of what remains of remnant East Timbalier Island.

F. August 2010 NAIP 2000

The 2010 morphology closely resembled that of the 2009 morphology, except for a few subtle differences. For example, a portion of the spits near the west end of West Belle Pass Barrier in 2009 appeared to be just under the water's surface in 2010. There seemed to be more dispersed sand on the west side of West Belle Pass Barrier that was exposed during low tide. Also, remnant East Timbalier had a *V*-shaped morphology with more sand deposition on the west side predominantly within the intertidal to subtidal zone. The channel of Raccoon Pass was poorly imaged in 2010 and consequently no conclusions can be drawn about the pass morphology.

G. October 2012 High Resolution Orthoimagery

In 2012 the morphology of West Belle Pass Barrier was completely altered due to the construction of the TE-52 restoration project (see Figure 2 for project infrastructure). West Belle Pass Barrier had approximately 3.4 km of shoreline and was 0.6 km wide. A containment dike was located on the bay side and a breakwater located on the southwest corner of the barrier. Conversely, remnant East Timbalier Island had undergone substantial erosion since 1989 and had minimal subaerial area.

In 2012 Hurricane Isaac made landfall as a category 1 system less than 19 km east of Raccoon Pass causing damage to Grand Isle and surrounding wetlands. However, the TE-52 project obscured the full impact of this storm near West Belle Pass Barrier. Nonetheless, Isaac's effects were visible along the island located just west of Raccoon Pass.

H. October 2013 NAIP 2000

The final image of the series showed a system that most closely resembled that of present day. The 2013 image shows the effects of natural processes, such as waves, acting on renourished sediment to create a 1.3 km-long spit on the west side of West Belle Pass Barrier. The barrier had a shoreline length of approximately 4.3 km and a width of 0.6 km. Although no major storms impacted the area since Hurricane Isaac in 2012, remnant East Timbalier Island has been reduced to a subaqueous shoal. Lastly, Raccoon Pass's orientation resembled that of the previous inlet orientations before the 2004-2005 hurricane season.

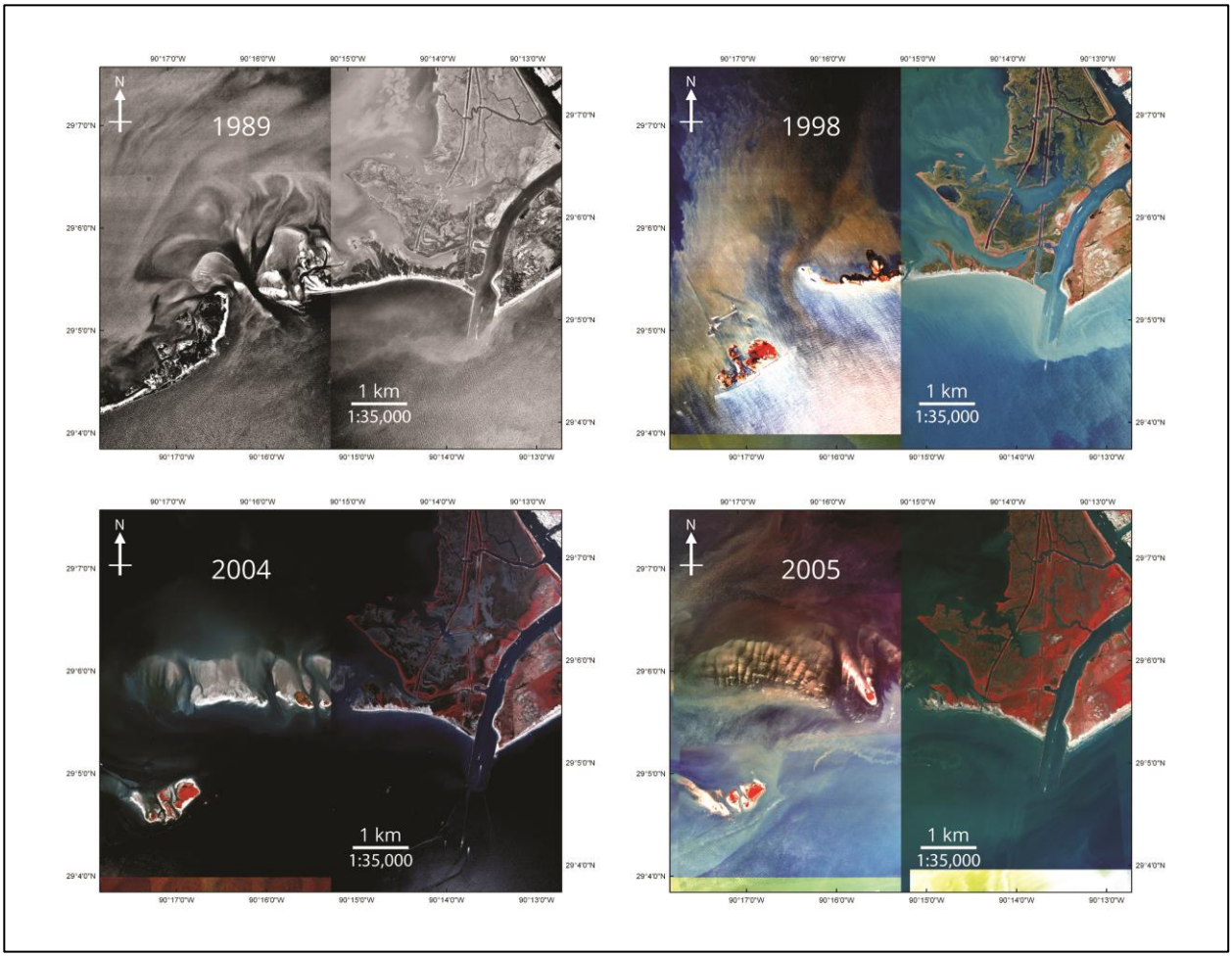

Figure 16. Imagery Part I. Four digital orthoquads that captured the morphological changes undergone by West Belle Pass Barrier and parts of East Timbalier Island between November of 1989 and October of 2005 (DOQs acquired from USGS Earth Explorer).

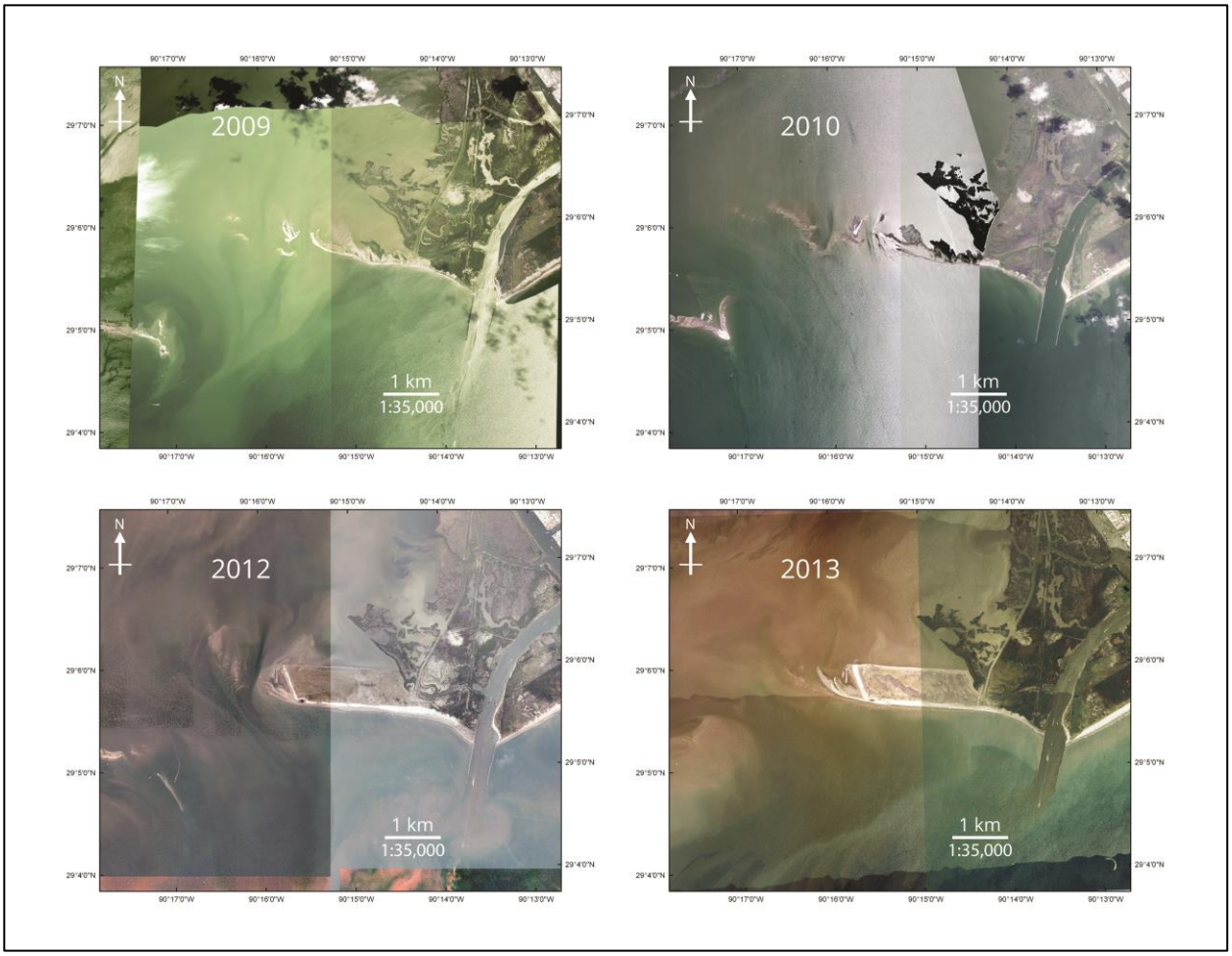

Figure 17. Imagery Part II. Four satellite images showing the morphological changes of West Belle Pass and parts of East Timbalier Island between August of 2009 and October of 2013 (NAIP imagery and orthorectified imagery from USGS Earth Explorer).

3.2.3 Modern Facies Classification

To classify surficial sediments of the identified geomorphic units, grab samples and vibracore tops (upper 2.5 – 5 cm) were classified using the Shepard (1954) grain-size scheme. The sand content of each of the samples was then plotted (Fig. 18). Once grain size was determined, each sample was placed within a geomorphic unit/depositional environment. Using the grain size data coupled with satellite imagery, a modern (2014) surficial facies map was created to better understand the likely distribution of consolidation-prone areas behind West Belle Pass Barrier (Fig. 19). Temporal resolution, however, is poor considering that the first and

last samples collected span roughly 13 years. It is worth noting that the majority of cores not acquired in 2014 were sampled between 2001-2003. The author assumes that most of the backbarrier sand percentages would not change significantly from 2001 to 2014; however, samples located near the fringe of the flood-tidal delta may experience an increase in sand. Nonetheless, sediment samples coupled with satellite imagery allowed for the classification of surficial sediments in and around Raccoon Pass.

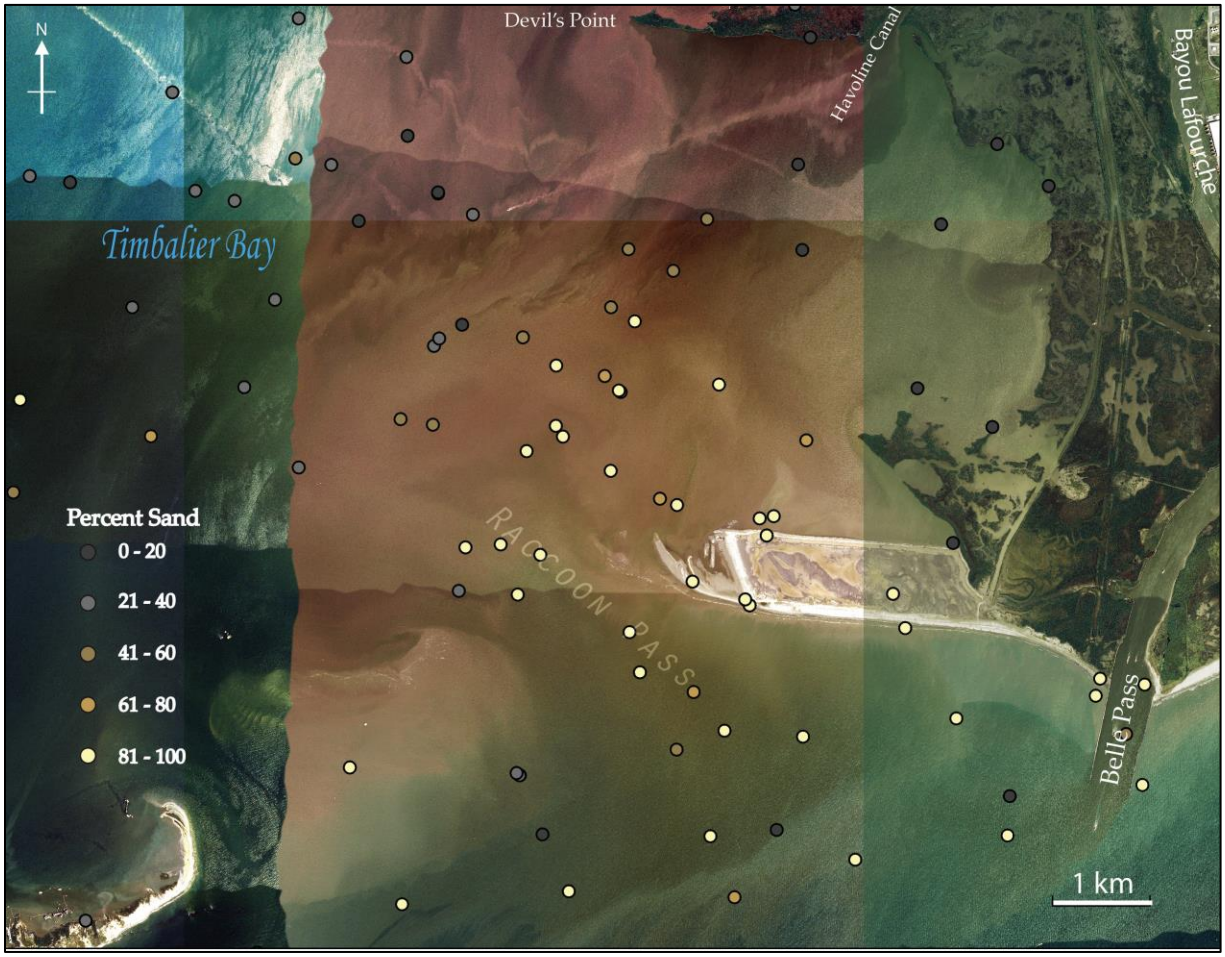

Figure 18. Grab Sample Sand Percentages. The location of grab and core samples used in this study to construct a surfial facies map. Color ranges show the percent sand of each sample using the Shepard (1954) scheme. Base map is the 2013 image of figure 10.

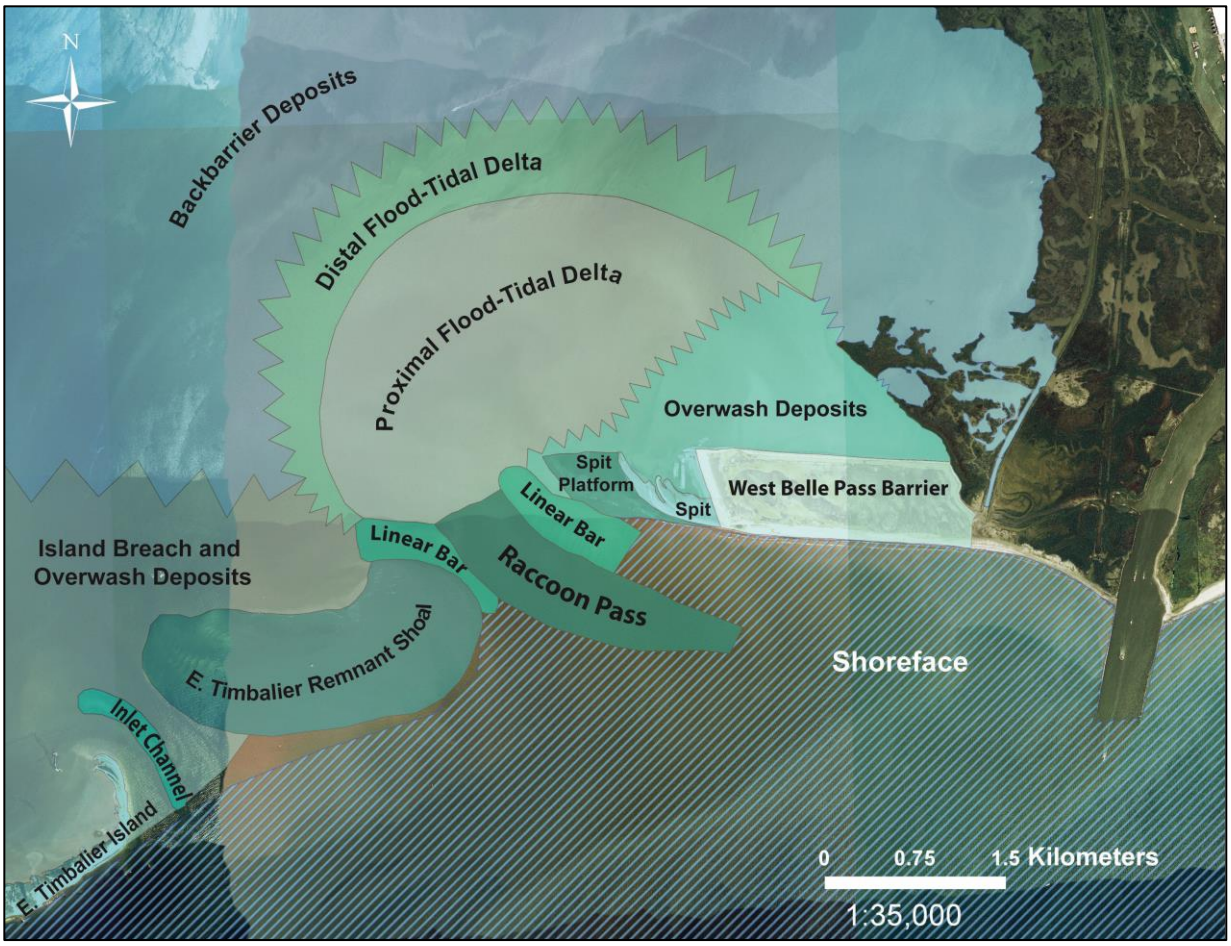

Figure 19. Surficial Facies Map. A modern day (2014) representation of depositional environments on the basis of sand content and spatial distribution from 61 grab samples, 7 push-cores, and 69 vibracore tops.

3.2.4 Subsurface Interpretation

A total of fifteen vibracores archived within UNO's CRL were used to construct two cross-sections, one depositional-dip parallel and the other coastline strike parallel, that depict the stratigraphic variability along the southwestern portion of the Caminada-Moreau Headland (Figs. 20 and 21). The deepest core penetrated 5.5 m into the subsurface, whereas the shallowest only penetrated 2.25 m. Vibracores descriptions, grain-size analysis, and vibracore photography allowed for the identification of sedimentary packages within a facies framework. For vibracores obtained during the summer of 2014, depositional environments were determined during vibracore processing. Facies determination for vibracores taken before the summer of

2014 were determined based on vibracore photography and previously completed description sheets along with any available grain size data. Using sedimentary characteristics and imagery, six facies classifications were used to distinguish sedimentary packages from one another. These six categories are as follows:

1) Barrier facies

2) Flood-tidal delta facies

3) Washover facies

4) Backbarrier facies

5) Deltaic facies

6) Marsh facies

Due to their backbarrier proximity to one another, relative similar timing in deposition, and similar textures, flood-tidal delta and washover sands were difficult to separate; therefore, they were treated as one backbarrier facies. Only one core (LH-03-06) contained likely marsh deposits. It was dominated by olive gray, organic-rich clay and will not be discussed further because it does not encompass a large portion of the stratigraphy. Three main facies are discussed in detail due to their significance and spatial extent: backbarrier facies, flood-tidal delta facies/washover facies, and deltaic facies.

A. Backbarrier Facies

This unit is generally 1 to 2 m thick, except in cores RP-14-07 and SCC01_56 where it is roughly 2.75 m thick and absent, respectively. This facies unit is dominated by light gray clay to medium dark gray clay and light gray to medium gray silty to sandy clay with rare 0.1–0.5 m-thick sand layers. Furthermore, this section is highly bioturbated and contains fragmented shells less than 5 mm in length with few whole shells of *Rangia.* Dark organic detritus similar in scale

to coffee grounds were found throughout the much of this facies. Backbarrier facies overlie deeper, regressive deltaic facies and are subjacent to flood-tidal delta and washover deposits except where it reaches the seafloor. It has a more or less gradational bottom contact with the deltaic facies and a sharp, erosional contact with flood-tidal delta and washover deposits.

B. Flood-tidal Delta and Washover Facies

One predominantly sandy package exists stratigraphically above backbarrier facies. This unit generally contains more than 50% sand and, in some cases, has up to 90-95% sand such as in RP-14-07. It is composed of mostly fine sand with color ranging from dark gray to light olive gray. It is in sharp contact with the underlying unit, represented by a noticeable increase in sand and silt relative to the clay dominated backbarrier facies. Due to the morphological changes illustrated in the shoreline datasets, it is evident that sand deposited from overwash processes and sand deposited through the inlet are overlapping and intermingled. However, an attempt to distinguish between the two can be made. Washover facies are generally lighter in color, ranging from light yellowish gray to moderate yellow. Washover deposits tend to have approximately 90-95% sand, whereas flood-tidal delta sand percentages range from 30-90%. Furthermore, roots are found within the sand interval near modern day West Belle Pass Barrier, which is indicative of washover vegetation. Specifically, washover facies are most likely to be found in cores RP-14-07 and RP-14-09 as opposed to SCC01_56.

Flood-tidal delta deposits are further separated in to either proximal or distal deposits on the basis of sand, silt, and clay percentages. Proximal deposits contain more sand and fragmented *Mulina* shells compared to distal portions due to the higher energy environment near the tidal inlet. Distal flood-tidal deposits are located along the fringe of the proximal flood-tidal

delta and a have visible increase in silt and/or clay. Further separation of these two facies would require a more in-depth analysis using more core samples.

C. Deltaic Facies

The deepest penetrated unit described herein is classified as deltaic facies. This unit consists of very fine-to-fine grained beds and lamina containing dark to medium gray and tan/reddish fat clay with thicknesses ranging from a few cm to several m interbedded with lenticular fine-grained sand. Numerous cores contain reddish brown fat clay that is discernibly different than the overlying clay-dominated strata. Shells are relatively non-existent. Kulp et al. (2003) noticed that the sand-rich intervals of this unit coincide updip with the trend of a distributary network located a few km northwest of the study site. The location and sedimentary characteristics of this unit are interpreted to be delta front and prodelta facies associated with a previous Bayou Lafourche occupation. Discrete sand packages ranging from 0.1-1.0 m in sharp contact with fat clay are interpreted to be a part of the distributary channel network. Overall clay content increases dramatically on the gulf side of West Belle Pass Barrier, suggesting that the sand deposition did not take place in these locations or was subsequently eroded during transgression.

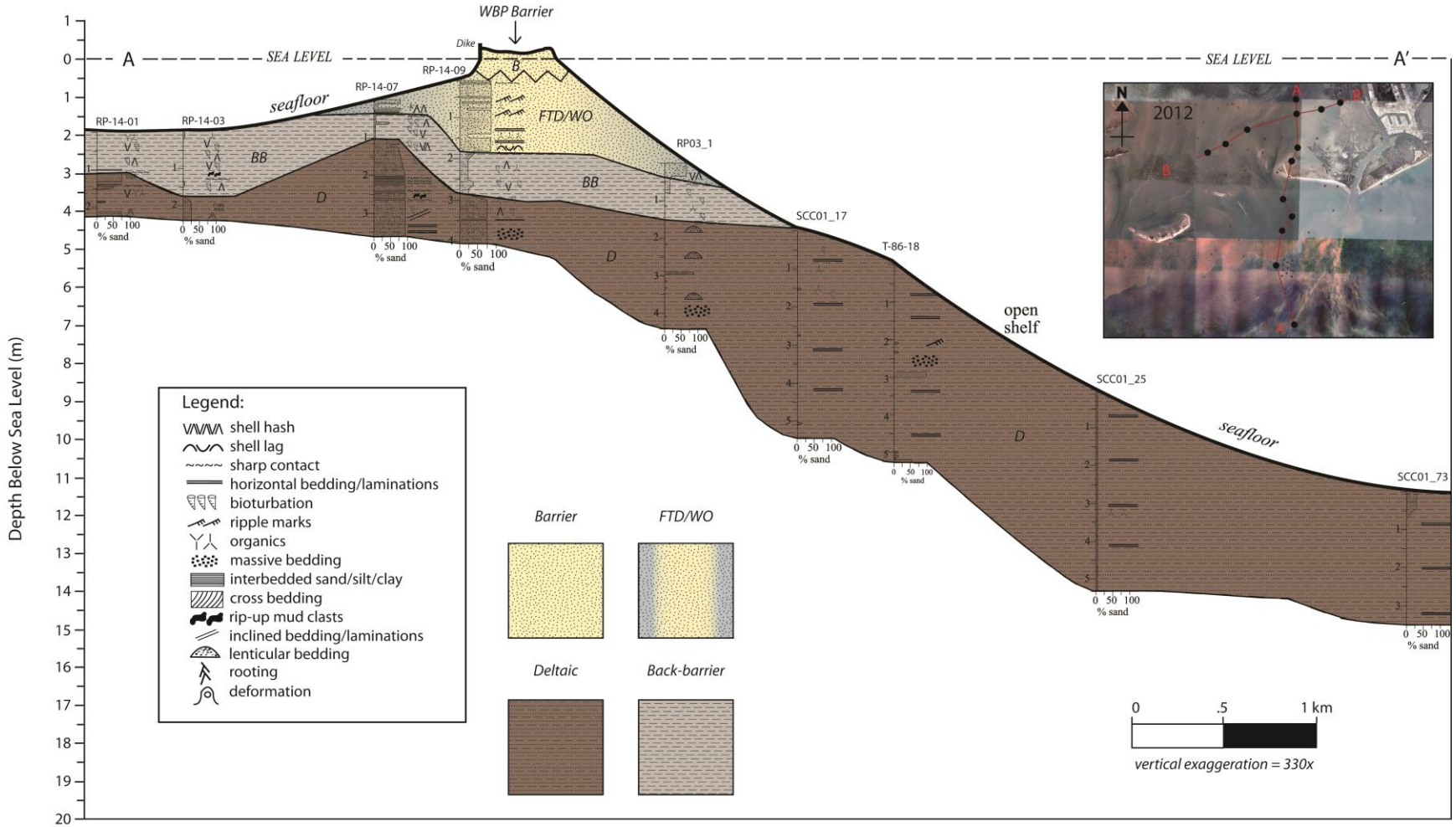

Figure 20. Stratigraphic Section A-A'. Stratigraphic line of section that shows the stratigraphic variability spanning from Timbalier Bay to the north to the Gulf of Mexico to the south. This line of section shows the potential consolidation that barrier islands undergo as they transgress landward over compactable backbarrier and deltaic strata. The inset shows the location of the cross sections with respect to the 2012 shoreline morphology.

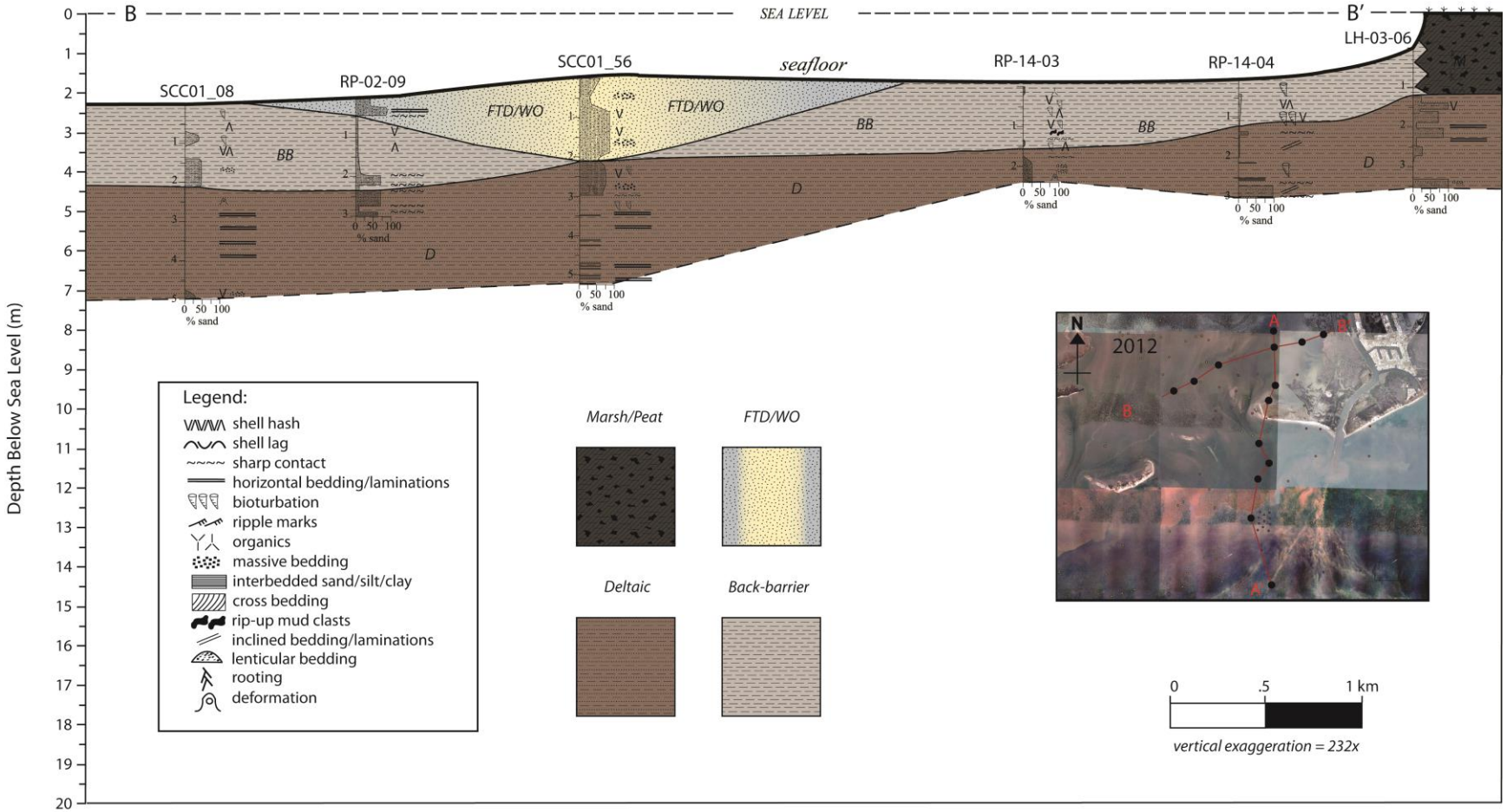

Figure 21. Stratigraphic Section B-B'. Stratigraphic line of section that shows the stratigraphic variability from west to east within the backbarrier environment of Timbalier Bay. This section shows the thick, primarily clay, backbarrier strata tested during the consolidation section of this study. The inset shows the location of the cross sections with respect to the 2012 shoreline.

3.3 Discussion

3.3.1 Morphological Evolution

West Belle Pass Barrier represents an immature flanking barrier influenced by the installation of hard structures, tidal inlet enlargement, and the occurrence of storms impacting the area. The results of this study clearly depict shoreline deterioration occurring downdrift of a jetty structure; however, hard structures are not the only cause of morphological change within the study area, and their influences are considered (i.e., an enlarging tidal inlet). Determining the exact cause of shoreline erosion and a particular event's role in altering the morphology has proven rather difficult. Nonetheless, the morphological evolution of West Belle Pass Barrier was most likely controlled by the alteration of littoral transport by the jetties, along with a change in tidal influence at Raccoon Pass. This discussion begins with the damming of Bayou Lafourche, since it is the earliest event influencing the study area. The evolution of the barrier system is discussed in two parts, which illustrate the main natural and anthropogenic events during their respective timeframes.

A. Early Influences (1904 – 1939)

While no published rates of littoral drift exist predating the damming of Bayou Lafourche in 1904, the closing of Bayou Lafourche indisputably had an affect on the study area. The damming of the bayou arguably signifies the end of fluvially transported sediment, which would have been a potential source of sediment for the area. This means that longshore sediment transportation after 1904 (and possibly before) is perhaps, the only source of sediment for West Belle Pass Barrier on a daily basis. Dantin et al. (1978) calculated rates of shoreline erosion directly east and west of Belle Pass between 1885 and 1974. Of particular interest is the interval between 1885 and 1932, wherein upstream controls (damming of Bayou Lafourche) and storm

impacts contributed to the deterioration of the study site. The shorelines directly east and west of Belle Pass experienced erosion rates of 21-35 m/yr between 1885 and 1932 (Dantin et al., 1978). The upper range of shoreline erosion (30-35 m/yr) occurred on the shoreline downdrift of Belle Pass. Dantin et al. (1978) argued that if most of the erosion during this period began in 1904, shoreline erosion rates increase to 35-58 m/yr for the 28-year period. Perhaps, one reason for the increased rates of erosion downdrift of the mouth of Bayou Lafourche is due to the damming at Donaldsonville, which deprived the study site of seasonal floodwater waters that supplied much needed sediment to the area. With a dominant wave approach from the southeast, it is possible that fluvial sediment would have been deposited near West Belle Pass Barrier and the surrounding shoreline.

Furthermore, the location of Dantin et al.'s (1978) shoreline transects are less than 700 m west from the west jetty rocks and over 1 to 2 km from Raccoon Pass. The distance of each transect from Raccoon Pass suggests that tidal influence was not a significant cause of shoreline erosion immediately west of the jetties before 1932. In addition to the damming of Bayou Lafourche, the unnamed 1915 category 3 hurricane played a role in shoreline erosion, and the effects are accounted for in Dantin et al.'s (1978) erosion rates during this time. The degree to which this storm affected the study site is not detectable due to the time between subsequent datasets. Nevertheless, the preferential erosion occurring downdrift of Belle Pass between 1885 and 1932 marks the beginning of shoreline reorientation. The increased rates of erosion at West Belle Pass Barrier caused the shoreline to transgress faster than the shoreline east of Belle Pass, and West Belle Pass Barrier exhibited slight clockwise rotation from 1884 to 1933 that was mainly due to natural causes.

B. Late Influences (1940 - 2013)

The West Belle Pass Barrier shoreline rotation was exacerbated by the completion of the Belle Pass jetties in 1940 and subsequent modifications. Although the jetties were completed in 1940, it seems that the initial construction (pre-modifications) was not enough to completely prohibit longshore sediment transport. Comparing the 1933 and 1956 shorelines validates this statement, especially since there does not appear to any major sediment accumulation on the east side of the jetty system. However, determining the source of sediment for longshore currents is rather difficult (i.e., from within West Belle Pass Barrier or updrift of the jetty system). Additionally, West Belle Pass Barrier extended over 2 km from 1933 to 1956. In essence, sediment supply to West Belle Pass Barrier and East Timbalier Island must have continued after 1940. However, it is possible that the amount of longshore transport reaching the west side of Belle Pass was reduced by the jetties in 1940 but not so much as too cause severe downdrift erosion if one assumes that longshore transport around the jetties was the dominant source of sediment for the area. Rather, it is more probable that the modifications to the jetties after 1956 contributed significantly to the deterioration of East Timbalier Island and West Belle Pass Barrier.

The most prominent morphological discrepancy between the shorelines immediately east and west of the Belle Pass jetties in 1956 was the shoreline strike. The two shoreline morphologies that predate jetty installation show a more or less uniform headland shoreline striking NE to SW. However, the 1956 shoreline dataset depicts a different orientation, particularly regarding the area directly west of the jetties. The shoreline strike of East Timbalier Island, the majority of West Belle Pass Barrier, and the shoreline of the Caminada-Moreau Headland exhibited the same strike orientation in 1956. Yet, the portion of shoreline

immediately west (> 1 km) of the jetties was oriented northwest to southeast. This discrepancy was most likely due to the jetties causing longshore transport to intersect the shoreline passed the point of shoreline inflection. Dantin et al. (1978) modeled the jetties' effect on sediment transport patterns around the Belle Pass jetties using current velocities acquired in the 1970's. Although the focus of Dantin et al.'s (1978) model was to predict changes in longshore transport for a proposed jetty modification, results showed that littoral sediment was deposited onshore anywhere from 1,530 m and 2,440 m west of Belle Pass depending on the rate of littoral flow and tidal currents. Overlaying this distance on to the historical shoreline morphologies shows that this distance was just past the point of shoreline inflection west of Belle Pass. However, Dantin et al.'s (1978) model was run using the jetty configuration at the time, which was not the same configuration in 1956. One can argue that this longshore transport pattern around the jetties began as early as 1969 when the jetties were extended over 300 m seaward (parameters for Dantin et al.'s (1978) model). Conceivably, the same longshore transport process occurred before 1969 but after 1940 to a lesser degree, and this resulted in the change in shoreline orientation seen directly west of the jetties in 1956. However, locating the site of longshore deposition on the West Belle Pass Barrier shoreline itself does not explain the erosion of the shoreline downdrift of this point after the 1956 shoreline dataset. One explanation for the erosion occurring downdrift of longshore deposition around the jetties after 1956 might be the location and influence of the nearest tidal inlet, Raccoon Pass.

In 1965 one of the largest storms to impact not only the Louisiana coastline but also West Belle Pass Barrier made direct landfall on the Caminada-Moreau Headland. The destruction incurred during Hurricane Betsy most probably damaged the existing jetty system, and possibly aided in the growth of Raccoon Pass visible in the 1978 dataset. Perhaps, one of the events

responsible for extending the Belle Pass jetties over 300 m was the same event that enabled tidal currents at Raccoon Pass to transport sediment bypassing the jetties into the backbarrier. Raccoon Pass tidal velocities around this time are not available; however, a 1930's to 1980's bathymetric change map from the BICM program illustrates approximately 1-3 m of accretion on the landward side of Raccoon Pass in the shape of a flood-tidal delta (Fig. 22) (Miner et al., 2009). Backbarrier accretion and flood-tidal delta formation suggests that tidal currents were sufficient enough to transport sediment from the shoreface to the backbarrier sometime between the 1930's and 1980's. Coupling the bathymetric change map along with shoreline modifications, longshore transport patterns, and one timely hurricane impact, the Belle Pass jetties created a system wherein longshore sediment was transported around the jetties, deposited on the shoreline, and funneled into the backbarrier in the form of a flood-tidal delta. Sustained shoreline deterioration and rotation at West Belle Pass Barrier during the 1980's, 1990's, and early 2000's allowed for the continual sequestration of longshore sediment through Raccoon Pass. Therefore, West Belle Pass Barrier appears to have been eroded from the west by tidal inlet expansion and the location of the jetties to the east.

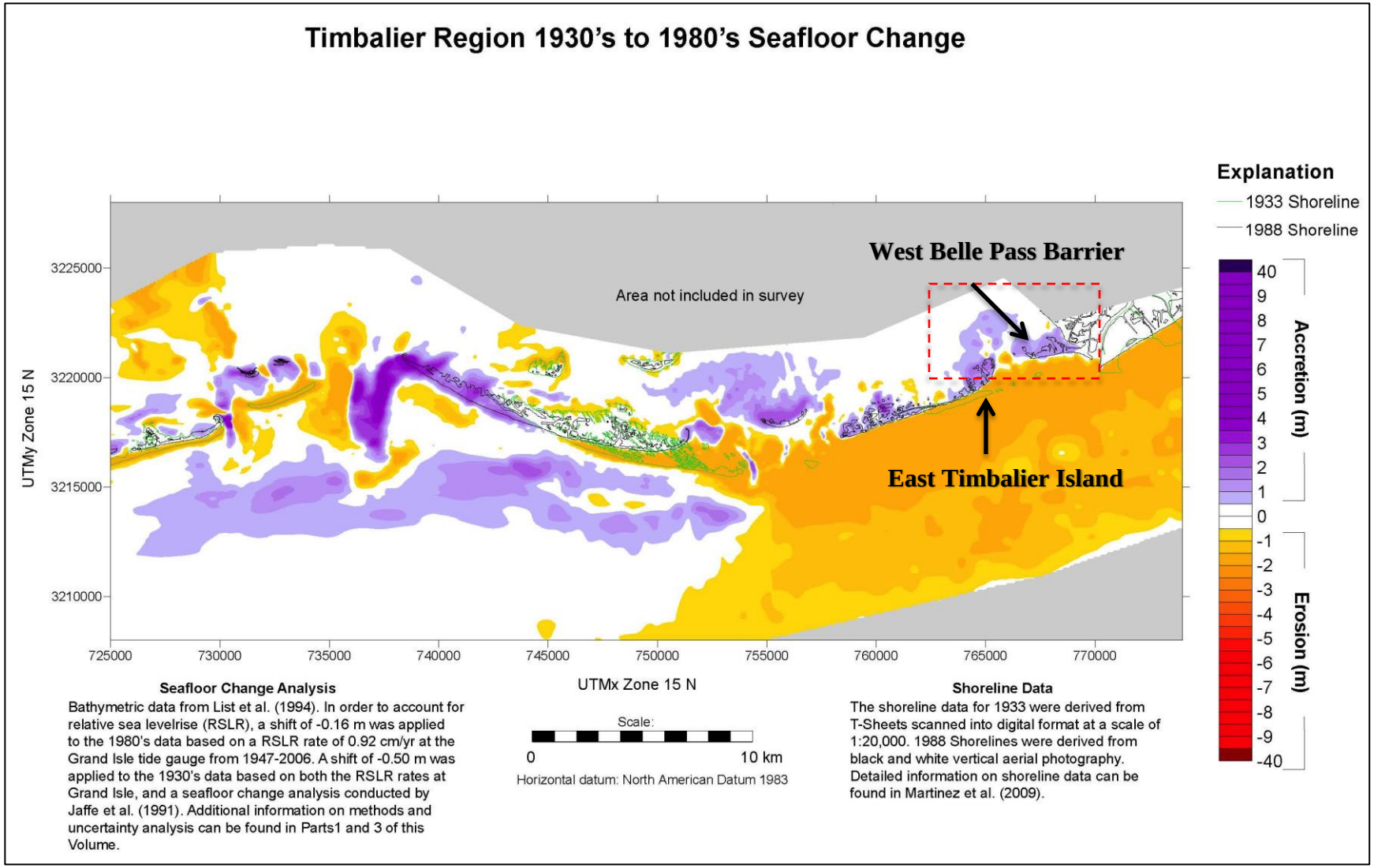

Figure 22. Bathymetric Change Map. A 1930's to 1980's bathymetric change map of the region between the Isles Deneries and Caminada-Moreau Headland (from Miner et al., 2009). During this time period, the backbarrier environment of West Belle Pass Barrier experienced approximately 1 to 3 m of net accretion (red box).

Tidal currents through Raccoon Pass, however, would have to be substantial enough to transport longshore-sourced sediment, as well as maintain the tidal inlet cross-sectional area after Hurricane Betsy. One explanation is that an increasing tidal prism during this time allowed for the stabilization and future enlargement of the inlet. NWRC Open File Report 94-01 measured wetland loss within the Timbalier/Terrebonne Basin at an average rate of 24 km^2/yr from 1956-1978 (Barras et al., 1994), which was highest rate of land loss of ten basins used in the study. The conversion of wetlands into open-water areas irrefutably increased the tidal prism associated with Raccoon Pass, which may have been the mechanism behind post-Betsy inlet stability and continued sediment funneling. Moreover, the paucity of flood-tidal deltas along the Louisiana coast suggests that tidal currents alone are not responsible the formation of the delta, and hence, the deterioration of West Belle Pass Barrier. Rather, a series of very unique and timely events surrounding the construction and extension of the Belle Pass jetties resulted in this quite unusual system. Storms, jetties, and tidal currents caused the barrier to alter its morphology through time causing state organizations to formulate a renourishment plan for the area (TE-52). The recent morphology of the barrier observed during several trips during the summer of 2014 suggests that processes are currently at work. An approximately 1.2 km-long spit has prograded into Raccoon Pass, confirming the transportation of littoral sediment in to the backbarrier. It is conceivable that some of the sediment from the TE-52 project will be deposited into the backbarrier as washover deposits or within the flood-tidal delta. The amount of sediment transported into the pass is unknown; however, the "recycling" of anthropogenically-sourced sediment may prove useful as the shoreline continues to translate landward.

Chapter 4. Consolidation of Backbarrier Facies

4.1 Principles of Consolidation

4.1.1 One-Dimensional Consolidation Theory

Terzaghi (1943) developed a model of one-dimensional consolidation in order to estimate the settlement rates of soils. This model quantifies the time-dependent, compressible behavior of soils using an incremental loading process and is possibly the most widely used consolidation theory in practice today. Consolidation is the process during which pore water pressure (u) leaves a soil particle matrix due to a change in effective stress ($\Delta\sigma'$) caused by loading (Terzaghi, 1943; Das and Sobhan, 2014). The consolidation of recently deposited, water-saturated sediment can take place quickly in very shallow, highly compressible clays. A load applied to a saturated, compressible substrate causes a sudden change in stress ($\Delta\sigma$), which results in an increase in pore pressure (Δu). This excess pore pressure eventually dissipates by outward flow of water, leading to a change in effective stress within the sediment matrix. The total stress (σ), pore water pressure (u), and effective stress (σ') relationship of a soil layer was developed first by Terzaghi (1936) and expanded upon by Skempton (1960). The principle of effective stress is as follows (Das and Sobhan, 2014):

$$\sigma = \sigma' + u$$

The effective stress principle is one the most widely used concepts in geotechnical engineering, and the effective stress concept is defined as (Das and Sobhan, 2014):

$$\Delta\sigma = \Delta\sigma' + \Delta u$$

Where:

At time = 0 immediately after an applied load:

$$\Delta\sigma = \Delta u, \ \ \Delta\sigma' = 0$$

At time = ∞, such that consolidation is complete:

$$\Delta\sigma = \Delta\sigma', \ \ \Delta u = 0$$

The rate of pore pressure dissipation (i.e., drainage) is dependent on the hydraulic conductivity of the soil; and, in highly permeable soils like sands, this dissipation occurs immediately (Das and Sobhan, 2014). Pore pressure dissipation of clayey and silty soils, on the other hand, occurs during a much longer time since clays and silts are less permeable than sands (Coduto et al., 1999). As excess pore water pressure translates to an increase in effective vertical stress, the soil particle skeleton starts to support the change in stress caused by loading. This process forces the voids between the grains to compress, resulting in the settling or compression of the layer and a net reduction in the original void space. The equation used to determine the change in effective stress caused by loading (i.e., subaqueous washover deposits) is as follows (Das and Sobhan, 2014):

$$\Delta\sigma' = H_{load} * (\gamma_{sat\ load} - \gamma_{water})$$

Where:

$$H_{load} = thickness\ of\ the\ load$$

$$\gamma_{sat\ load} = saturated\ unit\ weight\ of\ the\ load$$

$$\gamma_{water} = unit\ weight\ of\ water$$

There are different mechanisms that can change the effective stress on a compressible substrate. Such sources are large areal fills, loads placed on finite sized footings, and fluctuations in the groundwater table (Coduto et al., 1999). Since sediment additions from renourishment projects or washover deposits typically cover a large area (several m^2), changes in the groundwater table and loads placed on footings are not considered relevant to this examination.

4.1.2 Settlement

The total amount of settlement that a soil layer will experience after loading can be calculated as (Das and Sobhan, 2014):

$$Total\ settlement, S_T = S_C + S_S + S_e$$

Where:

$$S_C = primary\ consolidation\ settlement$$

$$S_S = secondary\ consolidation\ settlement$$

$$S_e = elastic\ settlement$$

The three types of settlement do not contribute equally to the total settlement, nor do they take place concomitantly. Elastic settlement (S_e) is the result of elastic deformation of a soil without a change in water content, and this settlement usually occurs immediately after a load is applied to a compressible soil layer (Das and Sobhan, 2014). Alternatively, primary consolidation settlement is the result of a change in void space in saturated soils due to the rearrangement of sediment grains and expulsion of fluid, and it is defined as follows (Das and Sobhan, 2014):

For normally consolidated soils:

$$S_C = \frac{C_C\, H}{1 + e_o} \log \frac{\sigma'_o + \Delta\sigma'}{\sigma'_o}$$

$$C_c = compression\ index$$

$$H = thickness\ of\ the\ compressible\ soil\ layer$$

$$e_o = the\ initial\ void\ ratio$$

$$\sigma'_o = insitu\ effective\ overburden\ pressure\ at\ midpoint$$

$$= H_{midpoint}\,(\gamma_{sat} - \gamma_{water})$$

$$\Delta\sigma' = increase\ in\ effective\ stress$$

This type of settlement is the result of a change in effective vertical stress due to an applied load, either natural or anthropogenic. If there is no change in effective stress on the soil matrix, then primary consolidation will not occur. Perhaps, the most time consuming settlement is secondary consolidation settlement, which is the settlement due to the plastic adjustment of soil fabrics after primary consolidation has occurred (Das and Sobhan, 2014). Secondary compression settlement occurs without a change in effective stress and usually is preceded by primary consolidation. It is generally understood that the largest contributor to total settlement is primary consolidation settlement; consequently, primary consolidation is the focus of this study.

The compressibility of soil is determined by calculating the compression index (C_c). In order to determine the compression index, a sample is tested using a consolidometer, which measures the change in height of a sample against an incremental loading schedule. A semi-log plot of the changing void ratio versus the log of the change in effective stress displays the sample's response to increasing pressures. The compression index is the slope between two points located on the straight portion of the resulting semi-log curve. It describes the relationship between voids ratios and corresponding pressures and is determined using the equation (Das and Sobhan, 2014):

$$Compression\ Index, C_c = \frac{e_1 - e_2}{\log\frac{\sigma_2}{\sigma_1}}$$

Where:

$$e_1, e_2 = void\ ratios\ from\ consolidation\ curve$$

$$\sigma_1 = corresponding\ e_1\ pressure\ from\ consolidation\ curve$$

$$\sigma_2 = corresponding\ e_2\ pressure\ from\ consolidation\ curve$$

4.1.3 Terzaghi's Assumptions

In order to quantify the magnitude and rate of consolidation of a soil layer using the theory of one-dimensional consolidation, Terzaghi made eight assumptions:

1) The compressible soil layer is homogenous.
2) The soil is completely saturated.
3) Solids and water within the soil layer are incompressible.
4) Compression and flow are one-dimensional (i.e., vertical).
5) Strains are small.
6) Darcy's law governs flow.
7) The coefficient of permeability (k) and the coefficient of compressibility (m_v) remain constant throughout the entire process.
8) There is a unique relationship between void ratio and effective stress that is independent of time.

Assumptions 1-5 are realistic enough that they do not pose any complications when applying Terzaghi's theory to practical problems. However, evidence suggests that pore water flow does not follow Darcy's law at very low gradients in regards to Assumption 6 (Hansbo, 1960). Typically, this is not an issue with fine-grained soils since the hydraulic gradient is sufficiently high, and Mitchell and Soga (1976) concluded that Darcy's law is valid. Also, the coefficient of permeability (k) and the coefficient of compressibility (m_v) have been shown to change with increasing effective stress, meaning the coefficient of consolidation (c_v) is not constant through time with regard to clay minerals (Robinson and Allam, 1998). However, using small stress increments throughout the consolidation process keeps Assumption 7 fairly practical. The majority of complications arise with Assumption 8 since experimental results show that the

relationship between void ratio and effective stress is not independent of time. Fine-grained soils usually undergo a reduction in void volume with time without a change in effective stress (secondary consolidation settlement). Therefore, Terzaghi's one-dimensional consolidation theory is useful for estimating the rate and magnitude of consolidation.

4.2 Methodology

4.2.1 Undisturbed Push-Cores

Due to the disruptive nature of the vibracoring process, all previously obtained cores were rendered inadequate for consolidation testing. Vibracoring alters the in situ soil conditions by increasing the pre-consolidation stress, reducing the volume, and increasing the unit weight of the soil sample. In order to accurately determine the primary consolidation settlement potential of backbarrier deposits, this study used a push-coring technique that minimizes compressive forces during sampling. Push-core locations were determined after vibracore processing to better understand areas prone to compaction (e.g., thick, clay-dominated substrates) (Fig. 23). This methodology requires an approximately 1.8 to 2.1 m-long, 7.62-cm diameter aluminum pipe with a 1.27-mm wall thickness for sampling.

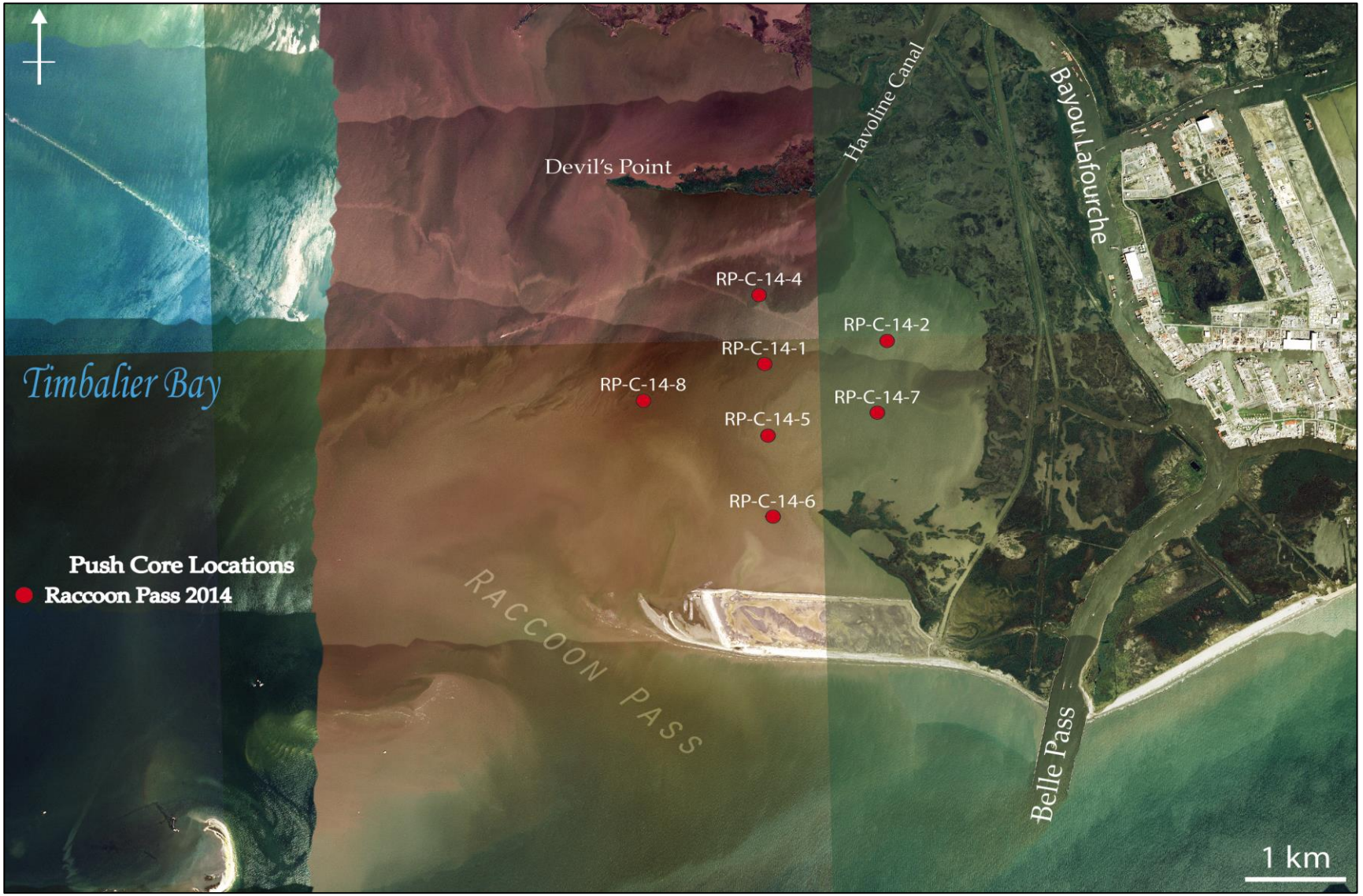

Figure 23. Push-Core Sample Locations. The locations of seven undisturbed push-cores are shown within the immediate vicinity of Raccoon (satellite image from USGS Earth Explorer, 2013 NAIP JPG 2000).

Water depth and core length measurements were taken before and after sampling. Table 2 shows the measurements and sample information for each push-core. The aluminum tubing is forced into the substrate by applying a smooth, constant force from top to bottom, minimizing any vibration or disturbances within the sediment. The average penetrable depth was 0.4 m, and the deepest and shallowest cores reached 0.61 and 0.25 m, respectively. The top end of the tube was then plugged, capped, and sealed. Before hoisting the sample out of the water, the bottom end of the tube was capped and sealed to ensure sample capture. A total of seven push-cores were labeled and readied for transport to UNO's CRL. Difficulties penetrating the subsurface at push-core location RP-C-14-03 made capturing an adequate amount of sediment nearly impossible; therefore, a sample was not recovered at this location. This is most likely attributed to the location of the coring site over the very sandy flood-tidal delta. Also, push-cores RP-C-14-05 and RP-C-14-06 did capture sediment; however, these cores did not capture enough sediment for testing (RP-C-14-05) or the soil sample was disturbed enough to render it inadequate (RP-C-14-06). These samples visually indicated sand, which was noted for future use. Cores RP-C-14-02 and RP-C-14-07 were in such pristine condition that samples were taken from the top (T) and bottom (B) of both cores. Cores were transported standing vertically, as to mimic in situ conditions and limit the amount of disturbance during transportation.

Table 2. Push-Core Samples. Push-core measurements from a total of seven cores (T = top, B = base).

Sample	Core Length (m)	Consolidometer Sample Depth Below Mudline (m)	Water Depth (m)
RP-C-14-01	0.4509	0.33	1.85
RP-C-14-02-T	0.3937	0.101	1.72
RP-C-14-02-B	0.3937	0.279	1.72
RP-C-14-04	0.4953	0.279	1.83
RP-C-14-05	0.0762	N/A	1.48
RP-C-14-06	0.3302	N/A	1.00
RP-C-14-07-T	0.6096	0.152	1.79
RP-C-14-07-B	0.6096	0.432	1.79
RP-C-14-08	0.254	N/A	1.51

Sample extrusion was done at Ardaman and Associates, Inc.'s laboratory in Jefferson, LA. A motorized soil extruder was used to remove the samples from the aluminum tubing. A 7.62-cm diameter plate attached to a steel rod powered by the motor successfully extruded push-core samples with minimal disturbance. Samples were visually described, measured, photographed, and prepared for transport to UNO's Civil Engineering laboratory. Upon arrival, one to two samples were cut from each push-core based on overall sample length and sediment characteristics. Once samples were prepared, they were readied for use in the consolidometer. Further discussion on sample preparation can be found in the consolidation section of this chapter. It should be stated that the sampling and transportation methods of any core sample from the field might alter the *in situ* soil conditions. However, the author assumes that this change was not significant enough to invalidate the results.

4.2.2 Geotechnical Analysis

Laboratory tests were completed on seven push-core samples representing five push-cores. Each push-core was sampled once in order to gain a representative core sample; however, two samples were acquired from push-cores of substantial length (RP-C-14-02 and RP-C-14-07).

Samples were tested based on the amount of clay that was visually estimated. Predominantly muddy samples underwent testing for moisture content, specific gravity, % passing No. 200 sieve, Atterberg limits, and consolidation. Fortunately, there was only one sample that contained a sizeable amount of sand (RP-C-14-08). A sieve analysis was run on RP-C-14-08 along with moisture content. All laboratory analyses were conducted in the UNO's Civil Engineering Laboratory by a certified technician according to the correct American Society for Testing and Materials (ASTM) standard.

A. Moisture Content

The water or moisture content (MC) of a soil is defined as the ratio of the mass of water removed from a sample by heating expressed as a percentage. Moisture contents were determined by the procedure outlined in ASTM standard D2974-13. The equipment used in this procedure adheres to the specifications outlined in the standard. First, a representative samples taken from push-cores were weighed to the nearest 0.01 grams. Samples were then dried uncovered in an oven for at least sixteen hours at 110 ±5°C. Once the samples were dried, they were removed and placed in a desiccator to cool. The mass of the sample was then reweighed to the nearest 0.01 grams. In order to determine the moisture content as a percentage of the initial mass of the sample, the mass of the moist specimen (m_w) is divided by the mass of the oven-dried specimen (m_d). The result was then multiplied by 100 to calculate the moisture content. The moisture content equation is as follows:

$$Moisture\ content, MC = \frac{m_w}{m_d} * 100$$

B. Specific Gravity of Soil Solids

The specific gravity of soil solids (G_s) is the ratio of the unit weight of material to the unit weight of water (Das and Sobhan, 2014). It is needed to calculate void ratios, degree of

saturation, and density of soil solids. ASTM Standard D854 was used to determine the specific gravity of soil solids of all push-core samples (excluding RP-C-14-08). The specific gravity of soil solids is determined by using a water pycnometer. In order to calculate G_s, determine the difference between the weight of the pycnometer filled with water (W_A) and the weight of the pycnometer filled with water and soil (W_B). Add the weight of the oven-dried soil sample (W_0) to the difference, and divide the weight of the oven-dried soil sample (W_0) by the result ($W_0 + (W_A - W_B)$).

$$Specific\ Gravity\ of\ soil\ solids, G_S = \frac{W_0}{W_0 + (W_A - W_B)}$$

C. Grain Size Analysis

Push-core samples suitable for consolidation testing were also examined for sand and mud content by washing some of the sample through the No. 200 sieve following the procedures outlined in ASTM standard D422. Washing the sample through this sieve allows for the separation of silts and clays from sand and gravel. However, it is rather difficult to pass predominantly fine-grained samples through the No. 200 sieve. Washing with water allows the sample to break down into individual soil grains making it easier to pass. The results of passing sediment through the No. 200 sieve are important for classifying soils using the Unified Soil Classification System (USCS).

Push-core RP-C-14-08 captured predominantly sandy sediment in enough quantity to be tested using traditional sieve analysis. The sample was sieved through No. 4, No. 10, No. 20, No. 60, No. 100, No. 120, No. 140, and No. 200 sieves in order to achieve a grain size distribution curve. All of the tests mentioned in this section are used for the classification of soil, as well as determining any successive tests.

D. Atterberg Limits

Atterberg limits are measurements of water content or consistency in predominantly fine-grained samples (Das and Sobhan, 2014). There are four consistency states: liquid, plastic, semi-solid, and solid. Water content increases from solid to liquid. These limits are crucial in understanding a soil's response with different water contents. Typically, geotechnical analysis focuses on the plastic (PL) and liquid limits (LL) of a soil sample. The plastic limit is the moisture content at which a soil changes from a semisolid state to a plastic state. The plastic limit is determined by rolling a 1/8" thread of soil until it begins to crack. First, create a soil paste made by mixing water and soil in a bowl and place in a cool dry area to allow for moisture expulsion (air-drying is acceptable). Before the sample completely dries out, roll a 1/8" thick soil sample on a rolling plate. Once the sample begins to crack and cannot be re-rolled, collect an appropriate amount of soil to measure the water content. The resultant water content is the plastic limit. For this study, two samples from the same depth were run to determine an average plastic limit of the sample. The liquid limit is the water content at which a fine-grained soil sample changes from a plastic state to a liquid state (Das and Sobhan, 2014). In order to determine the liquid limit, a soil paste must be prepared by mixing water and soil until the consistency is appropriate enough to close a standard groove in the soil by ½" upon 25 repeated drops of a Casagrande cup. A four point liquid limit test requires a total of four trials, wherein two tests use less than 25 blows to close the groove and two tests use more than 25 blows to close the groove. After each trial the water content of the sample was found. In order to determine the liquid limit, a graph of water content verse the number of blows is prepared. The liquid limit is the water content that corresponds to 25 blows using the graph. The next step is to find the plasticity index, which is the difference between the liquid limit and plastic limit. The

plasticity index is the range of water contents in which the soil sample behaves in a plastic (remoldable) manner. The methods described herein were followed according to the ASTM standard D4318.

E. Consolidation Testing

In order to accurately determine the primary consolidation settlement of backbarrier lithofacies contained within undisturbed push-cores, consolidation tests were performed on appropriate samples using the ASTM D2435 standard for one-dimensional consolidation. The soil properties determined from the consolidation test aid in the estimation in the degree and rate of primary and secondary consolidation of a particular soil sample. In order to accurately complete a consolidation test, the consolidation cell must be calibrated before use to ensure that the deformation of the system is known. The consolidation cell of known volume is constructed entirely of metal as to minimize any deformation of the sample directly related to fluctuations in the ring's size during loading. Once calibration was completed, an appropriate soil sample was prepared using a wire saw. The consolidation ring was used to trim a sample of 25.4 mm height and 63.5mm diameter. Figure 24 shows the setup of the consolidation cell and two porous stones, dial gauge, and a water reservoir used for testing. Other equipment necessary to complete the test includes filter paper, metal straight edge, and timer. Once the consolidation cell was fully prepared, it was applied to the loading machine. An incremental loading schedule was applied to the sample in order to accurately determine the consolidation curve. As noted in the loading process, each sample underwent an initial period of loading followed by unloading, and lastly, reloading. Various measurements were taken throughout the test in order to determine the soil compressibility, including the applied pressure, change in soil sample volume, and time.

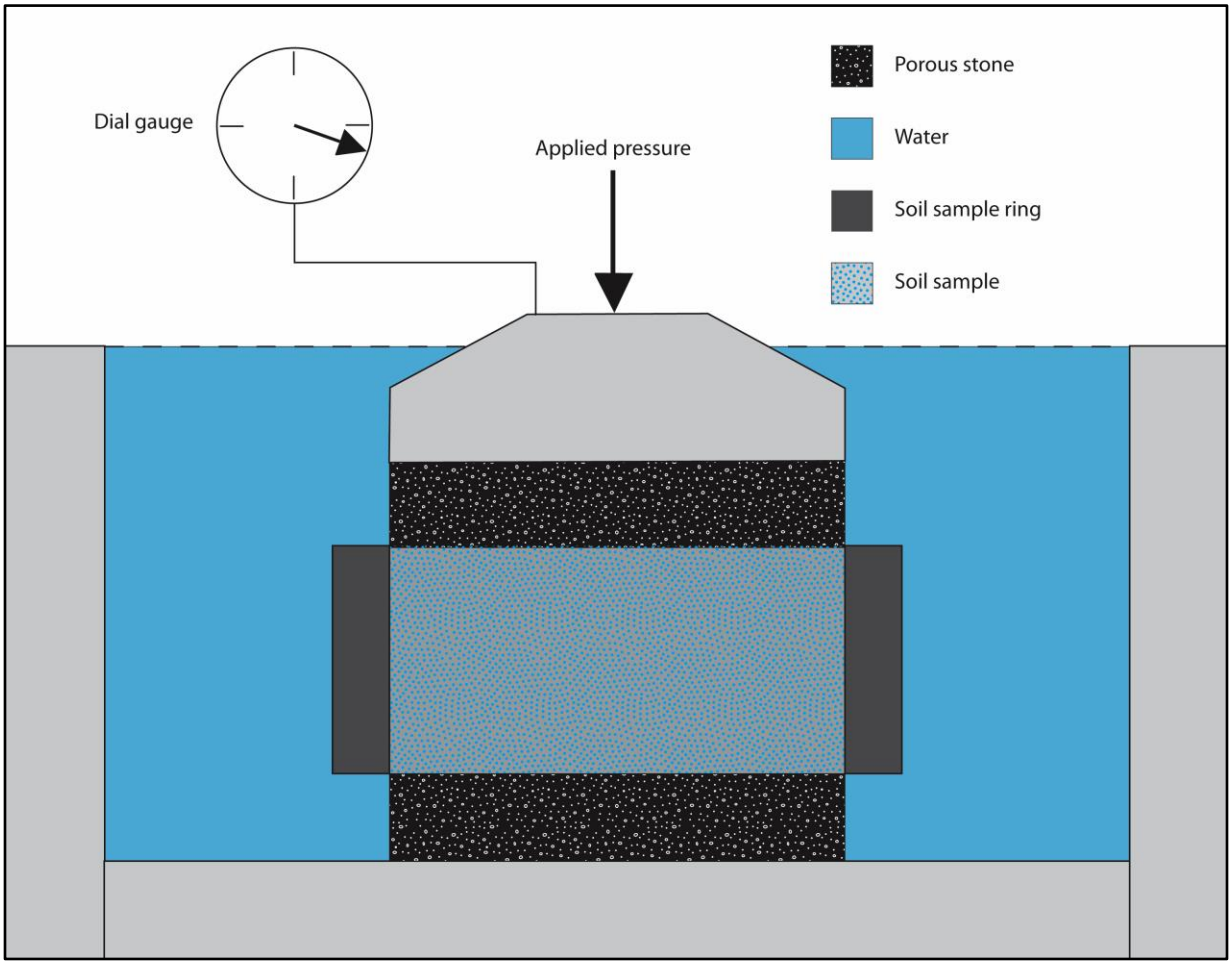

Figure 24. Consolidometer Diagram. Schematic of a consolidometer during testing.

4.3 Results

A total of seven samples were tested using standard geotechnical practices to assess the potential consolidation and variability within the backbarrier facies of West Belle Pass Barrier. Six samples from four push-cores underwent testing for moisture content, specific gravity, % passing No. 200 sieve, organic content, Atterberg limits, and consolidation testing. All of the results are provided in Appendix B. Push-cores RP-C-14-02 and RP-C-14-07 were sampled to depths that allowed for the analysis of two samples (top and bottom). All other push-cores were sampled once at a range of depths. Due to its lack of fines noted in the field, push-core RP-C-14-08 was only tested for grain size.

4.3.1 Soil Classification

In this study the Unified Soil Classification System (USCS) was used because it utilizes a textural and plasticity approach that has valuable engineering purposes. Since this study considers the role of compactable strata during natural loading along barrier shorelines, the USCS is an ideal approach for categorizing samples. The USCS uses symbols that combine the gradation (well-graded = W, poorly-graded = P), liquid limit (high LL = H, low LL = L), and grain size (sand = S, silt = M, clay = C, organic = O) of samples in to one easily understood soil group (e.g., SW, SP, SL, SM, CH, CL, MH, ML, OH, OH etc.)

A first step in USCS soil classification is to categorize the samples on the basis of grain size (coarse vs. fine) and organic content. All push-core samples (excluding RP-C-14-08) were visually categorized as predominantly fine-grained. Samples were subsequently passed through the No. 200 sieve in order to confirm the visual classification. Samples with more than 50% of the total sample passing through the No. 200 sieve were classified as fine-grained (<0.075 mm diameter), whereas samples with more than 50% of the total sample retained on the No. 200

sieve are classified as coarse-grained (0.075 to 75 mm diameter). In the USCS coarse-grained soils refers to gravels (4.75 to 75 mm diameter) and sands (0.075 to 4.75 mm diameter).

A. Atterberg Limits

In the next step samples were separated on the basis of an arbitrarily set liquid limit (%) of 50. Samples with a liquid limit less than 50% were classified as low liquid limits (L), while samples with a liquid limit greater than 50% were classified as high liquid limits (H). To further refine the sample separations, a plot of the liquid limit vs. the plasticity index (LL-PL) developed by Casagrande in 1948 is used (Fig. 25). The A-line of figure 25 separates clayey soils (C) from silty soils (M) as well as inorganic soils from organic soils. The U-Line represents the upper range of plasticity index and liquid limit pairs that are generally accepted as occurring in nature, and any samples plotting above this line should be cautiously interpreted or re-run.

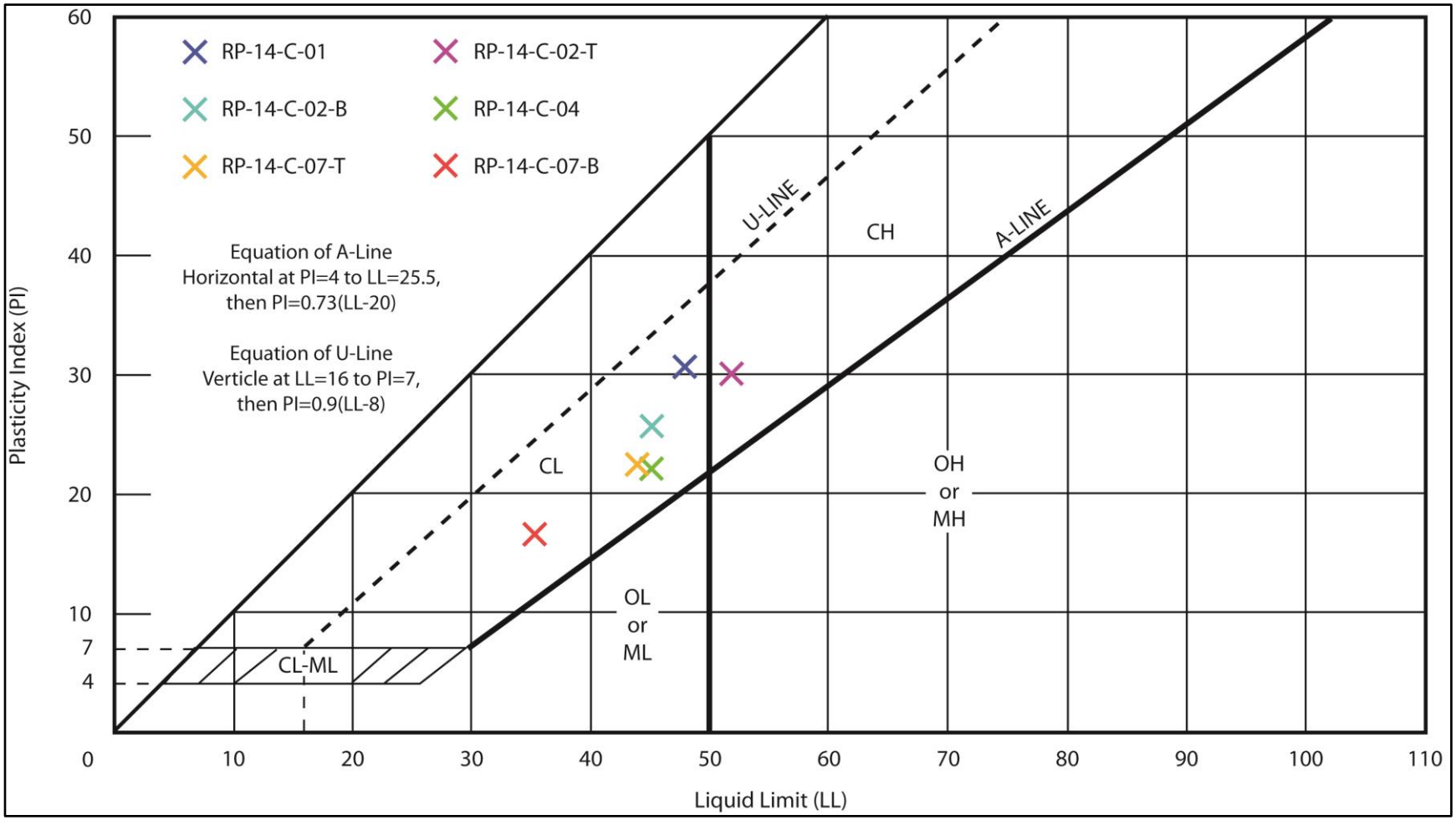

Figure 25. Plasticity Chart. Plasticity chart showing the classification of soil samples using their respective plasticity indexes (PI) and liquid limits (LL).

Low liquid limit (L) samples (<50%) that plot below the A-line or have a plasticity index less than 4 are classified as either organic (O) or inorganic silts (M). Therefore, these samples are classified as either OL or ML. Samples with a low liquid limit that plot within the hatched area are classified as CL-ML, while low liquid limit samples plotting above the A-line and have a plasticity index higher than 7 are considered inorganic clays (CL). High liquid limit (H) samples (>50%) that plot below the A-line are characterized by organic (OH) and inorganic (MH). High liquid limit samples plotting above the A-line are termed CH. A detailed breakdown of the characteristics of each category can be found in Holtz and Kovacs (1981).

B. Sieve Analysis

The only core to undergo sieve analysis in its entirety was RP-C-14-08, located within the extent of the flood-tidal delta and washover deposits. The result of sieving the sample is shown in Figure 26 and Table 3. The USCS considers sediments with particle sizes ranging from 0.075 to 4.0 mm as sand. The particle size of fine sand is from 0.075 to 0.425 mm. Based on the grain size distribution in figure 26, sand within RP-C-14-08 is classified as fine sand.

This classification is based on the percentage of the total sample retained on the No. 200 sieve. The USCS classifies soils that have 5-12% of sediment passing the No. 200 sieve as borderline soils. These soils plot along the border of two classifications and require a dual symbol based on gradation and plasticity characterisitics. RP-C-14-08 had 8% of the total sediment pass the No. 200 sieve. USCS requires the plasticity characteristics to be determined in order to better define the soil's properties; however, these tests are typically run on muddy soils. RP-C-14-08 was classified purely on the gradation curve and was assigned the classification of SP-SM.

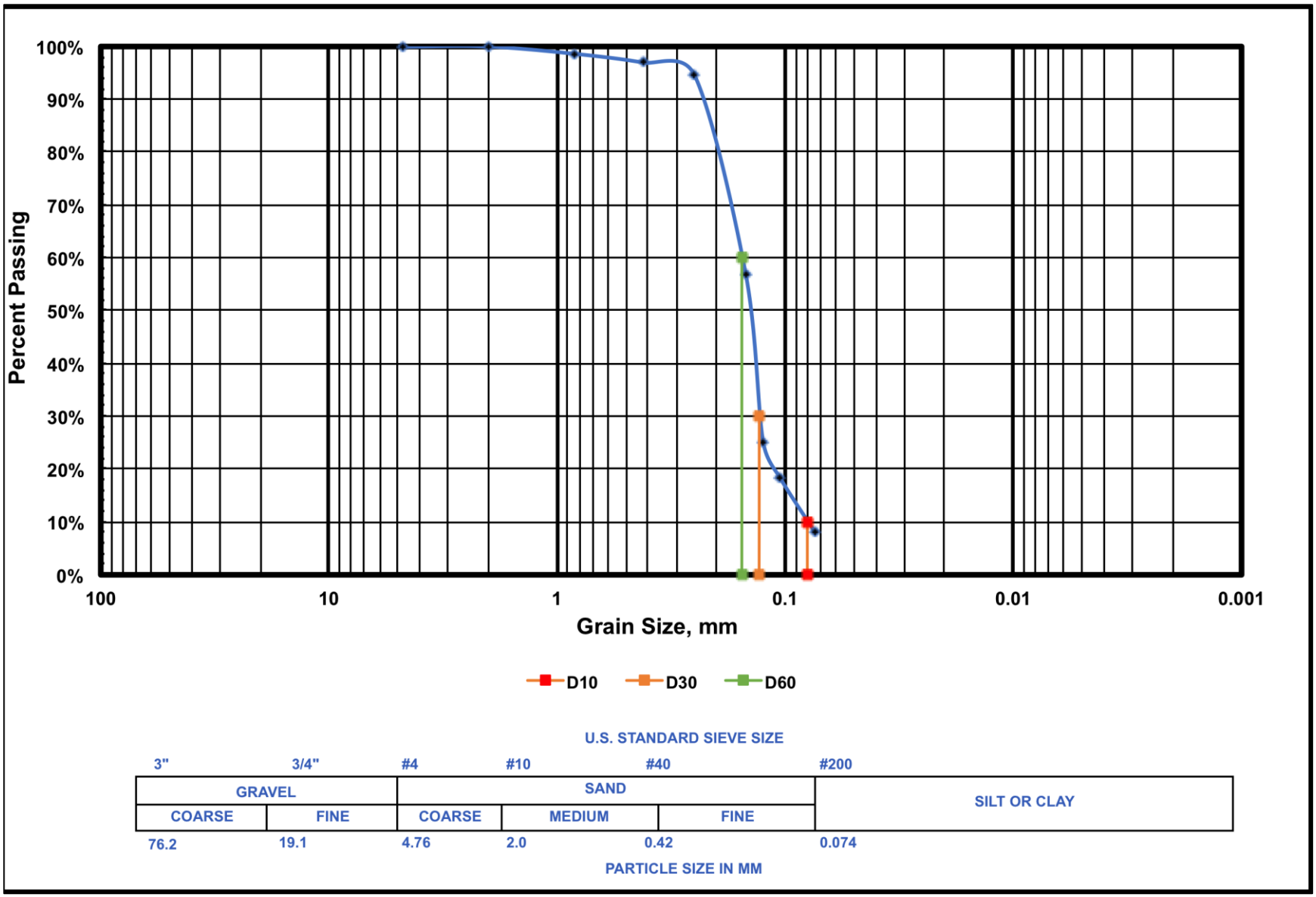

Figure 26. RP-C-14-08 Grain Size. Grain size distribution of push-core RP-C-14-08.

Table 3. RP-C-14-08 Grain Size Analysis. Sieve results showing the percent of sediment passing each sieve.

Sieve	Opening (mm)	% Passing
No. 4	4.760	100.00%
No. 10	2.000	99.97%
No. 20	0.840	98.62%
No. 40	0.420	96.96%
No. 60	0.250	94.60%
No. 100	0.149	56.96%
No. 120	0.125	25.22%
No. 140	0.105	18.26%
No. 200	0.074	8.06%

4.3.2 Consolidation and Settlement

Results from the consolidation tests were used to calculate the saturated unit weight (γ_{sat}) and compression index (C_c) of six samples taken from four push-cores acquired in the backbarrier environment of West Belle Pass Barrier. Table 4 lists the laboratory test results for all of the four cores tested. Values for cores with a top and bottom sample were averaged before calculating primary consolidation settlement. The top and bottom samples show minor variability in the results with respect to depth. Saturated unit weights of the samples were calculated using the volume of the specimen ring and the moist weight of the sample before testing. The saturated unit weights of the soil samples are between 16.43 and 18.81 kN/m^3, and the compression indexes ranged from 0.22 to 0.32 with an average of 0.25. The consolidation curves for each sample can be found in Appendix C.

Table 4. Push-core Laboratory Results. Results of laboratory tests performed on four of the seven push-cores. Values for cores with two samples were averaged to calculate the primary consolidation settlement.

Sample	γsat (kN/m3)	H (m)	Initial Void Ratio	Compression Index	Insitu Effective Stress at sample depth (kN/m2)	Insitu Effective Stress at midpoint depth (kN/m2)	Increase in Effective Stress (kN/m2)	Primary Consolidation Settlement (mm)	Primary Consolidation Settlement (in)	Sc:H
RP-C-14-01	17.07	1.45	0.7612	0.24881	2.3958	5.26	1	15.48	0.61	1.07%
							2	28.67	1.13	1.98%
							4	50.32	1.98	3.47%
							8	82.26	3.24	5.67%
							12	105.71	4.16	7.29%
							16	124.25	4.89	8.57%
							20	139.59	5.50	9.63%
							24	152.67	6.01	10.53%
RP-C-14-02-Avg	17.885	0.98	0.79735	0.249295	N/A	3.96	1	13.29	0.52	1.36%
							2	24.13	0.95	2.46%
							4	41.22	1.62	4.21%
							8	65.25	2.57	6.66%
							12	82.28	3.24	8.40%
							16	95.48	3.76	9.74%
							20	106.27	4.18	10.84%
							24	115.38	4.54	11.77%
RP-C-14-04	16.43	0.99	0.9453	0.31658	1.84698	3.28	1	18.62	0.73	1.88%
							2	33.31	1.31	3.36%
							4	55.79	2.20	5.64%
							8	86.43	3.40	8.73%
							12	107.66	4.24	10.88%
							16	123.93	4.88	12.52%
							20	137.13	5.40	13.85%
							24	148.22	5.84	14.97%
RP-C-14-07-Avg	16.96	0.96	0.79835	0.2229	N/A	3.43	1	13.22	0.52	1.38%
							2	23.74	0.93	2.47%
							4	39.94	1.57	4.16%
							8	62.20	2.45	6.48%
							12	77.71	3.06	8.09%
							16	89.62	3.53	9.34%
							20	99.29	3.91	10.34%
							24	107.44	4.23	11.19%

Typically, consolidation curves are interpreted using a technique developed by Casagrande (1936) to determine the pre-consolidation stress (σ'_c) of a soil. However, this technique only works if the pre-consolidation stress is greater than the initial load used during testing. In this case, all of the samples are currently experiencing an *in situ* effective stress less than 11.97 kN/m^2 (0.25 tsf). Therefore, Casagrande's simplistic method for determining the pre-consolidation stress does not work on soils with a maximum effective stress less than the first applied load during consolidometer tests. However, it should be noted that 11.97 kN/m^2 is generally accepted as the first load for consolidometer tests for normally consolidated soils.

Using the effective stress equation, the *in situ* effective stresses were calculated. The samples are experiencing an *in situ* effective of 0.9 to 3.0 kN/m^2 depending on the depth of the sample below the mudline. Furthermore, the *in situ* effective stress of the midpoint (H/2) was calculated and used to determine the magnitude of primary consolidation settlement for each sample. The effective stress at the midpoint was used since the water located within the pore spaces can flow upward or downward through overlying (water) and underlying (permeable sand) layers. A range of increasing effective stresses ($\Delta\sigma'$) was used to determine the soil's response to different loads independent of the loading mechanism (natural *vs*. anthropogenic). The change in effective stress calculations incorporated Kuecher's (1994) unit weight of beach sand of 19.72 kN/m^3 with variable thicknesses of washover deposits. The maximum possible thickness of overwash was set at the maximum water depth measurement recorded during coring (i.e., 1.85 m), although it is unlikely that this thickness could be achieved from one storm. However, this means that the highest possible change in effective stress is equal to 18.3 kN/m^2. Effective stresses higher than 18.3 kN/m^2 were used to cover changes in effective stress caused by renourishment projects (i.e., thicker deposits). The values used for changes in effective stress

for the settlement calculations are 1, 2, 4, 8, 12, 16, 20, and 24 kN/m^2. These values, in theory, should cover the majority of possible changes in effective stress caused by overwash and/or renourishment projects.

The primary consolidation settlement (S_c) equation for normally consolidated soils was used to calculate the settlement for four cores. Using the changes in effective stress previously mentioned, the primary consolidation settlement of the sampled backbarrier section ranges from 13 to 152 mm (depending on $\Delta\sigma$'). Using the primary consolidation settlement and change in effective stress, a settlement plot was constructed for each sample (Figure 27). Primary consolidation settlement caused by overwash deposits from one storm can be estimated using the plot if the thickness and saturated unit weight of the overwash deposit is known. For instance, a 0.35 m washover deposit with a saturated unit weight of 17 kN/m^3 yields a change in effective stress of 2.5 kN/m^2. Once the change in effective stress is calculated, the potential ranges of settlement for each of the four cores can be visually estimated using the graph of settlement verse change in effective stress. In this case, the potential primary consolidation settlement for the 0.35 m washover deposit with a saturated unit weight of 17 kN/m^3 ranges from 25-35 mm. In order to further estimate the settlement potential of washover settlement from a single storm, varying thickness were applied to a washover deposit with a saturated unit weight of 19.72 kN/m^3. Figure 27 shows an area in orange that represents the settlement ranges of each of the cores tested as a function of thickness and a saturated unit weight of 19.72 kN/m^3. The area in gray represents a deposit whose thickness is larger than the maximum accommodation space (i.e., restoration projects); however, it is not meant to represent the maximum potential settlement caused by such sediment additions (Figure 27). Lastly, the ratio between primary

consolidation settlement and original soil thickness (H) was calculated to find the change in thickness as a percentage of the original unconsolidated thickness (see Appendix D).

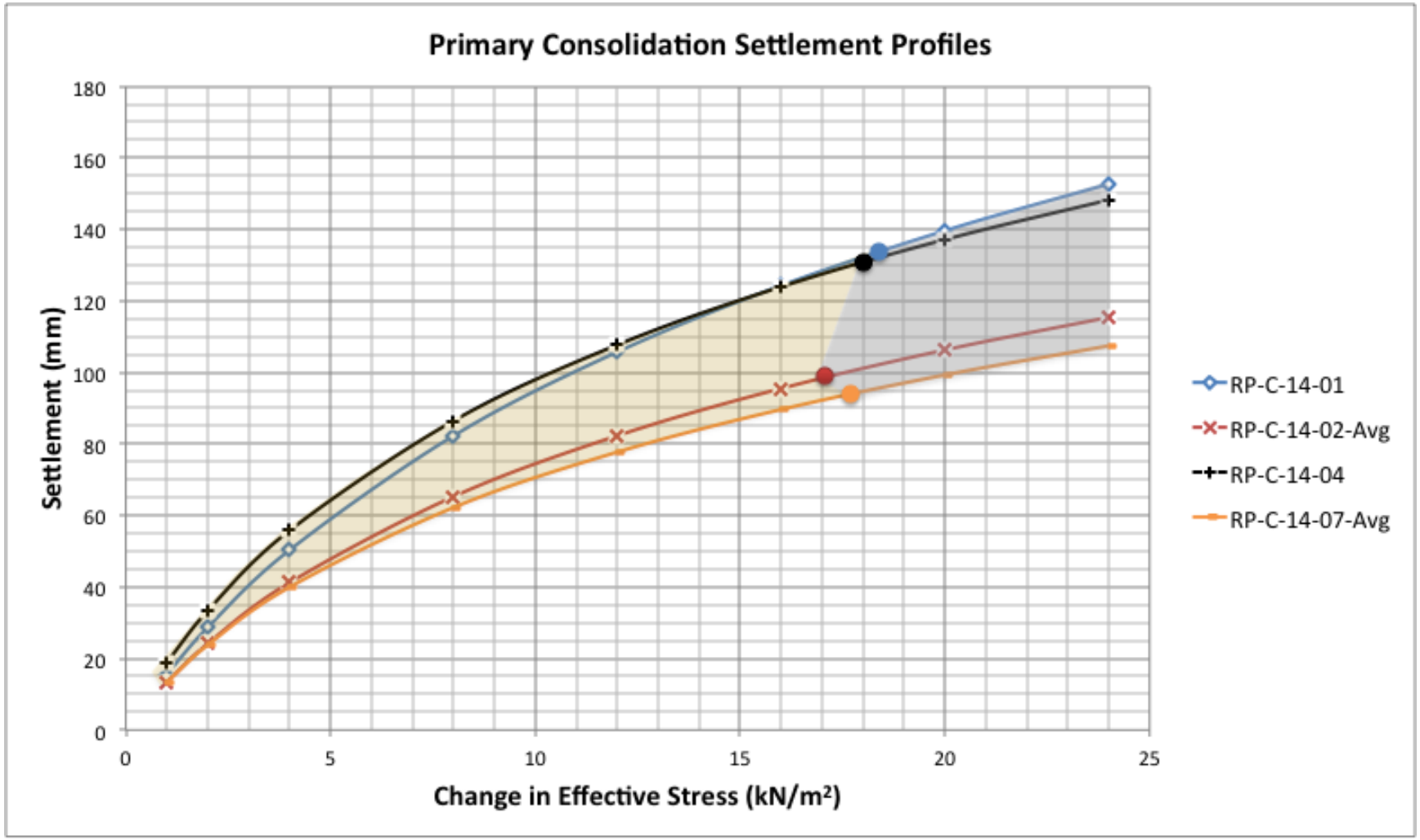

Figure 27. Settlement Profiles. The primary consolidation settlement of four cores plotted against the change in effective stress. The area in orange represents the possible primay consoidation settlement attributed to washover deposition from one storm, where the maximum washover thickness and corresponding change in effective stress are a function of the maximum accommodation space (i.e., water depth at time of sampling). The area in gray represents the primary consolidation settlement ranges attributed to potential restoration projects, when the load's thickness exceeds the maximum water depth at the time of sampling. The color-filled circles represent the maximum change in effective stress that corresponds to the complete infilling of accommodation space.

4.4 Discussion

4.4.1 Washover-Induced Consolidation

Consolidation of backbarrier facies affects nearly all barrier islands within the MRDP, and the resulting settlement is just one of many mechanisms of subsidence. The consolidation data described herein was used to evaluate the primary consolidation settlement caused by loading the backbarrier facies of West Belle Pass Barrier with washover deposits caused by overwash processes during one storm event. The primary consolidation settlement profile of each sample shows a range of possible settlement that can occur after loading regardless of the loading mechanism; therefore, it can be used to determine the possible ranges of primary consolidation settlement caused by washover deposits (fans, terraces, and sheets) and renourishment projects. It is important to note that the settlement profiles do not account for elastic settlement as well as secondary compression settlement, and one may confidently assume that the total settlement for a particular event will be larger in magnitude compared to primary consolidation settlement. Also, these results do not infer the time for primary consolidation settlement to take place. The time factor can be calculated using the data from the consolidation tests, but it is not the focus of this study.

In order to determine meaningful settlement predictions, practical areas and thicknesses of washover deposits should be used. Ritchie and Penland (1988) noted that overwash events occur regularly along the Louisiana coast, and the distribution and geomorphology of these deposits is governed, in part, by the passing of cold fronts and hurricanes. The amount and extent of settlement caused by overwash depends on the thickness, spatial extent, and unit weight of washover deposits. The area and thickness of overwash deposits is variable and somewhat unpredictable due to the amount of factors controlling the distribution of sediment from the

beach to the backbarrier (i.e., dune elevation, storm surge elevations, etc.). Furthermore, overwash deposits are not uniform in thickness. These deposits are expected to be thicker immediately behind the barrier island and thin as they move further out into the bay/lagoon; therefore, they do not apply stress evenly throughout the subsurface. Ritchie and Penland (1989) analyzed washover penetration distances from 1978 to 1984 just west of the Belle Pass jetties within the study site. The authors found that the average penetration of washover sheets was over 200 m, which was nearly twice the average of washover penetration immediately east of the Belle Pass jetties (Ritchie and Penland, 1989). Furthermore, Morton and Sallenger (2003) compared several washover deposit studies along the Gulf of Mexico and Atlantic coasts caused by a single storm event (category 3-5) and found that washover thicknesses range from 0.1 to 1.5 m with an average thickness of approximately 0.68 m. Even with the variability in size, location, and thickness of these deposits, simplistic settlement surfaces can be made if the thickness of the deposit is known at multiple locations. It is important to note that the location of the push-cores is much farther than the maximum washover penetration reported in either Ritchie and Penland (1989) or Morton and Sallenger (2003). Hence, the results in this study represent the settlement caused by an initial washover deposit onto the backbarrier and not the settlement caused by stacked overwash deposits typically observed in the field. Nevertheless, applying an average washover thickness of 0.68 m with a saturated unit weight of 19.72 kN/m^3 yields approximately 55 to 78 mm of primary consolidation settlement. Minimum and maximum washover thicknesses of 0.10 m and 1.5 m, respectively, were used to create a potential range of settlement. These thicknesses result in a range of 12 to 120 mm of settlement using the settlement profiles. If one assumes that this settlement is completed within one year of loading, these rates are anywhere from approximately 1.5 to 15.8 times higher than the time-averaged rate

of subsidence of 7.59 ±0.23 mm/yr at the Grand Isle tide gauge. However, using the average washover thickness of 0.68 m and corresponding settlement over a one-year period results in a rate 7.2 to 10.3 times higher than the Grand Isle rate of subsidence. It is important to note that the only way to correctly estimate the time required for the completion of primary consolidation is by calculating the coefficient of consolidation (C_v) using either the logarithm-of-time or square-root-of-time methods.

4.4.2 Barrier Island Overwash and Consolidation Model

A simplistic conceptual model illustrating an overwash event and subsequent consolidation of recently deposited backbarrier sediment from washover deposits is presented (Fig. 28). This model was adopted from Rosati et al.'s (2010) 2D MCO model that uses various geotechnical parameters and marine processes to estimate settlement. Stage 1 (time = 0) represents an immature barrier island along a microtidal, wave-dominated coast that has not been altered by storms and does not contain any tidal inlets or breaches. The backbarrier environment is void of any washover deposits and has not been loaded (other than its own weight) by any sediment. Dune and beach elevations are sufficient enough to prevent the occurrence of overwash. As time increases, the increase in effective stress from the barrier island along with marine reworking and other geologic processes causes the barrier island to subside. This change in elevation makes the barrier island susceptible to overwash during elevated water levels. Stage 2 (time = 1) marks the first storm event and overwash processes to impact the barrier resulting in the deposition of sediment within the backbarrier in the form of washover terraces, sheets, or fans. The initial deposition causes an increase in total stress, which is equal to the amount of pore pressure. Elastic settlement is the only settlement that has occurred as a result of loading. At Stage 3 (time 2), pore pressure begins translating into effective stress causing the expulsion of

water from voids. This expulsion signifies the beginning of primary consolidation settlement, and a reduction in volume is expected and can be estimated based on the consolidometer results. The barrier island enters Stage 4 (time = ∞) as all of the water has been expelled from the soil layer, and primary and secondary compression are completed. This theoretical model illustrates a barrier's response to a single overwash event wherein a washover deposit of some thickness loads previously unconsolidated backbarrier deposits. It is important to remember that the change in effective stress caused by any load is experienced to some depth, which is well below the depth of the facies in question. This means that compressible layers below backbarrier deposits will also consolidate leading to a larger amount of elevation change.

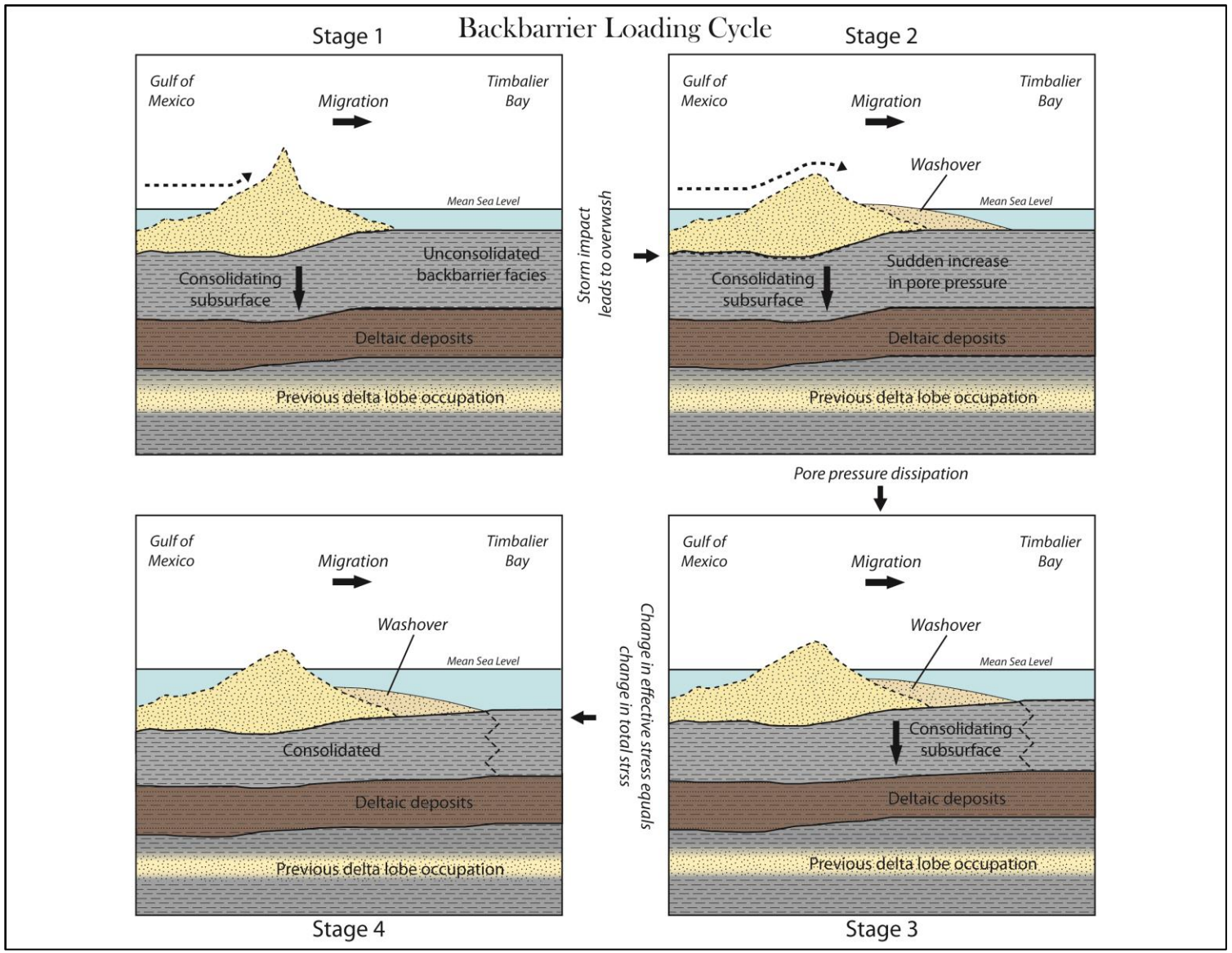

Figure 28. Washover Loading Model. A 4-stage conceptual model illustrating the processes involved before, during, and after loading by washover deposits (adopted from Rosati et al., 2010).

Chapter 5. Conclusion

Historical shoreline datasets and core samples were used to evaluate the morphological changes and primary consolidation potential of near-surface backbarrier facies at West Belle Pass Barrier. The morphological evolution of West Belle Pass Barrier was influenced by the addition and modification of the Belle Pass jetties, as well as an expanding tidal inlet complex at Raccoon Pass. Yet, jetty installation alone does not appear to be the main cause for shoreline deterioration at the study site. Expansion of the tidal complex at Raccoon Pass after 1956 appears to be the main factor that caused severe erosion downdrift of the jetty system. Specifically, erosion caused by Hurricane Betsy in 1965 initiated tidal inlet expansion. Longshore transport (sourced either updrift or downdrift of the jetties) and tidal inlet growth allowed for the transportation and sequestration of sediment within the backbarrier environment of West Belle Pass Barrier, creating a system wherein sediment is continuously "recycled" and deposited into the backbarrier. This deposit may serve as a future sediment source as the barrier system continues to translate landward. However, there may be only a handful of locations along Louisiana's coast where this system holds true.

Furthermore, the transportation of sediment from the shoreface/beach into the backbarrier creates an environment wherein previously unloaded strata consolidates and settles. Using numerous push-cores and accepted consolidation techniques, the primary consolidation settlement potential of backbarrier facies was determined in a framework of loading from storm overwash. A conceptual model of backbarrier loading adopted from Rosati et al. (2010) was presented; wherein washover deposits loaded a completely unconsolidated near-surface substrate. Although it is unlikely that washover deposits will reach the push-core locations with the thicknesses used in calculating the corresponding settlement (with respect to the modern

shoreline), the conceptual model and settlement calculations gives insight into the magnitude of potential settlement that could occur. However, as the modern shoreline transgresses these same backbarrier deposits will become prone to loading. Furthermore, it is likely that coastal restoration projects or potential river diversions as well as storm washover could result in the addition of sediment to previously unconsolidated backbarrier facies. The results could serve as a model for estimating the potential primary consolidation settlement as long as the loading characteristics (i.e., unit weight and thickness) are known. The results within this study may prove useful for evaluating and monitoring past, present, and future renourishment efforts of Louisiana's barriers, which are continuously starved from fluvially sourced sediment.

References

Barras, J.A., Bourgeois, P.E., and Handley, L.R., 1994. Land loss in coastal Louisiana 1956-90. National Biological Survey, National Wetlands Research Center Open File Report 94-01. 4 pp. 10 color plates.

Beven II, J.L. and Kimberlain, T.B., 2009. Tropical Cyclone Report Hurricane Gustav (AL072008) 25 August–4 September 2008. *National Hurricane Center*.

Blum, M.D. and Roberts, H.H., 2012. The Mississippi delta region: past, present, and future. *Annual Review of Earth and Planetary Sciences*, *40*, pp.655-683.

Casagrande, A., 1936. The determination of the pre-consolidation load and its practical significance. In *Proceedings of the international conference on soil mechanics and foundation engineering* (Vol. 3, pp. 60-64). Harvard University Cambridge.

Coduto, D.P., Yeung, M.C.R. and Kitch, W.A., 1999. *Geotechnical engineering: principles and practices* (Vol. 759). Upper Saddle River, NJ: Prentice Hall.

Coleman, J.M., 1988. Dynamic changes and processes in the Mississippi River delta. *Geological Society of America Bulletin*, *100*(7), pp.999-1015.

Coleman, J.M., Roberts, H.H. and Stone, G.W., 1998. Mississippi River delta: an overview. *Journal of Coastal Research*, pp.699-716.

Couvillion, B.R., Barras, J.A., Steyer, G.D., Sleavin, William, Fischer, Michelle, Beck, Holly, Trahan, Nadine, Griffin, Brad, and Heckman, David, 2011. Land area change in coastal Louisiana from 1932 to 2010: U.S. Geological Survey Scientific Investigations Map 3164, scale 1:265,000, 12 pp.

Dantin, E.J., Durbin, W.T. and Whitehurst, C.A., 1978. Littoral Drift and Erosion at Belle Pass, Louisiana. *Journal of the Waterway, Port, Coastal and Ocean Division*, *104*(4), pp.375-390.

Das, B. and Sobhan, K., 2014. *Principles of geotechnical engineering*. Cengage Learning.

De Beaumont, E., 1845. Leçons de Géologie Practique. Reproduced in Schwartz, M.L. (Editor), 1973. Barrier Islands. Benchmark Pap. in Geol., Vol. 9, Dowden, Hutchison and Ross, Stroudsburg, Pa., pp. 5-43.

Fairbanks, R.G., 1989. A 17, 000-year glacio-eustatic sea level record: influence of glacial melting rates on the Younger Dryas event and deep-ocean circulation. *Nature*, *342*(6250), pp.637-642.

Fisk, H.N., 1944. Geological investigations of the alluvial valley of the lower Mississippi River: Vicksburg, Miss., U.S. Army Engineers, Mississippi River Commission.

Fisk, H.N. and McFarlan, E., 1955. Late Quaternary deltaic deposits of the Mississippi River (Local sedimentation and basin tectonics). *Geological Society of America Special Papers*, *62*, pp.279-302.

Frazier, D.E., 1967. Recent Deltaic Deposits of the Mississippi River: Their Development and Chronology. *Gulf Coast Association of Geological Societies Transactions*, v. 17, p. 287-315.

Gilbert, G.K., 1885. The topographic features of lake shores: U.S. Geological Survey 5th Annual Report, p. 87-88.

Hansbo, S., 1960. Consolidation of clay with special reference to influence of vertical sand drains. Swedish Geotechnical Institute, *Proc. No. 18*, 41-61.

Holtz, R.D. and Kovacs, W.D., 1981. *An introduction to geotechnical engineering* (No. Monograph).

Hoyt, J.H., 1967. Barrier island formation. *Geological Society of America Bulletin*, *78*(9), pp.1125-1136.

Kolb, C.R. and Van Lopik, J.R., 1958. Geology of the Mississippi Deltaic Plain-Southeastern Louisiana. U.S. Army Corps of Engineers, Waterways Experiment Station, Technical Report 2, 482p.

Kolker, A.S., Allison, M.A. and Hameed, S., 2011. An evaluation of subsidence rates and sea-level variability in the northern Gulf of Mexico. *Geophysical Research Letters*, *38*(21).

Kuecher, G.J., 1994. Geologic Framework and Consolidation Settlement Potential of the Lafourche Delta, Topstratum Valley Fill; Implications for Wetland Loss in Terrebonne and Lafourche Parishes, Louisiana. PhD Dissertation, Department of Geology and Geophysics, Louisiana State University, 344p.

Kulp, M., FitzGerald, D., & Penland, S., 2005b. Sand-rich lithosomes of the Holocene Mississippi River Delta Plain', *Special Publication - Society For Sedimentary Geology*, 83, pp. 279-293.

Kulp, M., Penland, S., Flocks, J., and Kindinger, J., 2002. Regional geology, coastal processes, and sand resources in the vicinity of East Timbalier Island: Louisiana Department of Natural Resources Technical Report, 101 p.

Kulp, M., Penland, S., Williams, S.J., Jenkins, C., Flocks, J. and Kindinger, J., 2005a. Geologic framework, evolution, and sediment resources for restoration of the Louisiana coastal zone. *Journal of coastal research*, pp. 56-71.

Martinez, L., Penland, S., Fearnley, S., O'Brien, S., Bethel, M. and Guarisco, P., 2009. Louisiana Barrier Island Comprehensive Monitoring Program (BICM), Task 3: Shoreline change analysis: 1800's to 2005*: Pontchartrain Institute for Environmental Sciences* (No. 001-2008, p. 27). Technical Report

McBride, R.A., Penland, S., Hiland, M.W., Williams, S.J., Westphal, K.A., Jaffe, B.E. and Sallenger Jr, A.H., 1992. Analysis of barrier shoreline change in Louisiana from 1853 to 1989 in *Louisiana Barrier Island Erosion Study: Atlas of shoreline changes in Louisiana from 1853 to 1989*, pp.36-97.

McGee, W.J., 1890. Encroachments of the sea. Forum Publishing Company, vol. 9, p. 437-449.

McIntire, W.G., 1954. Correlation of prehistoric settlements and delta development. Louisiana State University, Coastal Studies Institute Technical Report 5, 65p.

Miner, M., Kulp, M., Penland, S., Weathers, D., Motti, J.P., McCarty, P., Brown, M., Martinez, L., Torres, J., Flocks, J.G. and Dewitt, N., 2009. Louisiana Barrier Island Comprehensive Monitoring Program (BICM) Volume 3: Bathymetry and Historical Seafloor Change 1869-2007 Part 1: South-Central Louisiana and Northern Chandeleur Islands, Bathymetry Methods and Uncertainty Analysis Final Report.

Mitchell, J.K. and Soga, K., 1976. *Fundamentals of Soil Behavior*, Wiley, New York.

Morton, R.A. and Sallenger Jr, A.H., 2003. Morphological impacts of extreme storms on sandy beaches and barriers. *Journal of Coastal Research*, pp.560-573.

Mossa, J., Penland, S. and Moslow, T.F., 1985. Coastal structures in Louisiana's Barataria Bight. Louisiana Geological Survey.

Penland, S., Boyd, R. and Suter, J.R., 1988a. Transgressive depositional systems of the Mississippi delta plain: a model for barrier shoreline and shelf sand development. *Journal of Sedimentary Research, 58*(6), pp.932-949.

Penland, S., Ritchie, W., Boyd, R., Gerdes, R.G. and Suter, J.R., 1986. The Bayou Lafourche delta, Mississippi River delta plain. *Geological Society of America, Decade of North American Geology*, pp.447-452.

Penland, S. and Suter. J.R., 1988b. Barrier Island Erosion and Protection in Louisiana: A coastal Geomorphological Perspective: *Gulf Coast Association of Geological Societies Transactions* v. 38, p. 331-342.

Poppe, L.J. and Eliason, A.E., 2008. A Visual Basic program to plot sediment grain-size data on ternary diagrams: Computers and Geosciences, v. 34, p. 561-565.

Reinson, G.E., 1979. Facies models 14. Barrier island systems. *Geoscience Canada, 6*(2).

Ritchie, W. and Penland, S., 1988. Rapid dune changes associated with overwash processes on the deltaic coast of South Louisiana. *Marine Geology*, *81*(1), pp.97-122.

Ritchie, W. and Penland, S., 1989. Erosion and washover in coastal Louisiana Coastlines of the world. pp. 253-264 United States: American Society of Civil Engineers : New York, NY, United States GeoRef, EBSCO*host*, viewed 22 March 2016.

Roberts, H.H., 1997. Dynamic Changes of the Holocene Mississippi River Delta Plain: The Delta Cycle. *Journal of Coastal Research*, 13(3), 605-627.

Robinson, R.G. and Allam, M.M., 1998. Effect of clay mineralogy on coefficient of consolidation. *Clays and clay minerals*, *46*(5), pp.596-600.

Rosati, J.D., Dean, R.G. and Stone, G.W., 2010. A cross-shore model of barrier island migration over a compressible substrate. *Marine Geology*, *271*(1), pp.1-16.

Roth, D., 2010. *Louisiana hurricane history*. National Weather Service.

Scott, L.C., 2008. The economic impacts of Port Fourchon on the national and Houma MSA economies. *Greater Lafourche Port Commission*. pp.1-28

Shepard, F.P., 1954. Nomenclature based on sand-silt-clay ratios. *Journal of Sedimentary Research*, *24*(3).

Skempton, A.W., 1960. Correspondence. *Geotechnique*, Vol. 10, No. 4, 186

Stewart, S.R., 2006. Tropical Cyclone Report, Hurricane Cindy, 3–7 July, 2005.

Terzaghi, K.V., 1936. Relation between soil mechanics and foundation engineering. In *Proceedings of the International Conference on Soil Mechanics and Foundation Engineering* (Vol. 3, pp. 13-18).

Terzaghi, K., 1943, *Theoretical Soil Mechanics*, John Wiley and Sons, Inc.

Törnqvist, T.E., Kidder, T.R., Autin, W.J. and van der Borg, K., 1996. A revised chronology for Mississippi River subdeltas. *Science*, *273*(5282), p.1693-1696.

Winehurst, C.A., 1974. A parametric study of water resources variables in a delta region of south Louisiana – Bayou Lafourche. *Technical Report to the Office of Water Research Technology*, Division of Engineering Research, Louisiana State University, Baton Rouge, La., Vol. 1, pp. 38-39.

Appendix A

UNIVERSITY OF NEW ORLEANS

DEPARTMENT OF GEOLOGY AND GEOPHYSICS

VIBRACORE DESCRIPTION SHEET

CORE ID: BP-14-01 DATE: 7/2/14 DESCRIBED BY: J. Kramer

ELEVATION: WD = 1.85 m LOCATION: Barataria Pass → Bay, SE of Devil's Point

CORE LENGTH: 2.54 m LAT/LONG: N 29.12952° W090.25602°

TOTAL DEPTH: 3.3824 m COMPACTION: 0.8424 m

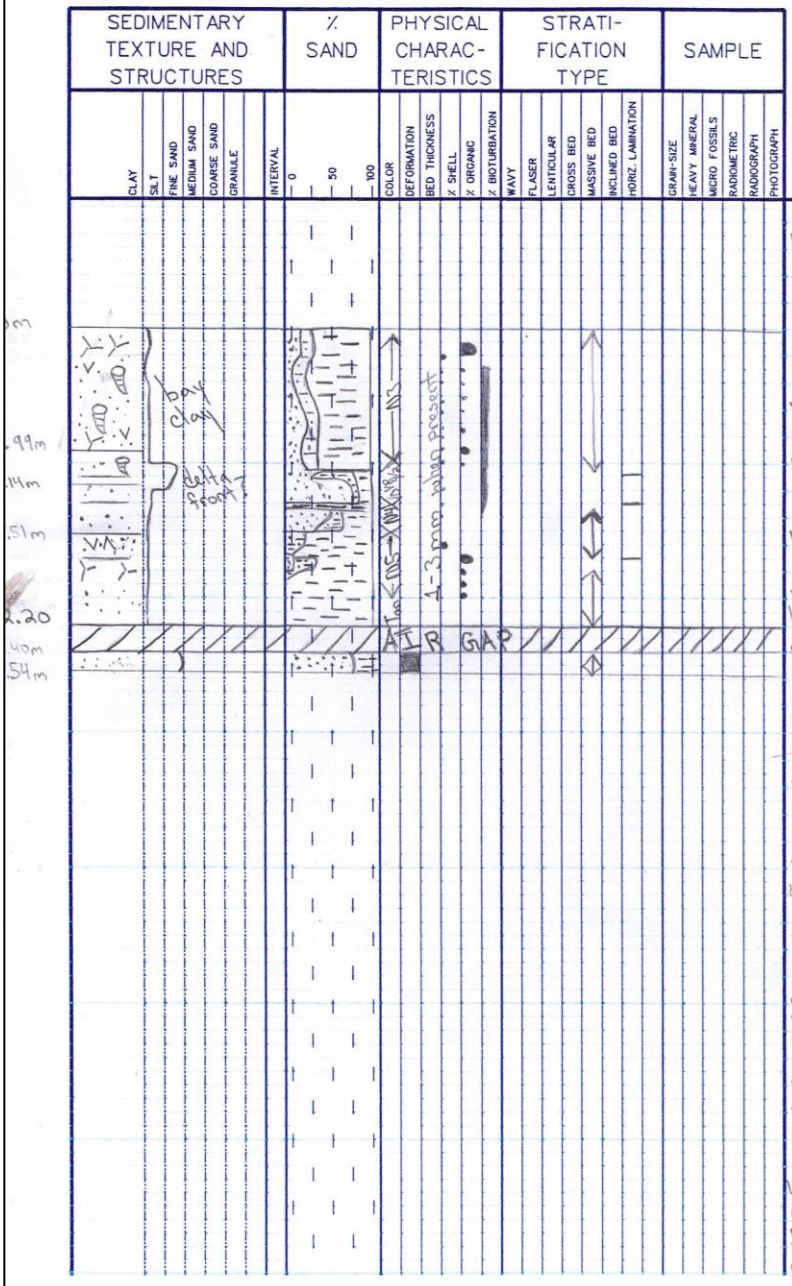

PHYSICAL DESCRIPTION

Unit A: 0.00 - 0.99 m
Clay with some silt and trace amounts of sand, dark gray (N3) with a grayish black (N2) organic layer from 0.10 - .17m, massive bedding throughout, moderate bioturbation from 0.20 - 0.99m, sprinkled w/ shell fragments < 2mm in length, peppered coffee grounds from 0.70 - .99m, large piece of wood (4cm x 1.5cm) at 0.95m, gradational bottom contact

Unit B: 0.99 - 1.14
Clay with sand lenses, dark yellowish brown (10YR 4/2), discontinuous horizontal sand lense at 1.08m, mainly massive bedding, mild bioturbation, gradational bottom contact, trace shell frag.

Unit C: 1.14 - 1.51 m
Clayey silty sand, med. dark gray (N4), massive bedding, trace shell fragments < 2mm in length, peppered organic content, 1.33 m interbedded clay & silt lenses, moderate burrowing, somewhat sharp contact

Unit D: 1.51 - 2.20 m
Clay, med. gray (N5) grading to dark yellowish brown (10YR 4/2) at 2.03m, Massive bedding with one silty organic lense at 1.70 m (3-4cm thick), large shell (4cm x 1.5cm) at 1.53 m, generously sprinkled w/ organic content (small chips < 1mm), sharp bottom contact

Unit E: 2.40 - btm
Clayey sand, med gray (N5), sand deformed: fell down to bottom of tube while sampling, no shells, no organics

UNIVERSITY OF NEW ORLEANS

DEPARTMENT OF GEOLOGY AND GEOPHYSICS

VIBRACORE DESCRIPTION SHEET

CORE ID: RP-14-03 DATE: 7/3/14 DESCRIBED BY: T. Kramer

ELEVATION: WD=1.83m LOCATION: Raccoon Pass, Bay-wash

CORE LENGTH: 2.4638 m LAT/LONG: N 29.12269° W 090.25567°

TOTAL DEPTH: 3.0913 m COMPACTION: 0.6275 m

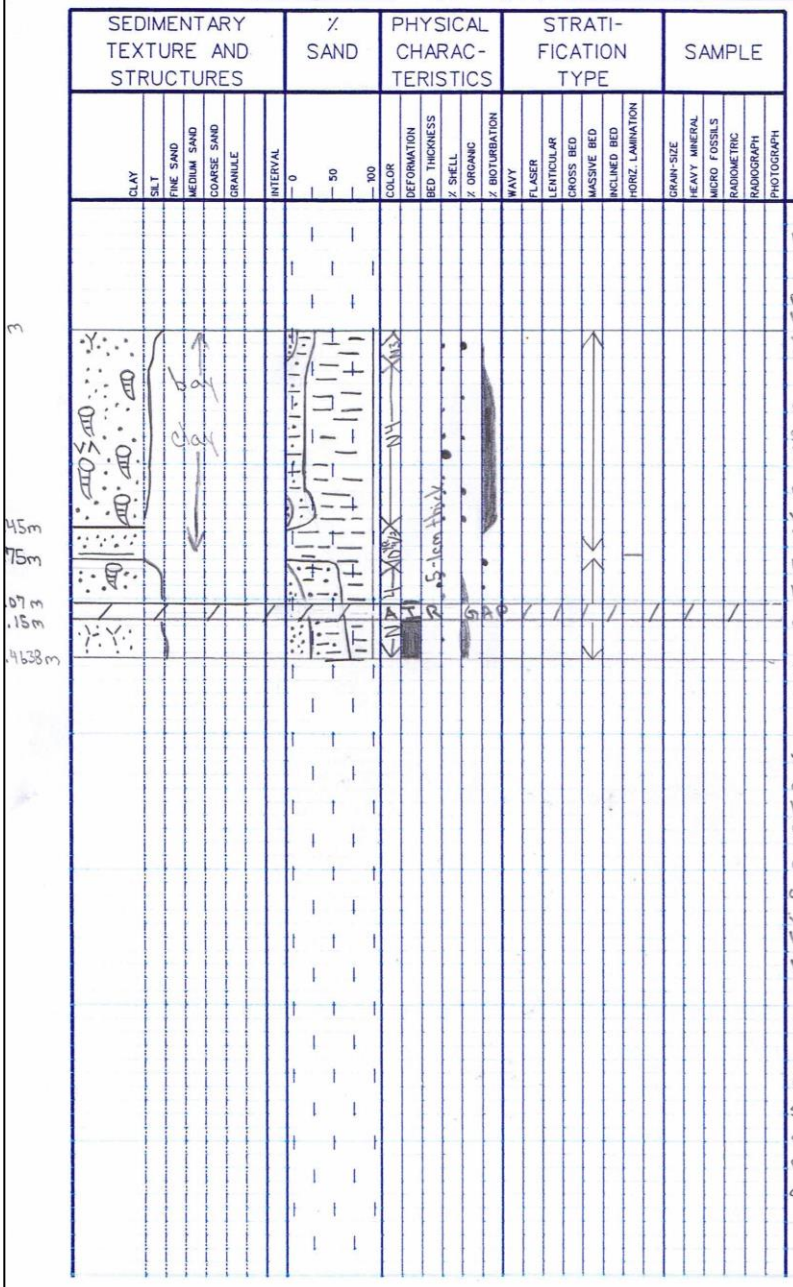

PHYSICAL DESCRIPTION

Unit A: 0.00 - 1.45 m
Unconsolidated silty clay, med. dark gray (N4), massive bedding to non discernable bedding due to bioturbation from 0.3 to 1.45m, 10cm thick dark gray (N3) organic silty clay layer from 0.07-0.17m, sprinkled w/ trace shell fragments 1-3mm in length throughout, some organics peppered throughout, piece of wood at 0.72m (.5cm x 3mm) and at 1.17m (1cm x 1cm), large intact shell at 0.92m (same kind found in RP-14-01 at 1.53m), sharp bottom contact (possibly erosional?) w/ rip up clay clasts

Unit B: 1.45 - 1.75m
Fat clay, dark yellowish brown (10YR 4/2), massive bedding with one horizontal silty clay lense at 1.65m (med dark gray color) roughly 1cm thick, 2-3 vertical burrows from 1.66-1.71m filled w/ silty clay (skolithos), some of the clay is oxidized more than the rest forming irregular coloration (most oxidation at beginning and end of unit), sharp bottom contact

Unit C: 1.75 - btm
Silty clay with trace sand, med dark gray (N4) grading to a darker silty clay, massive bedding, trace shell fragments < 2mm in length, minimal bioturbation, NOTE AIR GAP and DEFORMATION at bottom.

sheet 1 of 2

UNIVERSITY OF NEW ORLEANS

DEPARTMENT OF GEOLOGY AND GEOPHYSICS

VIBRACORE DESCRIPTION SHEET

CORE ID: RP-14-04 DATE: 7/7/14 DESCRIBED BY: T. Kramer

ELEVATION: M.D. = 1.72m LOCATION: Raccoon Pass, Northeast corner of bay

CORE LENGTH: 2.98m LAT/LONG: N29.12474 W90.2429

TOTAL DEPTH: 3.61m COMPACTION: 0.6295m

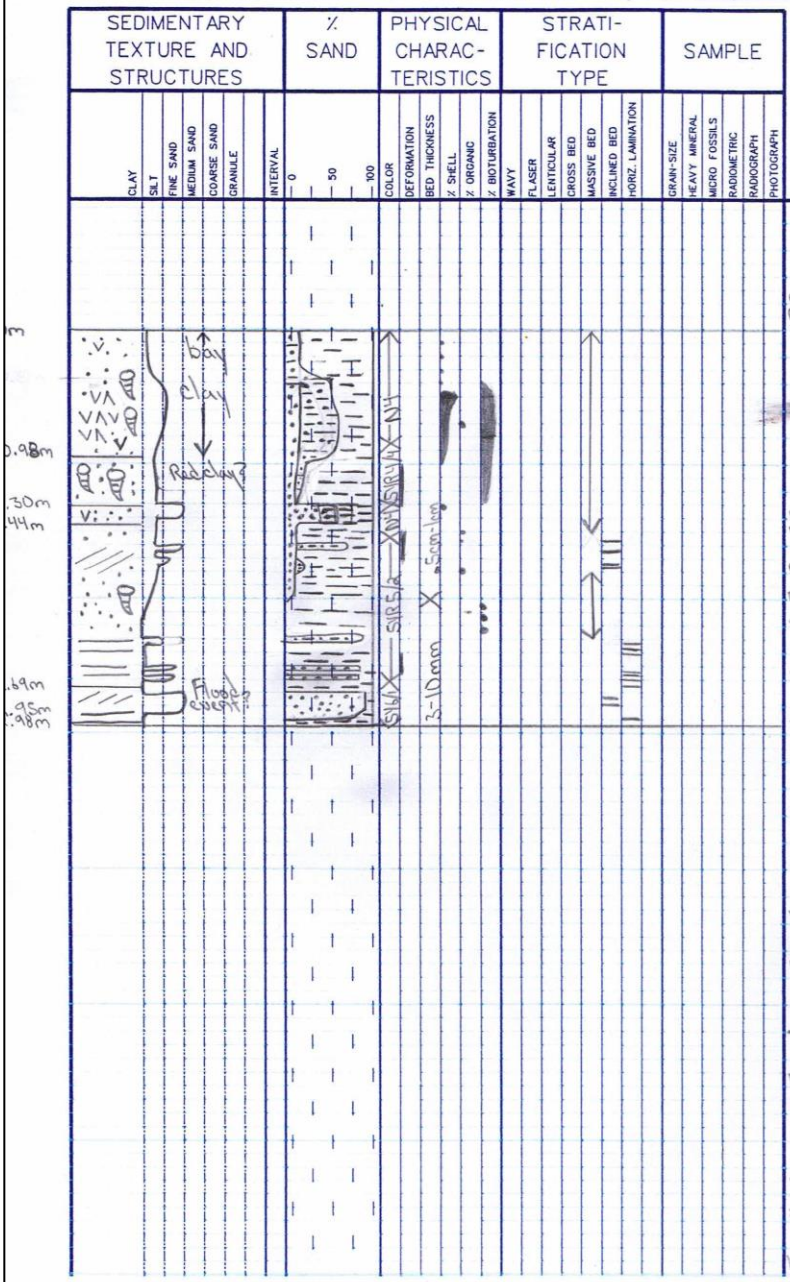

PHYSICAL DESCRIPTION

Unit A: 0.0 - 0.98m
Silty clay, med. dark gray (N4), massive bedding, sprinkled w/ shell fragments (<3mm in length), moderate bioturbation (some skolithos), trace organics, all grading to slightly sandier silty clay, med. dark gray (N4), with shells grading from large (4cm x 3cm) intact clams (Rangia) at 0.48cm to smaller shell fragments roughly 3-5mm in length), moderate to heavy bioturbation from 0.50 - 0.98m, rafted wood (2cm x .5cm) at 0.73m, massive to non discernable bedding in this sub unit (.38 - .98m) trace organics throughout, transitional bottom contact

Unit B: 0.98 - 1.30m
Clay with gray silty sand burrows, Moderate brown (5YR 4/4), massive bedding, moderate bioturbation throughout (vertical and curving/diagonal burrows: ( ), sharp bottom contact

Unit C: 1.30 - 1.44m
Sandy clay, dark gray (N4), massive bedding with shells at 1.34m (.5cm x .5cm) and trace organics, rip up mud clasts (.5cm x .5cm), erosional bottom contact

Unit D: 1.44 - 2.69 m
Mostly fat clay, pale brown (5YR 5/2), massive bedding with two large 4cm thick inclined dark gray silty sand lenses at 1.58m: 1.65m, smaller (3cm x 3mm) dark gray silty sand inclined laminae (ripples) from 1.70 - 1.80m, rafted wood (1cm x .5cm) at 1.81m, burrows at 2.02m (skolithos), horizontal bedding

sheet 2 of 2

UNIVERSITY OF NEW ORLEANS

DEPARTMENT OF GEOLOGY AND GEOPHYSICS

VIBRACORE DESCRIPTION SHEET

CORE ID: RP-14-04 DATE: 7/7/14 DESCRIBED BY: T. Kramer

ELEVATION: WD = 1.72m LOCATION: Raccoon Pass, NE corner of bay

CORE LENGTH: 2.98m LAT/LONG: N 29.12474 W 90.2429

TOTAL DEPTH: 3.61m COMPACTION: 0.6295m

SEDIMENTARY TEXTURE AND STRUCTURES								% SAND	PHYSICAL CHARACTERISTICS					STRATIFICATION TYPE							SAMPLE					PHYSICAL DESCRIPTION
CLAY	SILT	FINE SAND	MEDIUM SAND	COARSE SAND	GRANULE		INTERVAL	0 — 50 — 100	COLOR	DEFORMATION	BED THICKNESS	% SHELL	% ORGANIC	% BIOTURBATION	WAVY	FLASER	LENTICULAR	CROSS BED	MASSIVE BED	INCLINED BED	HORIZ. LAMINATION	GRAIN-SIZE	HEAVY MINERAL	MICRO FOSSILS	RADIOMETRIC	RADIOGRAPH	PHOTOGRAPH	
																											of sandy silt from 2.30 - 2.39m (avg. thickness = 5mm), interbedded sand : clay lenses from 2.51 - 2.69m avg. thickness 1-2cm (4-5 sand leases : 4-5 clay lenses), all have sharp/ erosional bottom contacts, except at the unit bottom contact where it looks like mud was deposited / draped on top of the Unit E sand. Unit E: 2.69 - 2.95m Sand, light olive gray (5Y 6/1) with horizontal laminations ~ avg. thickness = 5mm, some deformation at 2.90m, one tan clay lamination at 2.94m ~ .5cm thick on top a .5cm sand layer that has an erosional bottom contact (U-shaped, possible gully) Unit F: 2.95 - btm Clay, med. gray (N5), massive bedding, (short unit ~3-4cm

UNIVERSITY OF NEW ORLEANS

Sheet 1 of 2

DEPARTMENT OF GEOLOGY AND GEOPHYSICS

VIBRACORE DESCRIPTION SHEET

CORE ID: RP-14-06 DATE: 7/8/14 DESCRIBED BY: T. Kramer

ELEVATION: WD = 1.57m LOCATION: Raccoon Pass, SE corner of bay

CORE LENGTH: 2.53m LAT/LONG: N29.11161 W90.24507

TOTAL DEPTH: 2.97m COMPACTION: 0.44 m

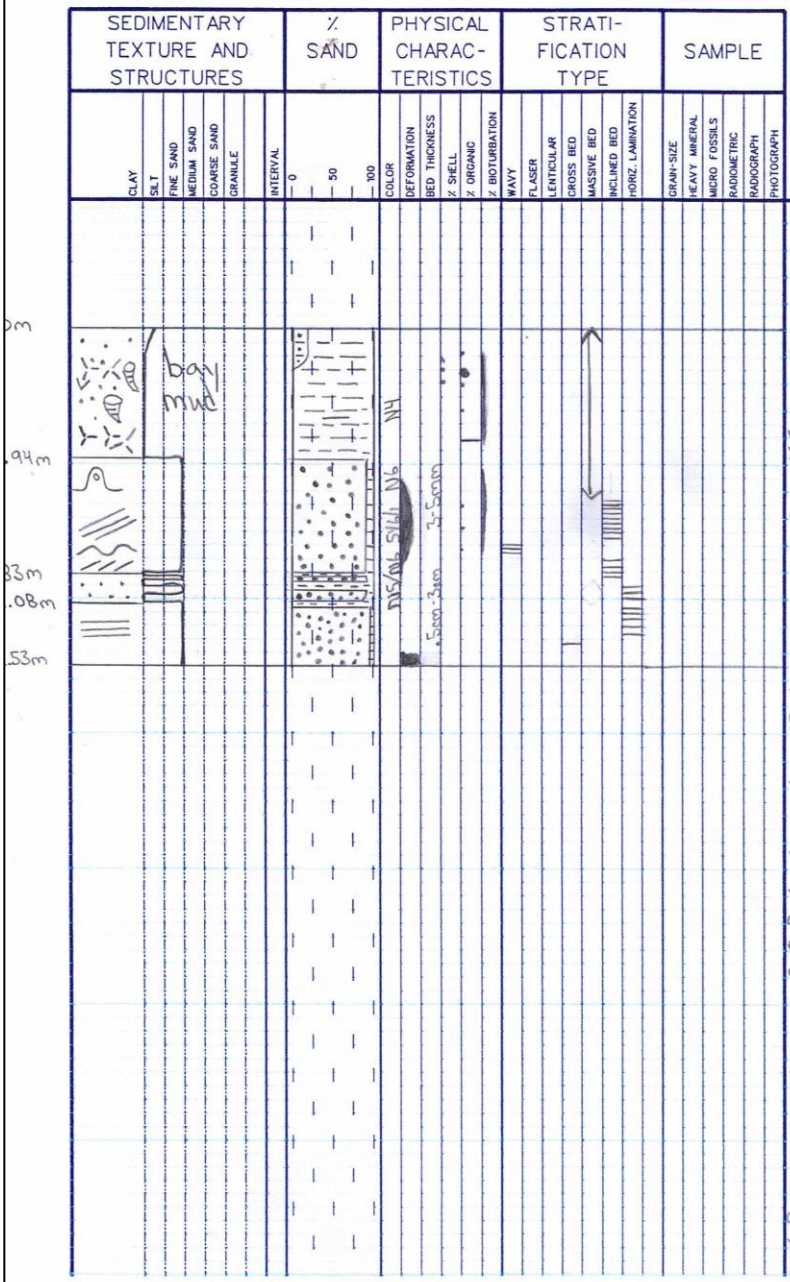

Unit A: 0.0 - 0.94m
Slightly silty clay grading to fat clay, med. dark gray (N4), massive bedding, mild to moderate rooting throughout, shell fragments from 0.10 - 0.30m (trace), horizontal organic bed at 0.82m (1cm thick) → marsh establishment, mild bioturbation throughout, 1 large (4cm x 2cm) burrow at 0.78m, erosional bottom contact over 3-4cm (alternating sand to clay lenses .5cm to 1cm thick, 1 sand lens at 0.93m, 1 clay lens at .935m

Unit B: 0.94 - 1.83m
Sand with trace silt and clay, med. light gray (N6) grading to a light olive gray (5Y 6/1), massive bedding from 0.94 - 1.25m, inclined bedding (some deformation) from 1.25 - 1.55m, wavy bedding from 1.55 - 1.63m (ripples) * deformation inclined bedding from 1.63 - 1.79m, avg. thickness of all beds 3-5mm, mild burrowing (circular burrows at 1.03 and 1.13m, vertical burrow at 1.43 and 1.65m, some organic speckled throughout, rip up mud clasts at 1.81m (1-2cm x 1-2cm), erosional bottom contact

Unit C: 1.83 - 2.08m
Interbedded med. gray (N5) clay and light olive gray (N6) sand, massive bedding, bed thickness → 3cm of fat clay; 3.5cm of sand; 7cm of fat clay; 6.5cm of sand; 2.5cm of fat clay; all bottom contacts are extremely sharp (erosional) with a small sand lens at 2.06m and another small clay lens at 2.07m,

Sheet 2 of 2

UNIVERSITY OF NEW ORLEANS

DEPARTMENT OF GEOLOGY AND GEOPHYSICS

VIBRACORE DESCRIPTION SHEET

CORE ID: RP-14-06 DATE: 7/8/14 DESCRIBED BY: T. Kramer

ELEVATION: WD = 1.57 m LOCATION: Raccoon Pass, SE corner of bay

CORE LENGTH: 2.53m LAT/LONG: N 29.11161 W 90.24507

TOTAL DEPTH: 2.97m COMPACTION: 0.44m

SEDIMENTARY TEXTURE AND STRUCTURES								% SAND	PHYSICAL CHARACTERISTICS					STRATIFICATION TYPE							SAMPLE					PHYSICAL DESCRIPTION
CLAY	SILT	FINE SAND	MEDIUM SAND	COARSE SAND	GRANULE		INTERVAL	0 — 50 — 100	COLOR	DEFORMATION	BED THICKNESS	% SHELL	% ORGANIC	% BIOTURBATION	WAVY	FLASER	LENTICULAR	CROSS BED	MASSIVE BED	INCLINED BED	HORIZ. LAMINATION	GRAIN-SIZE	HEAVY MINERAL	MICRO FOSSILS	RADIOMETRIC	RADIOGRAPH	PHOTOGRAPH	
																											Unit D: 2.08-bbm Sand, light olive gray (5Y 6/1), horizontal bedding throughout, slight cross bedding at 2.35m, deformation towards end of core, alternating / backed 5-8cm thick light gray and slightly tan sand throughout.

Sheet 1 of 2

UNIVERSITY OF NEW ORLEANS

DEPARTMENT OF GEOLOGY AND GEOPHYSICS

VIBRACORE DESCRIPTION SHEET

CORE ID: RR-14-07 DATE: 7/8/14 DESCRIBED BY: T. Krauss

ELEVATION: WD = 1.08m LOCATION: Raccoon Pass

CORE LENGTH: 3.6703m LAT/LONG: N 29.10745 W90.25527

TOTAL DEPTH: 4.1905m COMPACTION: 0.5202m

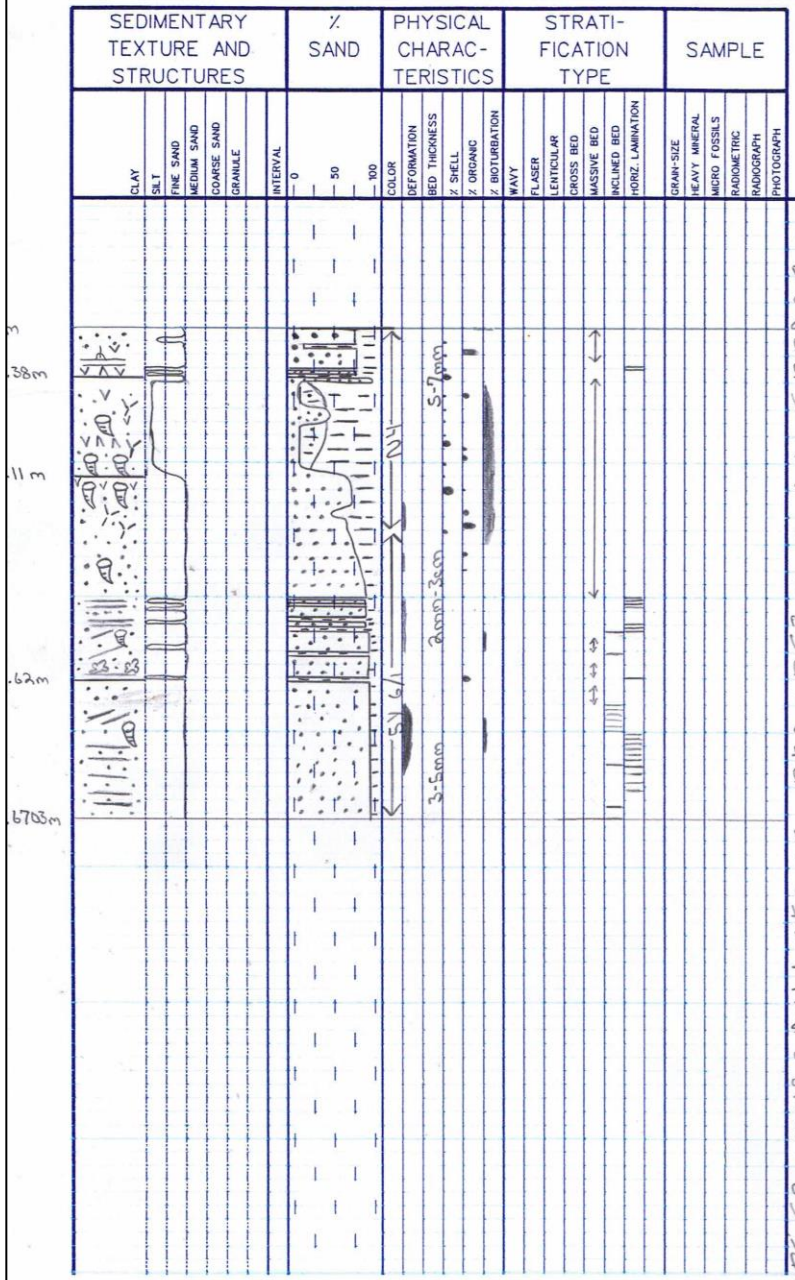

PHYSICAL DESCRIPTION

Unit A: 0-0.38m
Sand with silt & clay, med. dark gray (N4), massive bedding with two clay lenses at 0.30m & 0.32m ~ .5-1cm thick (dark gray color), organic layer w/ rooting from 0.10m - 0.20m, peppered w/ shell frag (1-3mm in length), very shelly-sand bed from 0.34m - 0.38m (mainly frag. 1-3mm length w/ occasional 1cm long shell, erosional bottom contact where shelly sand meets unit B

Unit B: 0.38-1.11m
Silty clay grading to sandy clay and back to silty clay, med. dark gray (N4), massive bedding, moderate to heavy bioturbation, peppered w/ 1-5mm shell frag except at 0.85 where shell frag abundance increases for 1-2cm, rafted wood at .82m, .88m, & .95m ~ <1cm x 1cm, some organics throughout, gradational bottom contact from silty clay to unit C

Unit C: 1.11 - 2.62m
Clayey sand (med. dark gray N4) grading to sand (light olive gray 5Y 6/1) w/ brownish tan clay lenses, massive bedding w/ clay lenses, 4 horizontal clay lenses from 2.02 - 2.07m ~ 3mm-1cm thick interbedded w/ 3 sand lenses ~3-5mm thick → all w/ sharp erosional contacts, a 3cm thick clay bed at 2.17m followed by interbedded sand and clay lenses ~ 3-7mm thick from 2.205m - 2.23m (3 clay lenses : 3 sand lenses), discontinuous clay lenses at 2.25m & 2.42m ~5-7mm thick → all w/ sharp erosional contacts, at 2.59m a 3-4cm thick clay bed w/ mm scale organics exists (top contact inclined, large Rangia at 1.17m, coffee grounds from 1.27 - 1.50m, circular burrows

UNIVERSITY OF NEW ORLEANS

DEPARTMENT OF GEOLOGY AND GEOPHYSICS

VIBRACORE DESCRIPTION SHEET

CORE ID: RP-14-07 DATE: 7/8/14 DESCRIBED BY: T. Kramer

ELEVATION: WD = 1.08m LOCATION: Raccoon Pass

CORE LENGTH: 3.6703m LAT/LONG: DD 29.10745 WD 90.25527

TOTAL DEPTH: 4.1905m COMPACTION: 0.5202m

SEDIMENTARY TEXTURE AND STRUCTURES								% SAND			PHYSICAL CHARACTERISTICS					STRATIFICATION TYPE							SAMPLE					PHYSICAL DESCRIPTION
CLAY	SILT	FINE SAND	MEDIUM SAND	COARSE SAND	GRANULE		INTERVAL	0	50	100	COLOR	DEFORMATION	BED THICKNESS	% SHELL	% ORGANIC	% BIOTURBATION	WAVY	FLASER	LENTICULAR	CROSS BED	MASSIVE BED	INCLINED BED	HORIZ. LAMINATION	GRAIN-SIZE	HEAVY MINERAL	MICRO FOSSILS	RADIOMETRIC	RADIOGRAPH	PHOTOGRAPH	

From 1.10-1.60m, vertical burrows from 2.27-2.55m, rip up mud clasts at 2.555m ~ .5cm x 1cm, bottom contact very sharp → erosional

Unit D: 2.62-btm
Sand, light olive gray (5Y 6/1), massive bedding from 2.62-2.78m, horizontal laminations w/ a few inclined laminations (most likely due to deformation) from 2.78-btm → avg. thickness = 3-5mm, a 16cm x 5mm vertical burrow starting at 2.89m, some small (.5cm) circular burrows (decreases as you get closer to the horizontal laminations

*Sheet 1 of 2

UNIVERSITY OF NEW ORLEANS

DEPARTMENT OF GEOLOGY AND GEOPHYSICS

VIBRACORE DESCRIPTION SHEET

CORE ID: RP-14-09 DATE: 7/1/14 DESCRIBED BY: T. Kramer

ELEVATION: W.D. = 0.52 m LOCATION: Raccoon Pass, NW corner of TE-52 polygon

CORE LENGTH: 4.08 m LAT/LONG: N 29.10140 W 90.25826

TOTAL DEPTH: 4.46 m COMPACTION: 0.38 m

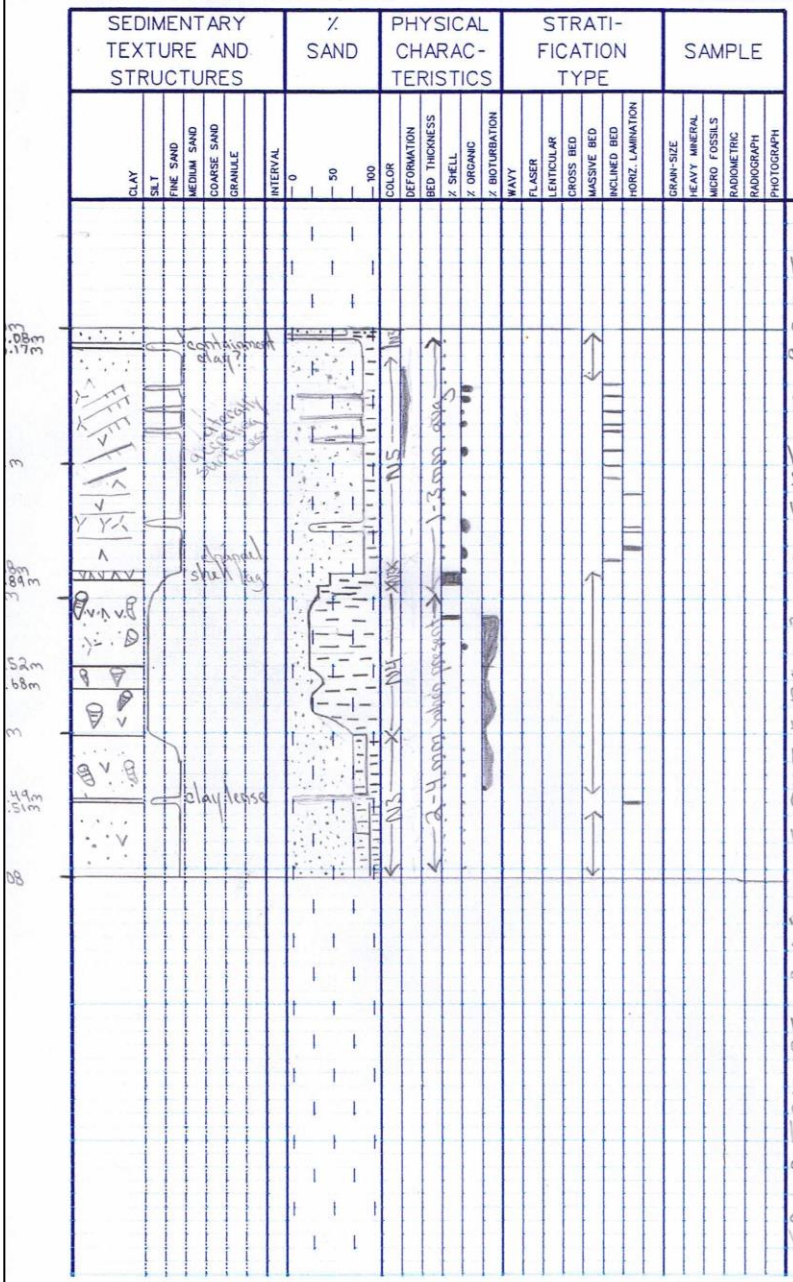

PHYSICAL DESCRIPTION

Unit A: 0 - 0.08 m
Loose to medium dense clayey sand, dark gray (N3), massive bedding w/ no shells or bioturbation, trace organics, sharp bottom contact

Unit B: 0.08 - 0.17m
Fat clay, medium dark gray (N4), massive bedding, organic content @ 0.09m containing trace shell fragments (<1mm long), sharp bottom contact

Unit C: 0.17 - 1.80m
Sand with some clay and silt, predominantly medium gray (N5) with some dark gray (N3) inclined to horizontal organic clay layers, inclined beds @ 0-5° (possible ripple marks from 0.40 - .90m), trace shell hash (<3mm length) throughout unit, low to mild rooting from 1.46 - 1.56 m, horizontal organic clay layers from 1.20 - 1.80m, roots 1-2mm in dia., sharp contact (cross bedding @ 1.10m)

Unit D: 1.80 - 1.89m
Sandy shell lag with some clay, dark gray (N3), massively bedded shell lag, shells ranging in length from <1mm to 2cm, sharp bottom contact (sand : clay ratio) erosional on to next unit but shells cease to exist

Unit E: 1.89 - 2.52m
Sandy clay to silty clay, medium dark gray (N4), massive bedding (non-discernable due to frequency and high degree of bioturbation), low to mild rooting throughout, large shells at 2.13m, unit has trace shell fragments <1mm scattered throughout, rafted wood at 2.33m ~5mm thick, gradational bottom contact

* Sheet 2 of 2

UNIVERSITY OF NEW ORLEANS

DEPARTMENT OF GEOLOGY AND GEOPHYSICS

VIBRACORE DESCRIPTION SHEET

CORE ID: RP-14-09 DATE: 7/1/14 DESCRIBED BY: T. Kramer

ELEVATION: WD = 0.52 LOCATION: Raccoon Pass, NW corner of TE-52 polygon

CORE LENGTH: 4.08m LAT/LONG: N 29.10140 W 90.25826

TOTAL DEPTH: 4.46m COMPACTION: 0.38m

SEDIMENTARY TEXTURE AND STRUCTURES								% SAND			PHYSICAL CHARACTERISTICS					STRATIFICATION TYPE							SAMPLE					PHYSICAL DESCRIPTION
CLAY	SILT	FINE SAND	MEDIUM SAND	COARSE SAND	GRANULE		INTERVAL	0	50	100	COLOR	DEFORMATION	BED THICKNESS	% SHELL	% ORGANIC	% BIOTURBATION	WAVY	FLASER	LENTICULAR	CROSS BED	MASSIVE BED	INCLINED BED	HORIZ. LAMINATION	GRAIN-SIZE	HEAVY MINERAL	MICRO FOSSILS	RADIOMETRIC	RADIOGRAPH	PHOTOGRAPH	

Unit F: 2.52 - 2.68 m
Clayey sand, medium dark gray (N4), Massive bedding with trace shell fragments <1mm long, little to no bioturbation, gradational contact

Unit G: 2.68 - 3.00m
Sandy clay grading to clayey sand, medium dark gray (N4), non-discernable bedding grading to massive bedding due to high degree of bioturbation, trace shell fragments <1mm long, little to no organic content, bottom contact gradational

Unit H: 3.00 - btm
Clayey sand, medium gray (N3), massive bedding with some inclined beds (5°) from 3.25 - 3.40m, one discontinuous clay lense at 3.50m, one burrow 3.37m (5x5mm), trace organics throughout, 3.69 - btm portion of core is destroyed / lost, vertical and diagonal burrows from 3.15 - 3.44m (possible skolithos), Ophiomorpha? at 3.17

Appendix B

Sample	Moisture Content (%)	Specific Gravity of Soil Solids (Gs)	Passing No. 200 Sieve (%)	Organic Content (%)	Sat. Unit Weight (kN/m3)	Liquid Limit (%)	Plastic Limit (%)	Plasticity Index (%)	Compression Index, Cc
RP-C-14-01	47	2.646	70	1.8	17.07	48	17	31	0.24881
RP-C-14-02-T	62	2.698	76	3.1	18.81	52	22	30	0.24479
RP-C-14-02-B	54	2.659	68	2.7	16.96	45	19	26	0.2538
RP-C-14-04	63	2.654	48	2.6	16.43	45	23	22	0.31658
RP-C-14-07-T	60	2.635	72	3.3	17.18	44	21	23	0.21725
RP-C-14-07-B	36	2.611	62	2.1	16.74	35	19	16	0.22855

Appendix C

RP-C-14-01:

Load Sequence	Cumulative Change in Height	Specimen Height	Delta e	New e
(kN/m2)	(in)	(in)		
0	0.0000	1.0000		0.7612
11.97	0.0253	0.9747	0.0446	0.7166
23.94	0.0524	0.9476	0.0477	0.6689
47.88	0.0865	0.9135	0.0601	0.6089
95.76	0.1311	0.8689	0.0786	0.5303
191.52	0.1736	0.8264	0.0749	0.4554
95.76	0.1719	0.8281	-0.0030	0.4584
47.88	0.1679	0.8321	-0.0070	0.4655
11.97	0.1541	0.8459	-0.0243	0.4898
23.94	0.1565	0.8435	0.0042	0.4856
47.88	0.1621	0.8379	0.0099	0.4757
95.76	0.1686	0.8314	0.0114	0.4643
191.52	0.1802	0.8198	0.0204	0.4438
383.04	0.2160	0.7840	0.0631	0.3808
766.08	0.2554	0.7446	0.0694	0.3114

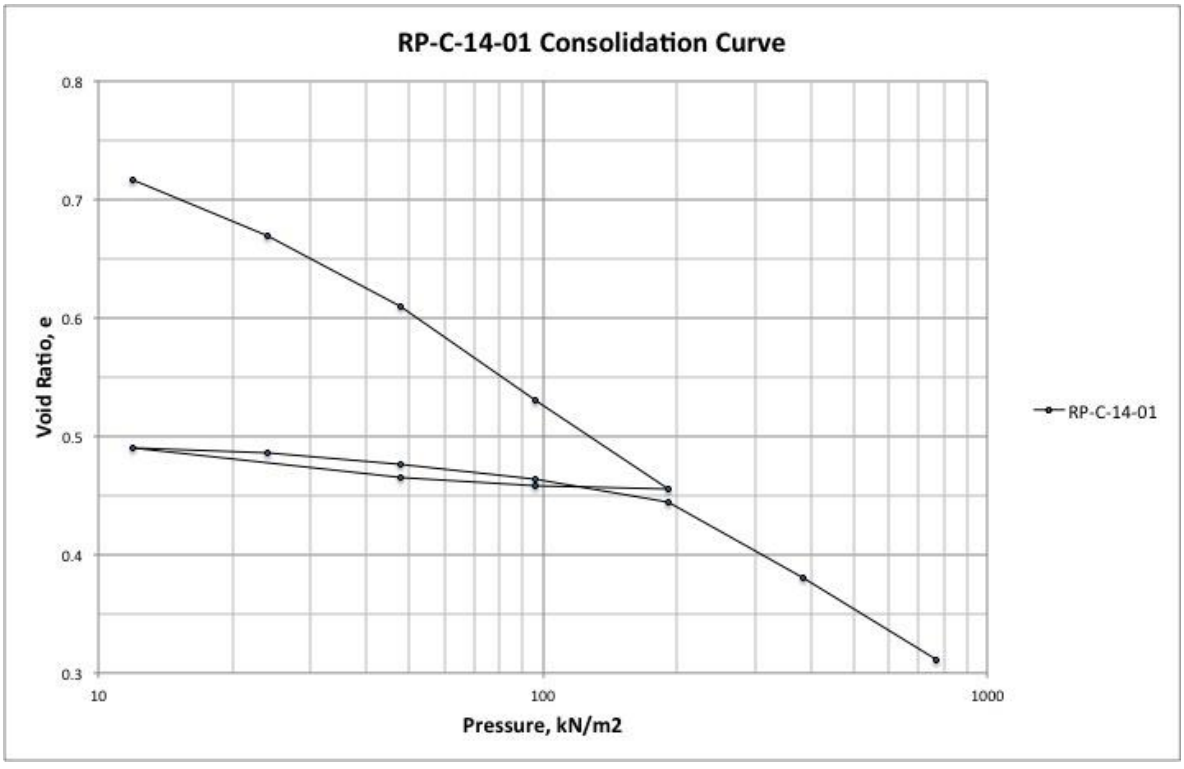

RP-C-14-02 Top:

Load Sequence	Cumulative Change in Height	Specimen Height	Delta e	New e
(kN/m2)	(in)	(in)		
0	0.0000	1.0000		0.7176
11.97	0.0487	0.9513	0.0836	0.6340
23.94	0.0884	0.9116	0.0682	0.5658
47.88	0.1241	0.8759	0.0613	0.5044
95.76	0.1711	0.8289	0.0807	0.4237
191.52	0.2140	0.7860	0.0737	0.3500
95.76	0.2149	0.7851	0.0015	0.3485
47.88	0.2119	0.7881	-0.0052	0.3536
11.97	0.2004	0.7996	-0.0198	0.3734
23.94	0.2020	0.7980	0.0027	0.3706
47.88	0.2055	0.7945	0.0060	0.3646
95.76	0.2106	0.7894	0.0088	0.3559
191.52	0.2187	0.7813	0.0139	0.3419
383.04	0.2512	0.7488	0.0558	0.2861
766.08	0.2927	0.7073	0.0713	0.2148

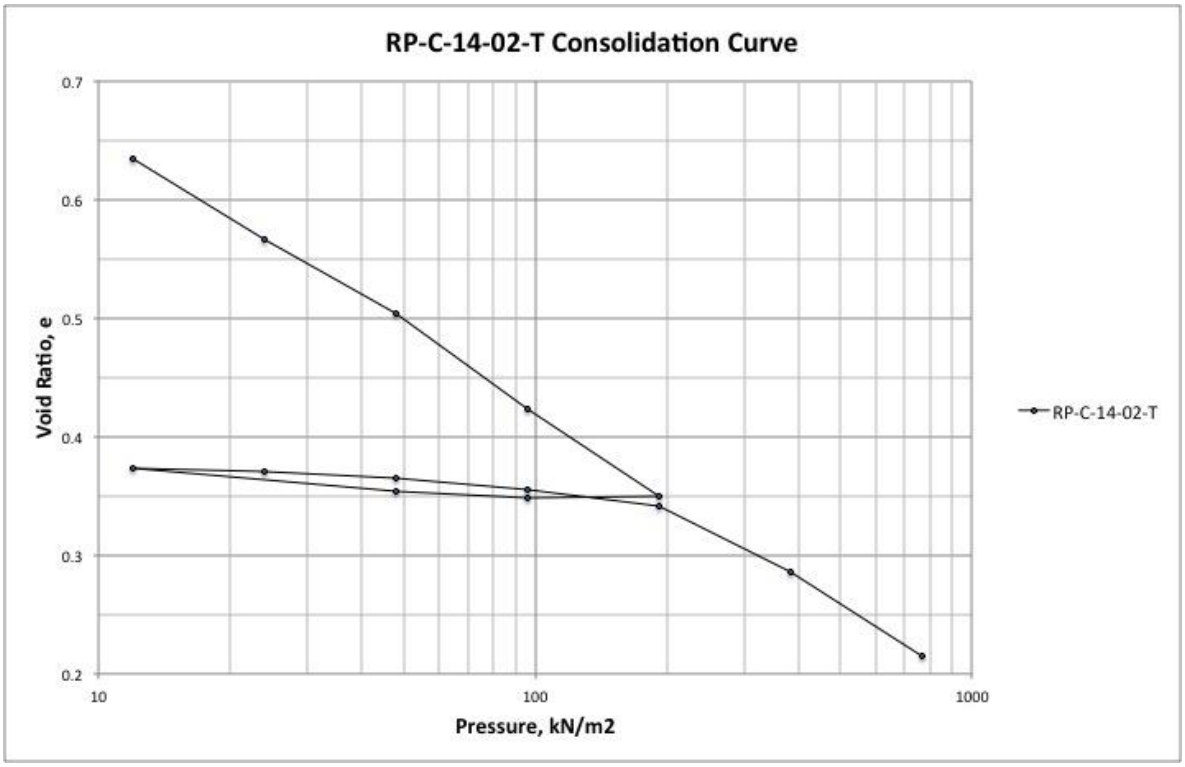

RP-C-14-02 Bottom:

Load Sequence	Cumulative Change in Height	Specimen Height	Delta e	New e
(kN/m2)	(in)	(in)		
0	0.0000	1.0000		0.8771
11.97	0.0644	0.9356	0.1209	0.7562
23.94	0.1027	0.8973	0.0719	0.6843
47.88	0.1459	0.8541	0.0811	0.6032
95.76	0.1944	0.8056	0.0910	0.5122
191.52	0.2351	0.7649	0.0764	0.4358
95.76	0.2340	0.7660	-0.0021	0.4379
47.88	0.2315	0.7685	-0.0047	0.4426
11.97	0.2216	0.7784	-0.0186	0.4611
23.94	0.2226	0.7774	0.0019	0.4593
47.88	0.2260	0.7740	0.0064	0.4529
95.76	0.2315	0.7685	0.0103	0.4426
191.52	0.2418	0.7582	0.0193	0.4232
383.04	0.2751	0.7249	0.0625	0.3607
766.08	0.3105	0.6895	0.0665	0.2943

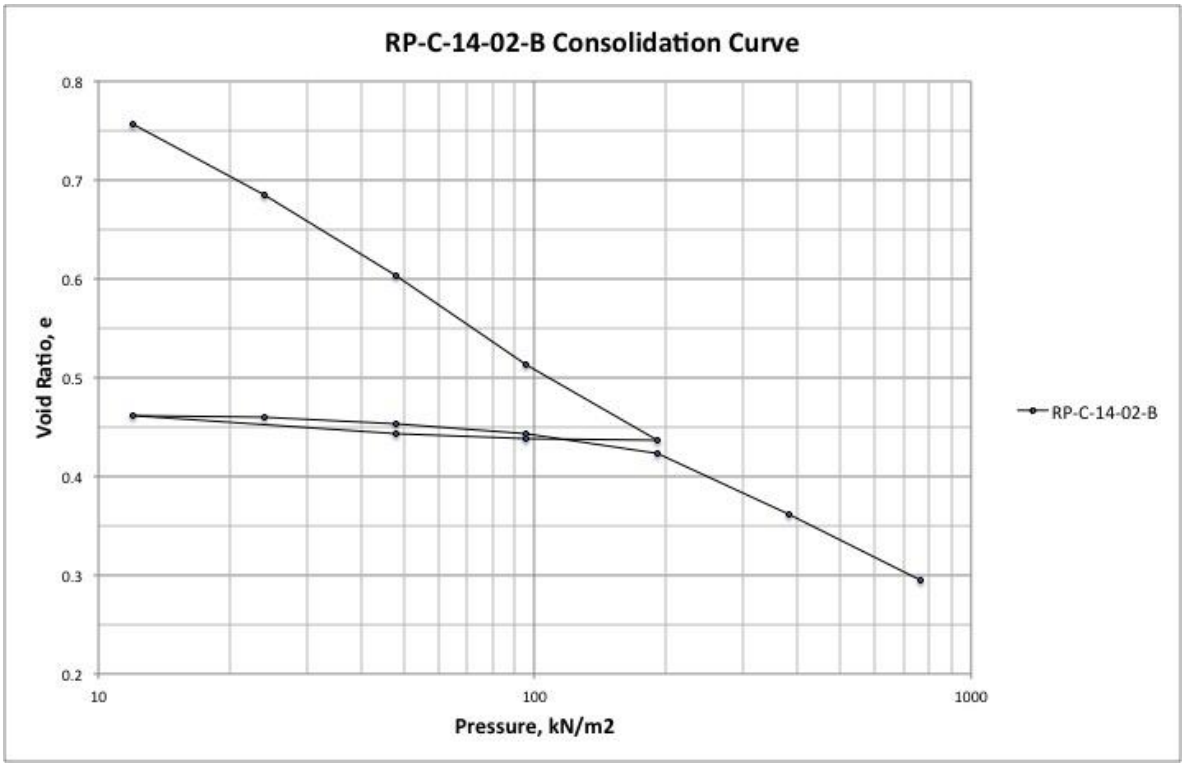

RP-C-14-04:

Load Sequence	Cumulative Change in Height	Specimen Height	Delta e	New e
(kN/m^2)	(in)	(in)		
0	0.0000	1.0000		0.9453
11.97	0.0306	0.9694	0.0595	0.8858
23.94	0.0646	0.9354	0.0661	0.8196
47.88	0.1244	0.8756	0.1163	0.7033
95.76	0.1795	0.8205	0.1072	0.5961
191.52	0.2285	0.7715	0.0953	0.5008
95.76	0.2266	0.7734	-0.0037	0.5045
47.88	0.2231	0.7769	-0.0068	0.5113
11.97	0.2119	0.7881	-0.0218	0.5331
23.94	0.2119	0.7881	0.0000	0.5331
47.88	0.2154	0.7846	0.0068	0.5263
95.76	0.2228	0.7772	0.0144	0.5119
191.52	0.2349	0.7651	0.0235	0.4883
383.04	0.2725	0.7275	0.0731	0.4152
766.08	0.3116	0.6884	0.0761	0.3391

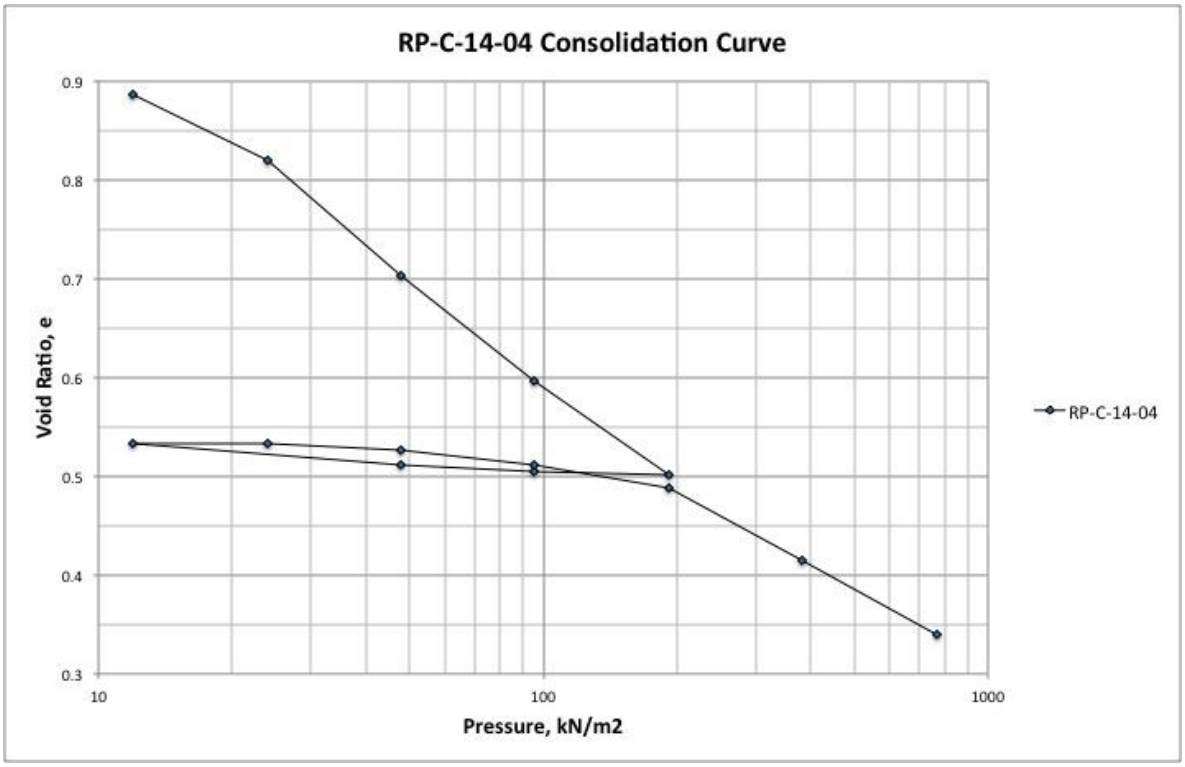

RP-C-14-07 Top:

Load Sequence	Cumulative Change in Height	Specimen Height	Delta e	New e
(kN/m2)	(in)	(in)		
0	0.0000	1.0000		0.7583
11.97	0.0524	0.9476	0.0921	0.6661
23.94	0.0857	0.9143	0.0586	0.6076
47.88	0.1210	0.8790	0.0621	0.5455
95.76	0.1627	0.8373	0.0733	0.4722
191.52	0.1999	0.8001	0.0654	0.4068
95.76	0.1989	0.8011	-0.0018	0.4085
47.88	0.1964	0.8036	-0.0044	0.4129
11.97	0.1884	0.8116	-0.0141	0.4270
23.94	0.1898	0.8102	0.0025	0.4245
47.88	0.1930	0.8070	0.0056	0.4189
95.76	0.1975	0.8025	0.0079	0.4110
191.52	0.2063	0.7937	0.0155	0.3955
383.04	0.2372	0.7628	0.0543	0.3412
766.08	0.2723	0.7277	0.0617	0.2795

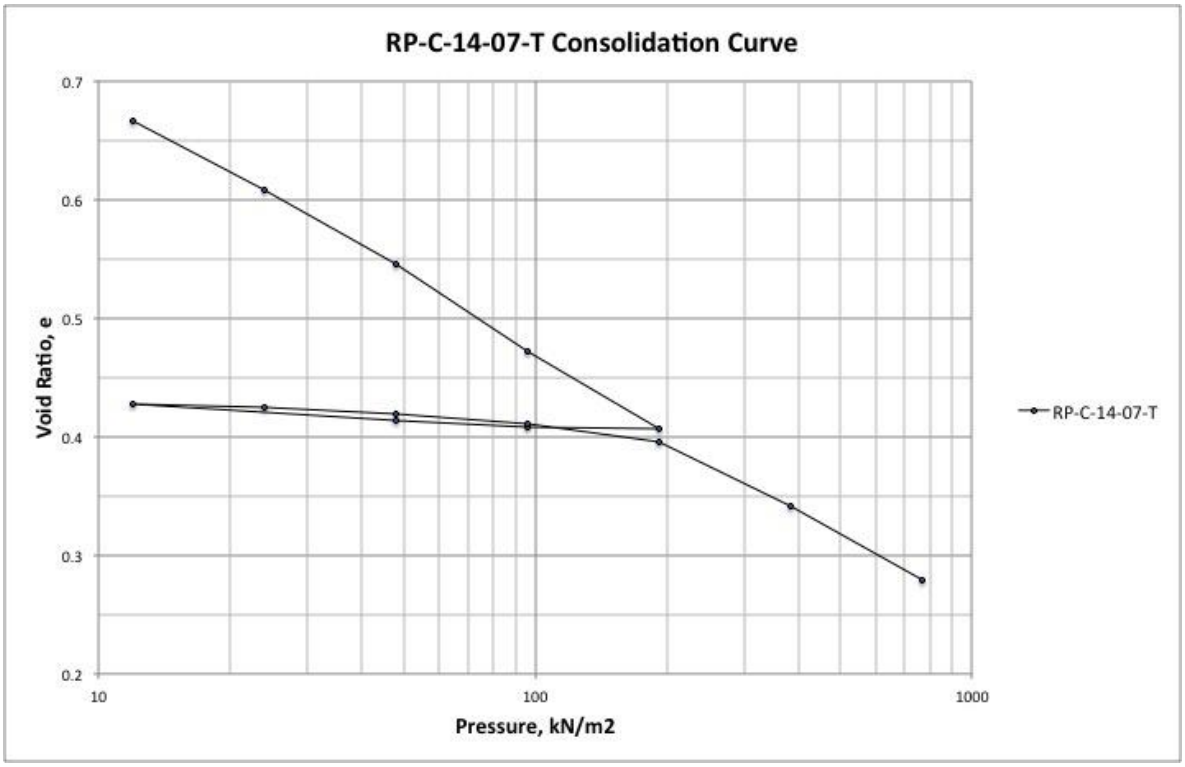

RP-C-14-07 Bottom:

Load Sequence	Cumulative Change in Height	Specimen Height	Delta e	New e
(kN/m2)	(in)	(in)		
0	0.0000	1.0000		0.8384
11.97	0.0527	0.9473	0.0969	0.7415
23.94	0.0871	0.9129	0.0632	0.6782
47.88	0.1241	0.8759	0.0680	0.6102
95.76	0.1645	0.8355	0.0743	0.5360
191.52	0.2019	0.7981	0.0688	0.4672
95.76	0.2005	0.7995	-0.0026	0.4698
47.88	0.1980	0.8020	-0.0046	0.4744
11.97	0.1900	0.8100	-0.0147	0.4891
23.94	0.1910	0.8090	0.0018	0.4872
47.88	0.1940	0.8060	0.0055	0.4817
95.76	0.1982	0.8018	0.0077	0.4740
191.52	0.2075	0.7925	0.0171	0.4569
383.04	0.2419	0.7581	0.0632	0.3937
766.08	0.2755	0.7245	0.0618	0.3319

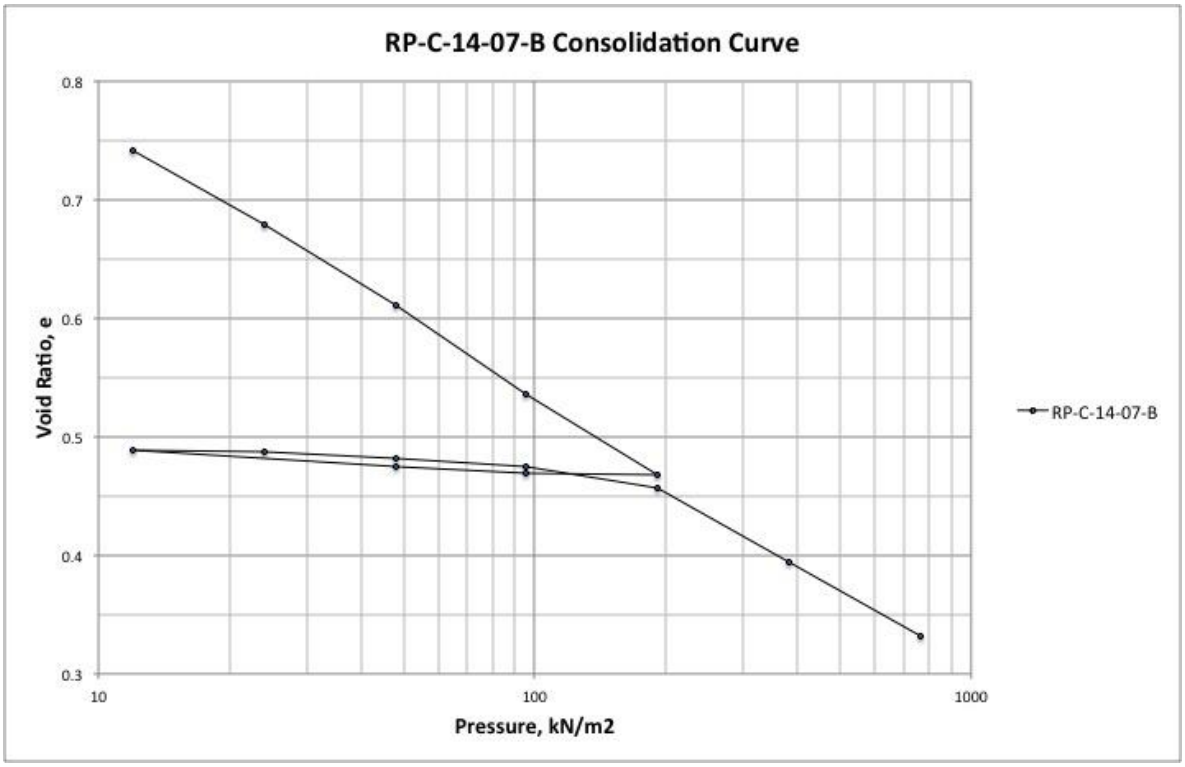

RP-C-14-08:

LABORATORY GRADATION WORKSHEET & AMOUNT OF MATERIALS IN SOILS FINER THAN #200 SIEVE (200 WASH)

ASTM C-33, ASTM C-117, ASTM C-136, & ASTM D-1140

Project Name: _____ **Date Tested:** _____
Project No.: _____ **Tested By:** _____
Scale: _____ **Sieve Shaker ID:** _____
Oven: _____

RP-C-14-08

Boring No.	998
Sample No. / Depth / Elev.	
Pan No.	998
Wt. Of Dry Soil Before Wash + Pan (g)	1006.60
Wt. Of Pan (g)	302.43
Wt. Of Dry Soil After Wash + Pan (g)	949.93
Unwashed Weight of Dry Soil (g)	704.17
Amount of Soil Passing (g)	56.67
% Passing	**8.05**
Moisture Content	
Wt. Of Pan (g)	302.43
Wt. Of Wet Soil + Can (g)	
Wt. Of Dry Soil + Can (g)	1006.60
Wt. Of Dry Soil (g)	704.17
Wt. Of Water (g)	-1007
Moisture (%)	**-143**
Remarks	
Group Symbol	

Sieve No.	Sieve Size	Cummulative Weight Retained (g)	% Retained	% Passing
	No. 4	0.16	0.02%	99.98%
	No. 10	1.64	0.23%	99.77%
	No.20	12.01	1.71%	98.29%
	No. 40	24.88	3.53%	96.47%
	No. 60	38.57	5.48%	94.52%
	No. 100	263.33	37.40%	62.60%
	No. 120	481.88	68.43%	31.57%
	No. 140	559.10	79.40%	20.60%
	No. 200	647.50	91.95%	8.05%
998	PAN	702.10	99.71%	
	Total Weight (g)	704.17	100.00%	

Boring No.	
Sample No. / Depth / Elev.	
Pan No.	10
Wt. Of Dry Soil Before Wash + Pan (g)	915.00
Wt. Of Pan (g)	266.89
Wt. Of Dry Soil After Wash + Pan (g)	862.80
Unwashed Weight of Dry Soil (g)	648.11
Amount of Soil Passing (g)	52.20
% Passing	**8.05**
Moisture Content	
Wt. Of Pan (g)	266.89
Wt. Of Wet Soil + Can (g)	
Wt. Of Dry Soil + Can (g)	915.00
Wt. Of Dry Soil (g)	648.11
Wt. Of Water (g)	-915
Moisture (%)	**-141**
Remarks	
Group Symbol	

Sieve No.	Sieve Size	Cummulative Weight Retained (g)	% Retained	% Passing
	No. 4	0.00	0.00%	100.00%
	No. 10	0.17	0.03%	99.97%
	No. 20	8.93	1.38%	98.62%
	No. 40	19.73	3.04%	96.96%
	No. 60	35.03	5.40%	94.60%
	No. 100	278.94	43.04%	56.96%
	No. 120	484.67	74.78%	25.22%
	No. 140	529.74	81.74%	18.26%
	No. 200	595.90	91.94%	8.06%
10	PAN	648.60	100.08%	
	Total Weight (g)	648.11	100.00%	

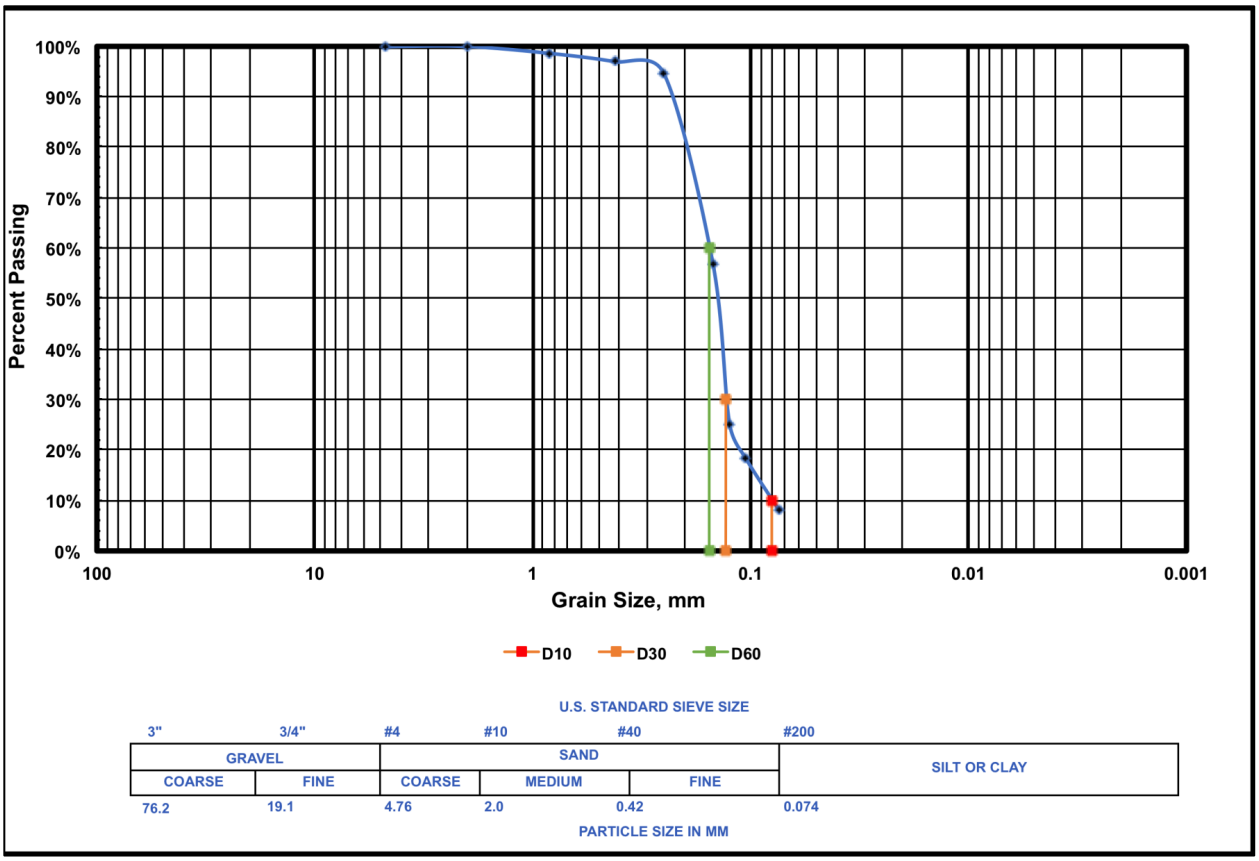
100%
90%
80%
70%
60%
50%
40%
30%
20%
10%
0%
Percent Passing
100
10
1
0.1
0.01
0.001
Grain Size, mm
D10
D30
D60
U.S. STANDARD SIEVE SIZE
3"
3/4"
#4
#10
#40
#200
GRAVEL
SAND
SILT OR CLAY
COARSE
FINE
COARSE
MEDIUM
FINE
76.2
19.1
4.76
2.0
0.42
0.074
PARTICLE SIZE IN MM

Appendix D

Sample	Sat. Unit Weight (kN/m3)	H (m)	Initial Void Ratio, eo	Compression Index, Cc	Insitu Effective Stress at MIDPOINT σ'o (kN/m2)	Increase in Effective Stress, Δσ'(kN/m2)	Settlement, Sc (mm)	Ratio of Sc & H (%)
RP-C-14-01	17.07	1.45	0.7612	0.24881	5.26	4	50.29	3.47%
						8	82.22	5.67%
						12	105.67	7.29%
						16	124.21	8.57%
						20	139.54	9.62%
RP-C-14-02-T	18.81	0.98	0.7176	0.24479	4.41	4	39.16	4.00%
						8	62.76	6.40%
						12	79.70	8.13%
						16	92.94	9.48%
						20	103.79	10.59%
RP-C-14-02-B	16.96	0.98	0.8771	0.2538	3.50	4	43.83	4.47%
						8	68.42	6.98%
						12	85.59	8.73%
						16	98.80	10.08%
						20	109.53	11.18%
RP-C-14-04	16.43	0.99	0.9453	0.31658	3.28	4	55.82	5.64%
						8	86.47	8.73%
						12	107.72	10.88%
						16	123.99	12.52%
						20	137.18	13.86%
RP-C-14-07-T	17.18	0.96	0.7583	0.21725	3.54	4	38.97	4.06%
						8	60.90	6.34%
						12	76.23	7.94%
						16	88.03	9.17%
						20	97.63	10.17%
RP-C-14-07-B	16.74	0.96	0.8384	0.22855	3.33	4	40.93	4.26%
						8	63.51	6.62%
						12	79.18	8.25%
						16	91.20	9.50%
						20	100.95	10.52%

Vita

John N. Kramer III was born and raised in New Orleans, LA in Midcity. He spent many days in the marshes of Louisiana at an early age and is still an avid fisherman to this day. John is also passionate about soccer and a career in the petroleum industry. After graduating from Jesuit High School of New Orleans in 2009, he decided to play soccer and pursue a B.S. in Environmental Science at the University of West Florida. He graduated from the University of West Florida in 2013 and chose to attend the University of New Orleans to pursue a M.S. in Earth and Environmental Science with a focus in coastal geology. During his time at U.N.O. John participated in AAPG's Imperial Barrel Award, where his team took 1st place in the Gulf Coast Section. In the summer of 2015, John completed an internship as an exploration geoscientist with Stone Energy in New Orleans. He is now preparing to for his next internship in the summer of 2016 with Anadarko Petroleum Corporation.